MAX-PLANCK-INSTITUT
FÜR METEOROLOGIE

Unravelling climate conditions preceding the End-Permian Mass Extinction: Insights from latest Permian interannual tropical variability and extreme events

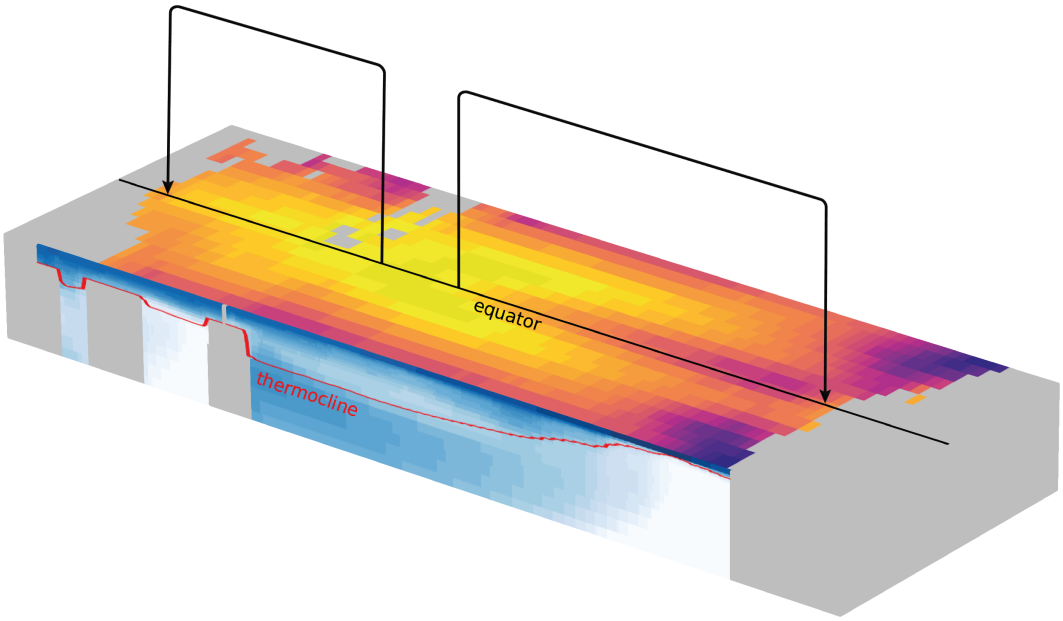

Daniel Burt

Hamburg 2024

Berichte zur Erdsystemforschung
Reports on Earth System Science

283
2024

Hinweis

Die Berichte zur Erdsystemforschung werden vom Max-Planck-Institut für Meteorologie in Hamburg in unregelmäßiger Abfolge herausgegeben.

Sie enthalten wissenschaftliche und technische Beiträge, inklusive Dissertationen.

Die Beiträge geben nicht notwendigerweise die Auffassung des Instituts wieder.

Die "Berichte zur Erdsystemforschung" führen die vorherigen Reihen "Reports" und "Examensarbeiten" weiter.

Anschrift / Address

Max-Planck-Institut für Meteorologie
Bundesstrasse 53
20146 Hamburg
Deutschland

Tel./Phone: +49 (0)40 4 11 73 - 0
Fax: +49 (0)40 4 11 73 - 298

name.surname@mpimet.mpg.de
www.mpimet.mpg.de

Notice

The Reports on Earth System Science are published by the Max Planck Institute for Meteorology in Hamburg. They appear in irregular intervals.

They contain scientific and technical contributions, including PhD theses.

The Reports do not necessarily reflect the opinion of the Institute.

The "Reports on Earth System Science" continue the former "Reports" and "Examensarbeiten" of the Max Planck Institute.

Layout

Bettina Diallo and Norbert P. Noreiks
Communication

Copyright

Unravelling climate conditions preceding the End-Permian Mass Extinction: Insights from latest Permian interannual tropical variability and extreme events

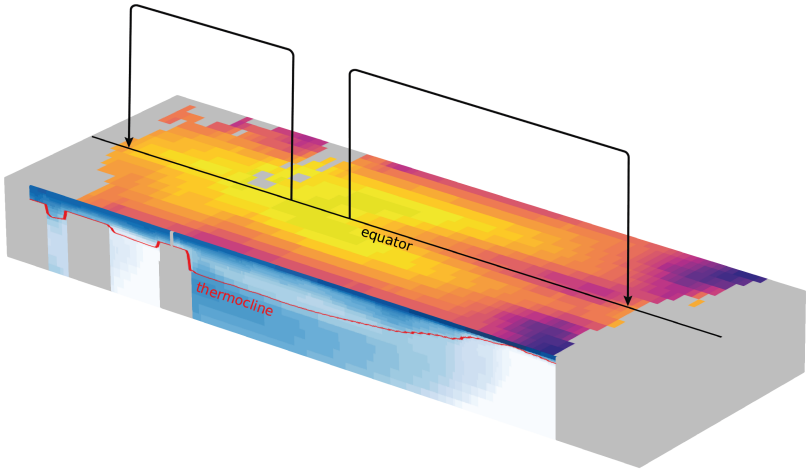

Daniel Burt

Hamburg 2024

Daniel Burt
aus Oban, Vereinigtes Königreich

Max-Planck-Institut für Meteorologie
The International Max Planck Research School on Earth System Modelling
(IMPRS-ESM)
Bundesstrasse 53
20146 Hamburg

Tag der Disputation: 4. Juni 2024

Folgende Gutachter empfehlen die Annahme der Dissertation:
Prof. Dr. Tatiana Ilyina
Prof. Dr. Gerhard Schiedl

Vorsitzender des Promotionsausschusses:
Prof. Dr. Hermann Held

Dekan der MIN-Fakultät:
Prof. Dr.-Ing. Norbert Ritter

Titelgrafik vom Autor: *A schematic illustration of the tropics during the latest Permian (252 Ma) with arrows indicating the mean atmospheric Walker Circulation, a contour map of the Sea Surface Temperatures (°C) with the equator highlighted, a contour map of the meridional mean oxygen concentrations (mol m-3) around the equator in the surface 300m and a line plot of the thermocline depth (m).*

Berichte zur Erdsystemforschung / Max-Planck-Institut für Meteorologie 283
Reports on Earth System Science / Max Planck Institute for Meteorology 2024

ISSN 1614-1199 - doi: 10.17617/2.3604961

This document was typeset using the typographical look-and-feel **classicthesis** developed by André Miede and Ivo Pletikosić and inspired by Robert Bringhurst. Available at https://bitbucket.org/amiede/classicthesis/.

ABSTRACT

In the present, anthropogenic greenhouse gas emissions are dramatically changing the climate and threatening ecosystems. Evidence of extinction in the present makes it essential that we learn from past analogues such as the End-Permian Mass Extinction, the Earth's most severe mass extinction. During the End-Permian Mass Extinction, more than 90% of species were extinguished by intense climate change driven by large-scale volcanic greenhouse gas emissions. Previous studies exploring the End-Permian Mass Extinction focus on geological timescales of 10s or 100s of thousands of years. These studies therefore overlook the most relevant annual and decadal timescales of environmental change at which ecosystems respond. In this thesis, I use the Max-Planck Institute Earth System Model to investigate the dominant-mode of interannual variability and patterns of marine extreme events in the latest Permian climate, to better understand the conditions preceding the End-Permian Mass Extinction.

I contribute towards bridging the disparity of timescales by identifying patterns of short-term variability in tropical sea surface temperatures and their implications for marine biota. For the first time, I reveal the dominant-mode of interannual tropical variability in the latest Permian as an atmosphere-ocean feedback system centred in the equatorial West Panthalassic Ocean. This mode of variability is characterised by a periodicity of 2-4 years and affects the patterns of precipitation, temperature, mixing and transport across the tropical Tethys and Panthalassic Oceans. I relate the pattern of surface tropical marine heatwaves to the leading-mode of variability and determine maximum marine heatwave durations of up to 22 months and intensities of up to 5.9°C in the equatorial East Panthalassic.

I explore the spatial pattern of the deadly trio of marine stressors (ocean warming, acidification and deoxygenation) across the major shelf regions of the latest Permian and their relationship with evidence of higher extinction severity at extratropical latitudes. I find that contrary to previous studies, hypoxia is unlikely to drive extinction across high latitude shallow shelf regions and rather poses the greatest stress to the tropical Tethys Ocean. Uniquely among the latest Permian shelf regions, the East Panthalassic shelf is likely exposed to the full deadly trio. The southern high latitudes are exposed to intense marine heatwaves but both northern and southern high latitudes have a similar expected intolerance to pH extremes. My results support previous studies that suggest the extratropical extinction selectivity described by the fossil record may primarily be explained by ocean acidification rather than warming.

My results clearly indicate that the End-Permian Mass Extinction occurred earlier and faster in response to the climate perturbation than previously described. I suggest that better understanding of regional mass extinction triggers in the past can be applied to aid conservation efforts in the present. This can be achieved through a better comprehension of the evolving spatial patterns of environmental stress in response to climate change.

ZUSAMMENFASSUNG

Gegenwärtig verändern die vom Menschen verursachten Treibhausgasemissionen das Klima drastisch und bedrohen ganze Ökosysteme. Angesichts der Hinweise auf das gegenwärtige Artensterben ist es von entscheidender Bedeutung, dass wir aus den Analogien der Vergangenheit lernen, wie z. B. aus dem Massenaussterben gegen Ende des Perms, dem schwersten Massenaussterbeereignis in der Erdgeschichte. Während des Massenaussterben gegen Ende des Perms wurden mehr als 90% der Arten durch intensive Klimaveränderungen ausgelöscht, die durch großflächige vulkanische Treibhausgasemissionen verursacht wurden. Bisherige Studien zur Erforschung des Massenaussterben gegen Ende des Perms konzentrieren sich auf geologische Zeiträume von 10- oder 100-tausend Jahren. Diese Studien vernachlässigen daher die bedeutenden jährlichen und dekadischen Zeitskalen der Umweltveränderungen, auf die die Ökosysteme reagieren. In dieser Doktorarbeit verwende ich das Erdsystemmodell des Max-Planck-Instituts, um den vorherrschenden Modus der interannualen Variabilität und die Muster mariner Extremereignisse im Klima des jüngsten Perms zu untersuchen, um die Verhältnisse vor dem Massenaussterben gegen Ende des Perms besser zu verstehen.

Ich trage dazu bei, die Diskrepanz der Zeitskalen zu überbrücken, indem ich die Muster der kurzfristigen Variabilität der tropischen Meeresoberflächentemperaturen und ihre Auswirkungen auf die Meeresbiota identifiziere. Erstmals zeige ich den dominanten Modus der interannualen tropischen Variabilität im jüngsten Perm als ein atmosphärisch-ozeanisches Rückkopplungssystem auf, das im äquatorialen westlichen Panthalassa Ozean zentriert ist. Dieser Modus der Variabilität ist durch eine Periodizität von 2 bis 4 Jahren gekennzeichnet und beeinflusst die Muster von Niederschlag, Temperatur, Durchmischung und Transport über den tropischen Tethys- und Panthalassischen Ozean. Ich bringe das Muster der tropischen marinen Hitzewellen an der Oberfläche mit dem führenden Modus der Variabilität in Verbindung und identifiziere maximale marine Hitzewellen mit einer Dauer von bis zu 22 Monaten und einer Intensität von bis zu 5,9°C im äquatorialen östlichen Panthalassikum.

Ich analysiere das räumliche Muster des tödlichen Trios mariner Stressfaktoren (Ozeanerwärmung, Ozeanversauerung und Ozeansauerstoffentzug) in den wichtigsten Schelfregionen des jüngsten Perms und untersuche ihre Beziehung zu den Anzeichen für ein stärkeres Aussterben in außertropischen Breitengraden. Im Gegensatz zu früheren Studien komme ich zu dem Ergebnis, dass es unwahrscheinlich ist, dass Hypoxie das Aussterben in flachen Schelfregionen in hohen Breitengraden vorantreibt; vielmehr stellt sie die größte Bedrohung für den tropischen Tethys-Ozean dar. Unter den Schelfregionen des jüngsten Perms ist das Östliche Panthalassa Schelf wahrscheinlich dem gesamten tödlichen Trio ausgesetzt. Die südlichen hohen Breiten sind intensiven marinen Hitzewellen ausgesetzt, aber sowohl die nördlichen als auch die südlichen hohen Breiten weisen eine ähnliche erwartete Intoleranz gegenüber pH-Extremen auf. Meine Ergebnisse unterstützen frühere Studien, die darauf hindeuten, dass die im fossilen Datensatz beschriebene Selektivi-

tät des außertropischen Aussterbens in erster Linie durch die Versauerung der Ozeane und nicht durch die Erwärmung erklärt werden kann.

Meine Ergebnisse deuten darauf hin, dass das Massenaussterben gegen Ende des Perms als Reaktion auf die Störung im Klima früher und schneller stattfand als bisher angenommen. Ich schlage vor, dass ein besseres Verständnis der Auslöser regionaler Massenaussterben in der Vergangenheit zur Unterstützung von Naturschutzmaßnahmen in der Gegenwart genutzt werden kann. Dies kann durch ein besseres Verständnis der sich entwickelnden räumlichen Muster der Umweltbelastung als Reaktion auf den Klimawandel erreicht werden.

PUBLICATIONS

This dissertation is based on the following two first-author publications, which are included in the appendices:

APPENDIX A

Burt, D.J., Putrasahan, D., Günther, M. & Ilyina, T. (in preparation). Characterising interannual tropical variability and marine heatwaves in the latest Permian [*to be submitted to Climate of the Past*].

APPENDIX B

Burt, D.J. & Ilyina, T. (in preparation). The Deadly Trio of marine stressors varied regionally in the latest Permian [*to be submitted to Climate of the Past*].

Furthermore, I contributed to an additional publication based on the results of my masters thesis:

Burt, D.J., Fröb, F. & Ilyina, T. (2021). The sensitivity of the marine carbonate system to regional ocean alkalinity enhancement. *Frontiers in Climate*, *3*(624075). DOI: 10.3389/fclim.2021.624075

CONTENTS

LIST OF ACRONYMS

CIE	Carbon Isotope Excursion
DO	Dissolved Oxygen
ECS	Equilibrium Climate Sensitivity
ENSO	El Niño Southern Oscillation
EOF	Empirical Orthogonal Function
EPME	End-Permian Mass Extinction
MHW	Marine Heatwave
MPI-ESM	Max-Planck Institute Earth System Model
OAE	Oceanic Anoxic Event
OMZ	Oxygen Minimum Zone
PTB	Permian-Triassic Boundary
SST	Sea Surface Temperature

Part I

UNIFYING ESSAY

Unifying Essay

Limits of survival are set by climate,
those long drifts of change which a generation may fail to notice.
And it is the extremes of climate which set the pattern.

– Herbert [1976]

1 INTRODUCTION

This thesis describes my research into the patterns of variability and extremes of the "deadly trio" during the latest Permian period and their implications for extinction stress preceding the Permian-Triassic transition. I model the palaeoclimate of the latest Permian period using the Max Planck Institute Earth System Model and analyse the modes of variability of sea surface temperature, ocean acidity and dissolved oxygen concentration across interannual timescales, which have not previously been investigated, and the pattern of extremes of these properties. As a palaeo-analogue to present-day anthropogenic climate forcing, the Permian-Triassic transition represents the greatest loss of species diversity associated with carbon-emission driven climate change in the geologic record. Investigating the Permian-Triassic transition and other palaeo-analogues will improve our understanding of anthropogenic climate change and the subsequent responses of ecosystems to these environmental stresses in the future.

context and subject of thesis

This cumulative thesis is structured in two parts: the unifying essay and the appendices. The unifying essay integrates and provides context for the two first-author manuscripts produced as a result of my research into latest Permian variability and extremes. I first provide the context of the latest Permian palaeoclimate and thereby establish the knowledge gaps that I seek to close through my research. Then, I summarise each manuscript presented in the appendices and finally provide overarching conclusions and outlook following my research.

thesis structure

1.1 ANTHROPOGENIC CLIMATE CHANGE

Climate variability is an inescapable fact of nature but as humanity has developed, we have had an increasingly dominant role in the climate system [Messerli et al., 2000; Y. Li et al., 2023]. For the majority of the species' existence, humans had to adapt or migrate in response to natural environmental change and only relatively recently, in the last 1-2 kyr, have humans begun to dominate their environment [Messerli et al., 2000; Y. Li et al., 2023]. Humanity now drives regional and global climate change at unprecedented scales through carbon dioxide (CO_2), nitrous oxide (N_2O) and methane (CH_4) emissions [Arias et al., 2021]. Humans have emitted 695 GtC from 1850 to 2022 at an increasing rate of emission with an increase in atmospheric CO_2

humanity's role in climate

of 2.4 ppm yr^{-1} in the last decade alone [Friedlingstein et al., 2023]. These emissions primarily contribute to climate change by inhibiting the natural radiative energy loss from the Earth's surface through the greenhouse effect. Such greenhouse gases are transparent to incoming shortwave solar radiation but absorb and later re-emit outgoing longwave infrared radiation from the Earth's surface [Fourier, 1824]. The increasing concentration of CO_2 and other GHGs in the Earth's atmosphere leads to warming at the Earth's surface [Eyring et al., 2021].

ocean in the climate system

The ocean also plays an important role in the climate system and mitigates anthropogenic forcing through heat and carbon uptake. The ocean has taken up 91% of the excess heat resulting from the enhanced greenhouse effect in the Earth's atmosphere [Forster et al., 2021] and 26% of total anthropogenic CO_2 emissions [Friedlingstein et al., 2023] since the pre-industrial era. However, the ocean also represents one of the world's largest ecosystems and the physical and chemical changes produced by the heat and carbon uptake of the ocean are also related to three major stressors on marine life, termed the "deadly trio": ocean warming, ocean deoxygenation and ocean acidification [Gruber, 2011; Bijma et al., 2013; Kwiatkowski et al., 2020].

ocean warming

The uptake of excess heat from the enhanced greenhouse effect leads directly to ocean warming but also indirectly to increased stratification within the ocean and sea level rise [Fox-Kemper et al., 2021]. The mean temperature of the ocean's surface has risen by 0.88°C in the last century at an increasing rate with a rise of 0.6°C in the last 40 years alone. A further 0.86-2.89°C warming is expected by the end of the century under the current Shared Socio-economic Pathways (SSP) scenarios. The global mean sea level has also risen by 0.2 m over the period 1901-2018 and at a rate of 3.7 mm yr^{-1} in the last decade. The melting of ice on land due to the changing climate also contributes to both the rising sea levels and the enhanced stratification of the ocean through freshening [Fox-Kemper et al., 2021].

The majority of marine life are ectotherms, meaning that they are dependent upon their ambient environmental temperature and therefore vulnerable to environmental warming. Temperature impacts the survival, metabolism, reproduction and many other biological processes of marine biota. However, the responses of organisms to warming are non-uniform, with some species performing better or worse upon exposure to environmental change [Yao & Somero, 2014; Stuart-Smith et al., 2015]. It is already evident that ocean warming, coupled with inhibited nutrient supply through enhanced stratification is reducing global primary productivity in the oceans [Lewandowska et al., 2014; Yao & Somero, 2014]. It is also clear that many crucial ecosystems, such as seagrass meadows [Nguyen et al., 2021] and coral reefs [Cornwall et al., 2021; Hoegh-Guldberg et al., 2007], are particularly vulnerable to environmental change. Stuart-Smith et al. [2015] indicate that under the SSP5-8.5 scenario, that the majority of tropical and sub-tropical marine ecosystems may exceed their thermal tolerances by the end of the century.

ocean deoxygenation

Marine organisms are also threatened by ocean deoxygenation, which is largely driven by factors also related to ocean warming [Levin, 2018]. The increased ocean temperatures resulting from the enhanced heat uptake concurrently reduces the solubility of oxygen in seawater and increases the rate of respiration of organisms present, which increases biological oxygen demand. The increased stratification of the ocean from warming and freshening also reduces ventilation of the ocean interior, reducing the invasion of atmospheric oxygen into the ocean. The decreased solubility,

increased respiration and decreased ventilation are attributed as the major drivers of ocean deoxygenation [Keeling et al., 2010; Levin, 2018; C. Li et al., 2020] and have led to a reduction in the global oceanic oxygen inventory of approximately 2% since 1960 [Schmidtko et al., 2017; Levin, 2018; Gulev et al., 2021]. Additionally, in oceanic regions associated with high production or restricted ventilation, there are Oxygen Minimum Zones (OMZs) where the prevailing oxygen concentrations are so low that they are hypoxic. Ocean deoxygenation has also led to a horizontal and vertical expansion of these OMZs in the ocean, which further impacts biogeochemical cycling and feedbacks in the climate system such as increased N_2O emissions [Stramma et al., 2008; Keeling et al., 2010; Stramma et al., 2010; Gulev et al., 2021].

All complex life on Earth relies on aerobic respiration, which is dependent upon oxygen and therefore deoxygenation has dramatic impacts on marine life. Oxygen is the electron acceptor in aerobic respiration and simpler forms of life which depend on anaerobic respiration, using alternative, less efficient electron acceptors, become abundant at low oxygen concentrations [Keeling et al., 2010]. Low oxygen concentrations have consistent negative impacts on survival, abundance, development, metabolism, growth and reproduction across a wide range of taxonomic groups, which illustrates the threat presented to many marine ecosystems [Vaquer-Sunyer & Duarte, 2008; Keeling et al., 2010; Sampaio et al., 2021].

ocean acidification

Where ocean warming and ocean deoxygenation are primarily related to heat uptake, ocean acidification is driven by the alteration of the chemical relationship in seawater due to the uptake of carbon. Ocean acidification is often referred to as "the other CO_2 problem" with respect to anthropogenic CO_2 emissions [Doney et al., 2009]. When CO_2 dissolves in water it is present largely as dissolved CO_2 and in very minor concentrations as the weak carbonic acid (H_2CO_3), which dissociates into bicarbonate (HCO_3^-) and carbonate (CO_3^{2-}) ions depending on the acidity of the solution. This dissociation relationship increases how much CO_2 can be dissolved in the ocean with a negative feedback relationship: the more CO_2 that is dissolved in the ocean, the more acidic the ocean becomes as a result of this dissociation relationship and the less additional CO_2 that can be dissolved in future [Zeebe & Wolf-Gladrow, 2003; Doney et al., 2009]. So far, the ocean has absorbed around 26% of anthropogenic CO_2 emissions [Friedlingstein et al., 2023] and globally pH in the open ocean has declined by -0.017 to -0.026 units per decade since the late 1980s [Canadell et al., 2021].

The responses of marine organisms and ecosystems to ocean acidification remain largely unclear with the exception of calcifying organisms, which already experience declines in net calcification [Orr et al., 2005; Doney et al., 2009; Doney et al., 2020]. Calcifiers are directly affected by the change in the dissociation relationship which controls the saturation state of their skeletal structures, increasing dissolution and inhibiting calcification [Orr et al., 2005; Doney et al., 2009; Doney et al., 2020; Cornwall et al., 2021]. Many other organisms are also affected from phytoplankton and zooplankton to fish with studies revealing varying responses depending on intensity and duration of exposure to acidic environments [Cattano et al., 2018; Wang et al., 2018; Doney et al., 2020; Cornwall et al., 2021]. However, the current consensus is that ocean acidification will significantly impact ecosystem function and reduce biodiversity [Godbold & Calosi, 2013; Doney et al., 2020; Agostini et al., 2021].

the deadly trio

With the pace of current environmental change and the pressure of the

"deadly trio" [Gruber, 2011; Bijma et al., 2013], there is increasing risk of a modern great extinction [Penn & Deutsch, 2022]. Given the severity of the threat, relatively few studies have investigated the combined effects of exposure to the "deadly trio" of stressors at organismal or ecosystem levels [Götze et al., 2020; Santos et al., 2021; Sampaio et al., 2021]. However, many studies have investigated the effects of exposure to one or two "deadly trio" stressors and identified additive or even synergistic impacts [Kroeker et al., 2013; Gobler & Baumann, 2016; Steckbauer et al., 2020; Baag & Mandal, 2022; Morée et al., 2023]. Furthermore, it is becoming clear that ocean warming and ocean deoxygenation have the most consistent negative impacts across the broadest range of taxa, with deoxygenation emerging as the most impactful despite being the least well-researched [Götze et al., 2020; Santos et al., 2021; Sampaio et al., 2021]. Tropical ecosystems have also been shown to exhibit limited resilience with regards to singular "deadly trio" stressor exposure. For example in tropical coral reefs, cnidarian hosts can endure periods of low oxygen concentrations due to oxygen production by their zooxanthellae symbionts. However, under warming, the cnidarian hosts may their zooxanthellae in response to toxic by-products, making them less tolerant to oxygen decline when exposed to thermal stress [Altieri et al., 2021].

1.2 A PALAEOCLIMATE ANALOGUE: THE PERMIAN-TRIASSIC TRANSITION

The End-Permian Mass Extinction (EPME) is the most severe extinction event in the Earth's history and the marine extinction is attributed to the "deadly trio" of stressors [Payne & Clapham, 2012; Bijma et al., 2013; Cui & Kump, 2015; Dal Corso et al., 2022]. More that 90% of all species went extinct across the Permian-Triassic transition in response to a dramatic carbon cycle perturbation approximately 252 million years ago, marking the end of the Paleozoic era [Erwin, 1994; S.-Z. Shen et al., 2011; Payne & Clapham, 2012; Song et al., 2013; Cui & Kump, 2015; Dal Corso et al., 2022]. This large perturbation, referred to as a Carbon Isotope Excursion (CIE), resulted in impacts to the marine environment and communities which are analogous to the current and predicted expressions of ocean warming, acidification and deoxygenation in response to anthropogenic climate change [Knoll et al., 2007; Clapham & Payne, 2011; Harnik et al., 2012; Payne & Clapham, 2012; Bijma et al., 2013; Cui & Kump, 2015; Dal Corso et al., 2022].

Siberian Traps volcanism

The global carbon cycle perturbations across the Permian-Triassic transition were driven by volcanic activity at the Siberian Traps [Ganino & Arndt, 2009; Brand et al., 2012; Ogden & Sleep, 2012; Burgess et al., 2017; Cui, Li, et al., 2021]. The Siberian Traps (Fig. 1) are a 6 million km^2 Large Igneous Province associated with flood basalts and intrusive sills [Burgess et al., 2017; Cui, Li, et al., 2021]. The initial effusive volcanic loading is attributed to the leading pulse of emissions which is preserved as a perturbation of the $\delta^{13}C$ isotopic record as early as 300 kyr in advance of the Permian-Triassic boundary and may be linked with terrestrial extinctions and northern high latitude marine environment stress [Dal Corso et al., 2022; Gliwa et al., 2022]. While the later intrusive emplacement of the lateral sill complex and subsequent liberation of greenhouse gases from organic-rich sediments is hypothesised as the trigger for the marine extinction [Song et al., 2013; Burgess et al., 2017; Dal Corso et al., 2022].

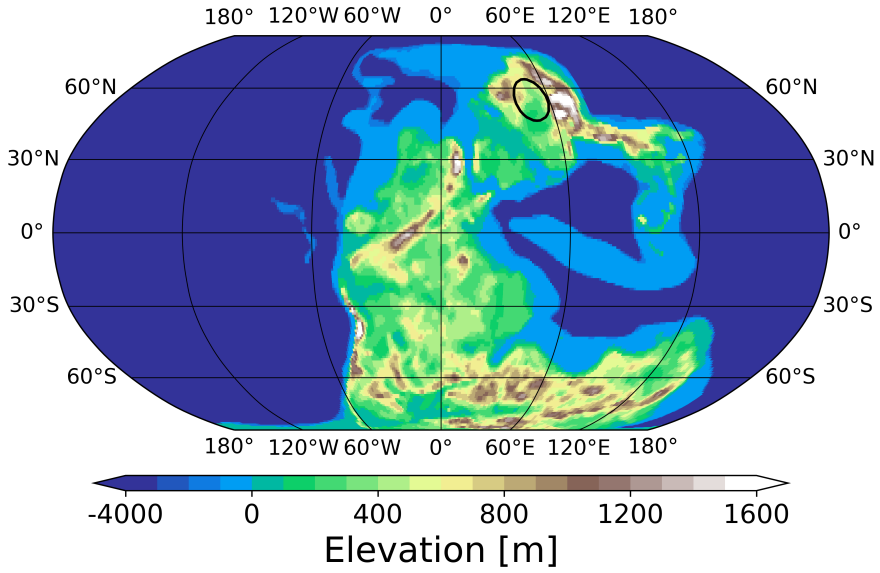

Figure 1: Contour map of elevation for the latest Permian (252 Ma) and approximate location of Siberian Traps indicated by black circle following [Dal Corso et al., 2022]. Topographic data provided by Kocsis and Scotese [2021]. Note the change in scale below 0 m.

carbon cycle perturbation

There remains considerable uncertainty with regards to the source, magnitude and rate of carbon emissions during the End-Permian. Svensen et al. [2009] estimate a potential emission of 27300 GtC through metamorphism of organic material and petroleum during the Siberian Traps formation. However, the uncertainty of the geochemical carbon isotopic record ($\delta^{13}C$) leaves a broad spectrum of potential emission magnitudes and ratios between CO_2 and CH_4. Initial estimates of the atmospheric CO_2 mixing ratio were as high as 8000 ppm with possible increases from 2800 to 4300 ppm, 5400 ppm or 8300 ppm depending on the emission of biogenic CH_4, thermogenic CH_4 or organic matter respectively [Cui et al., 2013; Joachimski et al., 2020]. However, recent studies have constrained the atmospheric CO_2 mixing ratio to a significantly lower 2500 ppm, still with significant uncertainty [H. Li et al., 2019; Y. Wu et al., 2021; Joachimski et al., 2022]. The emission rate still controls the total magnitude of the emissions though, Y. Wu et al. [2021] estimate 3900-12000 GtC through mass balance calculation based on their pCO_2 estimate. Mass balance calculations cannot account for fundamental carbon cycling processes such as continental weathering or burial rates and therefore may significantly underestimate the total injection of carbon into the Earth system. The land and ocean carbon uptake represent significant sinks in the present-day [Friedlingstein et al., 2023] and slower rates of emission could allow these sinks to take up more carbon over the period of the extinction, mitigating the impact. For instance, Jurikova et al. [2020] simulate an injection of 106000 GtC over 1 Myr which did not reproduce the global acidification response of the $\delta^{11}B$ record, however Cui, Li, et al. [2021] simulate an emissions of 36000 GtC in two distinct pulses of 8.3 kyr and 9.1 kyr and compute a better representation of the global acidification signal. It should be noted that the higher emission rate simulated by Cui, Li, et al. [2021] is still less than half the rate of present-day anthropogenic CO_2 emissions [Friedlingstein et al., 2023].

mass extinction stressors

There is abundant evidence in the geologic record that the carbon cycle perturbation is also associated with the "deadly trio" of stressors and these are considered the primary drivers of the EPME [Knoll et al., 2007; Clapham & Payne, 2011; Harnik et al., 2012; Bijma et al., 2013; Dal Corso et al., 2022]. The oxygen isotopic record ($\delta^{18}O$) is used to illustrate the global temperature perturbation, the uranium ($\delta^{238}U$) and sulphur ($\delta^{34}S_{CAS}$) isotopic records are used to infer ocean anoxia and the boron ($\delta^{11}B$) and calcium ($\delta^{44/40}Ca$) isotopic records are used to indicate ocean acidification [Dal Corso et al., 2022]. Perturbations in each of these records are detected concurrently with a dramatic decline in biodiversity in the fossil record [Erwin, 1994; Payne & Clapham, 2012; Cui et al., 2013; Foster & Twitchett, 2014; Dal Corso et al., 2022].

Investigations of the Permian-Triassic transition are reasonably consistent in their conclusions of the intensity and extent of ocean warming and ocean deoxygenation. The geologic material in which sea surface temperature proxies are preserved, most commonly originates from low-palaeolatitude locales, which limits the spatial extent of temperature reconstructions. However, geochemical studies are confident that there was an 8-10°C temperature rise in low-latitude sea surface temperatures across the Permian-Triassic transition [Joachimski et al., 2020; Grossman & Joachimski, 2022]. Ocean deoxygenation is perhaps the best investigated of the "deadly trio" of stressors in the context of the Permian-Triassic transition [Wignall & Twitchett, 1996; Isozaki, 1997; Wignall & Twitchett, 2002; Kaiho et al., 2012; Song et al., 2012; Feng & Algeo, 2014; Lau et al., 2016; Schobben et al., 2020; Cui, Zhang, et al., 2021; Müller et al., 2023]. In addition to the $\delta^{238}U$ and $\delta^{34}S_{CAS}$ isotopic records, the End-Permian Oceanic Anoxic Event (OAE) is also represented by abundant pyritic minerals and organic carbon-rich laminated sediments, indicating an absence of bioturbation and aerobic respiration during sediment deposition [Wignall & Twitchett, 2002; Payne & Clapham, 2012; Dal Corso et al., 2022]. Only the extent of the OAE during the Permian-Triassic transition remains debated, where initial studies suggested a superanoxic event throughout the global oceans [Isozaki, 1997; Wignall & Twitchett, 2002], more recent studies suggest that oceanic anoxia was more regionally limited [Sun et al., 2019] and potentially episodic [Y. Shen et al., 2011].

The role and occurrence of ocean acidification in the Permian-Triassic transition is still under debate. Jurikova et al. [2020] identify an acidification signal in the $\delta^{11}B$ isotopic record of 0.5 in ocean pH concurrent with the onset of the EPME which persisted into the Earliest Triassic. However, Foster et al. [2022] find an absence of morphological deformities and disordered shell ultrastructures in their analysis of the fossil record and therefore reject the occurrence of extensive ocean acidification in the Early Triassic. There is also evidence of Ooidal limestones across the inferred low pH interval suggesting that calcium carbonate undersaturation was not achieved and instead there was a more complex response of the marine carbonate system. Therefore, it is likely that if ocean acidification were present, it was limited to the latest Permian and EPME [Dal Corso et al., 2022; Foster et al., 2022]. Despite the controversial evidence of acidification, there is evidence that there was extinction selectivity for poorly buffered taxa and taxa with calcareous shells [Knoll et al., 2007; Clapham & Payne, 2011; Clarkson et al., 2015; Dal Corso et al., 2022].

1.3 STATE OF THE ART: PALAEOCLIMATE MODELLING

There has been considerable research in recent decades towards reconstructing the events across the Permian-Triassic transition from the exceedingly sparse geological record and models are a crucial tool in these efforts [Cui & Kump, 2015; Haywood et al., 2019; Dal Corso et al., 2022]. The sparse proxy record can be used to identify static and regional states within the Earth system, such as temperature, but are limited to which conclusions can be inferred with regards to the dynamics of the system or the processes and mechanisms of its evolution through time. For instance, Y. Wu et al. [2021] estimate the atmospheric CO_2 mixing ratio from the $\delta^{13}C$ isotopic record and use a mass balance calculation to infer the mass of carbon released into the ocean-atmosphere system. However, such mass balance calculations neglect fundamental processes and mechanisms of biogeochemical cycling, which can be better elucidated through the wealth of models now available. Furthermore, palaeoclimate studies present an opportunity to test and refine models using out-of-sample conditions, which will undoubtedly improve model skill in future projections [Haywood et al., 2019; Burls & Sagoo, 2022; J. Zhu et al., 2022].

evolution of model complexity

Over time, models have become more advanced, growing in sophistication with more complex models being applied towards reconstructing the EPME over time. Early modelling studies of the Permian-Triassic transition applied Energy Balance and conceptual models which were able to simulate broad climate indicators but could not reproduce high-latitude warming [Cui & Kump, 2015]. Geochemical box models were the next step in complexity and are able to produce improved estimates over mass balance calculations. Geochemical box models are still commonly used for palaeoclimate research due to fast integration times and good first-order representations of the climate system and biogeochemical cycles [R. Zhang et al., 2001; Berner, 2002; Grard et al., 2005; Rampino & Caldeira, 2005; Schobben et al., 2015; Stordal et al., 2017; Jurikova et al., 2020].

General Circulation Models (GCMs) with simple representations of ocean biogeochemistry represent a leap forward in complexity of models used for palaeoclimate reconstructions. There have also been studies with GCMs without ocean biogeochemistry [R. Smith et al., 2004; Kiehl & Shields, 2005; A. Winguth & Maier-Reimer, 2005] and while these represent a step forward in complexity, they cannot contribute significantly to reconstructing the ocean biogeochemical cycles of the Permian-Triassic transition and will not be discussed further. Hotinski et al. [2001] presented the first study of the Permian-Triassic transition using an ocean GCM with a simple representation of ocean biogeochemistry. They illustrated the spatial distribution of dissolved oxygen in response to surface wind, temperature and salinity forcing simulated by the GENESIS version 2 model with 2760 ppm CO_2 forcing. Some latter studies have applied the cGENIE model, an Earth System Model of Intermediate Complexity (EMIC), to Permian-Triassic reconstructions [Meyer et al., 2008; Cui et al., 2013; Cui, Zhang, et al., 2021; Hülse et al., 2021] and have provided considerable contributions towards constraining the magnitude, rate and type of carbon emissions and the evolution of ocean acidification and deoxygenation across the extinction interval. However, the representation of ocean biogeochemical cycling in cGENIE is limited, Maier-Reimer [1993] describes such implementations as "conceptually not a model of biology in the ocean but rather a model of biogenically induced chemical

fluxes (from the surface ocean)" [Ridgwell et al., 2007]. Kiehl and Shields [2005] were the first to apply a fully coupled Atmosphere-Ocean General Circulation Model (AOGCM) to the Permian-Triassic transition but their implementation lacked a representation of ocean biogeochemistry. Therefore, the study of C. Winguth and Winguth [2012] was the first study to investigate the Permian-Triassic transition using an AOGCM with a representation of ocean biogeochemistry because they applied the Community Climate System Model version 3 (CCSM3) with an additional carbon cycle model. This version of CCSM3 with carbon cycling has been applied to studies of the evolution of the climate system and ocean deoxygenation [C. Winguth & Winguth, 2012; A. Winguth et al., 2015] as well as the drivers and dynamics of monsoon variability during the Permian-Triassic transition [A. Winguth & Winguth, 2013; Shields & Kiehl, 2018].

Now, even fully-coupled Earth System Models (ESMs) are being applied to the problem of the EPME in order to better understand the extinction drivers and the implications for our future under anthropogenic climate forcing. ESMs represent the next step in the evolution of AOGCMs in that they consider additional components of the Earth system beyond the physical. The current generation of ESMs typically have complex representations of ocean biogeochemical processes which represent not only "biogenically induced chemical fluxes" [Maier-Reimer, 1993] but also various biological functional groups such as phytoplankton and zooplankton [Six & Maier-Reimer, 1996; Moore et al., 2001], diazotrophic Nitrogen cycling [Paulsen et al., 2017] and particle sinking schemes [Maerz et al., 2020]. The Community Earth System Model version 1 (CESM1) is the first of the current generation of ESMs to tackle the topic of the Permian-Triassic transition and has already enhanced our understanding of the biogeographic extinction selectivity in the EPME and wider climate implications of carbon and non-carbon emissions during the formation of the Siberian Traps [Black et al., 2018; Penn et al., 2018].

changing boundary conditions

Over time, more geologic evidence has become available to constrain the boundary conditions of the Permian-Triassic transition, particularly surface temperatures and atmospheric CO_2 mixing ratios [Payne & Clapham, 2012; Cui & Kump, 2015; Dal Corso et al., 2022]. Early climate modelling studies were conducted at a time where there were large pCO_2 uncertainties for both the background latest Permian and Permian-triassic transition atmospheres, with an estimate range from 300-7000 ppm [Cui & Kump, 2015]. Within this pCO_2 uncertainty range, models aimed to reproduce a temperature rise of approximately 6°C [Holser et al., 1991]. Many studies therefore applied high pCO_2 forcings to both the background latest Permian climate (1120-2800 ppm) [Cui et al., 2013; A. Winguth et al., 2015; Cui, Zhang, et al., 2021] and in their forced simulations for the Permian-Triassic transition (3550-8300 ppm) [Kiehl & Shields, 2005; A. Winguth & Maier-Reimer, 2005; Cui et al., 2013; A. Winguth & Winguth, 2013; A. Winguth et al., 2015].

The analyses by Joachimski et al. [2012] suggest a larger low-latitude temperature change of 8-10°C occurred at the Permian-Triassic transition. Model studies were able to reproduce this temperature rise by increasing atmospheric CO_2 mixing ratios from relatively low levels to relatively high levels within the pCO_2 estimates of the time. Penn et al. [2018] simulate a temperature change from the latest Permian to Early Triassic of approximately 10°C by increasing the atmospheric CO_2 forcing from 150 ppm to 5580 ppm. Similarly, Shields and Kiehl [2018] reproduce the estimated temperature change by increasing atmospheric CO_2 mixing ratios from 355 ppm

to 3550 ppm. However, the pCO_2 estimates of H. Li et al. [2019] suggest that the background atmospheric CO_2 mixing ratio of 355 ppm implemented in Shields and Kiehl [2018] is relatively low but within their reconstruction estimate, while the background mixing ratio of 150 ppm described by Penn et al. [2018] is significantly lower than the range of their stomatal ratio pCO_2 reconstruction [H. Li et al., 2019].

As the atmospheric CO_2 mixing ratio has become better constrained, it has revealed that many CO_2 forcings implemented in modelling studies may have been overestimated [H. Li et al., 2019; Y. Wu et al., 2021; Joachimski et al., 2022]. Recent modelling studies have attempted to reproduce the various isotopic excursions from the geologic record for the Permian-Triassic transition while following improvements in boundary condition constraints. Black et al. [2018] illustrate a global mean surface temperature rise of around 5°C by increasing their CO_2 forcing from 710 ppm to 2800 ppm and then further to 5600 ppm to produce a global mean surface temperature change of over 8°C. The background forcing of 710 ppm is higher than the proxy estimate by H. Li et al. [2019] for the latest Permian, while 2800 ppm agrees well with and 5600 ppm remains within the uncertainty range of the proxy estimate for the Permian-Triassic transition [Y. Wu et al., 2021]. However, Black et al. [2018] describe the change in global mean surface temperature and compare with estimates of low-latitude SST change [Joachimski et al., 2012; Joachimski et al., 2020], parameters which are not directly comparable. Therefore, the representativeness of the CESM1 forcing response remains unclear. Hülse et al. [2021] uses a similarly high pCO_2 forcing for the latest Permian of 700 ppm and produce a 7.4°C warming in the mean SST across the Tethys Ocean by increasing the atmospheric CO_2 mixing ratio to 5600 ppm. Taken together, these cGENIE and CESM1 simulations may suggest that the models underestimate the equilibrium climate sensitivity of the Permian-Triassic transition or that further understanding of the boundary conditions revealed by the proxy record are required. Furthermore, this could imply that less carbon emissions are required to force the climate system than simulated by Cui, Li, et al. [2021] to achieve a temperature change that agrees with low-latitude proxy temperature estimates. A higher equilibrium climate sensitivity and lower emission magnitude could permit better agreement between models and proxy estimates of carbon emissions [Svensen et al., 2009; Y. Wu et al., 2021] and low-latitude temperature change[Joachimski et al., 2012; Joachimski et al., 2020].

1.4 BRIDGING TIMESCALES

disparity of abrupt timescales

In spite of the wealth of prior research, there remains considerable disparity between the timescales which are investigated in the geological record of the EPME and the ecological timescales at which organisms and ecosystems are recognised to respond. The geologic record indicates that the Permian-Triassic CIE occurred over a period of 450-500 kyr [Song et al., 2013; Burgess et al., 2014] with the extinction taking place over an estimated 64±48 kyr interval [Burgess et al., 2014], which represents a geologically abrupt event. Even such an abrupt geological event is orders of magnitude longer than the annual to decadal timescales linked with abrupt ecosystem change [Bestelmeyer et al., 2011; Di Lorenzo & Ohman, 2012]. Furthermore, A. Winguth and Winguth [2013] and Black et al. [2018] conclude from their studies that the extinction

is likely related to periodic or rapid environmental shifts, rather than the slow climatic forcings simulated in their models.

rapid environmental shifts

Marine Heatwaves (MHWs) are an example of such periodic or rapid environmental shifts in ocean temperature and have been observed to have significant negative impacts on marine ecosystems [Harris et al., 2018; Smale et al., 2019; Jacox et al., 2020; K. Smith et al., 2023]. MHWs refer to discrete periods of unusually high seawater temperatures and are typically highly regional events [K. Smith et al., 2023]. In addition to extensive observations of negative ecosystem impacts, model projections illustrate the increased severity of impacts to critical ecosystem groups such as corals from exposure to natural variability and extreme events [Kleypas et al., 2015; McManus et al., 2019; Klein et al., 2022]. Furthermore, observations and models suggest that under anthropogenic climate forcing, extreme events such as MHWs are intensifying and becoming more frequent and that this trend will continue into the future [Frölicher et al., 2018].

latest Permian extremes

Given the significance of marine extreme events in the present and the severity of the extinction across the Permian-Triassic transition, it is essential to have a better understanding of the patterns of variability and extremes of marine stressors. Due to the limits of temporal resolution and uncertainty in the geologic record, it is rare for rapid environmental shifts to be recorded or detected. However, Y. Shen et al. [2011] detect evidence of potential episodic anoxic events in the Meishan section, South China. Such isotopic evidence could support the hypothesis of A. Winguth and Winguth [2013] that "the associated extinction of species are related rather to periodic anoxia in near surface-to-intermediate depth than to widespread anoxic events in the Panthalassic deep-sea". However, no studies have so far investigated environmental shifts of the latest Permian at the most relevant timescales at which ecosystems respond.

1.5 RESEARCH QUESTIONS

In the previous sections, I describe the vast body of evidence which has been collected through studies of the Permian-Triassic transition but also the dearth of research into environmental change at ecologically-relevant timescales. I hypothesise that the End-Permian Mass Extinction developed through more regional extinctions which occurred both more rapidly and earlier during the Permian-Triassic transition than previously described. I define the following research questions in order to explore my hypothesis through this dissertation.

I establish that previous studies of the Permian-Triassic transition focus on analyses of the isotopic record or long-term external climate forcing, which can be detected in the isotopic record. There have been no previous studies of the most rapid scales of environmental change in the latest Permian. Therefore, the first research question I address is:

RQ1: What was the dominant mode of internal climate variability at interannual timescales in the latest Permian?

Earth System Models provide a novel tool to investigate interannual timescales of environmental change that cannot be explored through the temporal resolution available in the isotopic record. Characterising the dominant mode

of internal climate variability illustrates the capacity of the latest Permian climate system to generate ecologically threatening extreme events.

Previous investigations of the End-Permian Mass Extinction focus on identifying the trigger mechanisms but are unable to constrain the timing of extirpations. Burgess et al. [2014] define an extinction interval of 60±48 ka using a high-precision timeline of the End-Permian Mass Extinction, which does not adequately explain the mechanism of extinction. Later modelling studies characterised the extinction through two distinct pulses of carbon emissions, each less than 10 ka in duration [Song et al., 2012; Cui, Li, et al., 2021]. All of these works have aimed at constraining the extinction interval but are still described on geological timescales. The second research question I address is:

RQ2: What was the spatial pattern of the deadly trio of marine stressors in the latest Permian?

Geochemical evidence from the low latitude Tethys and Panthalassa Oceans indicates 8-10°C warming across the Permian-Triassic transition [Joachimski et al., 2020] but modern marine heatwaves of 1-2°C have been observed to have dramatic negative impacts on tropical ecosystems [Thomson et al., 2015; Harris et al., 2018; McManus et al., 2019; Holbrook et al., 2021]. Therefore, we expect the extinctions to occur more rapidly and earlier in the extinction interval than required for the peak climate warming to occur.

2

PAPER I: CHARACTERISING INTERANNUAL TROPICAL VARIABILITY AND MARINE HEATWAVES IN THE LATEST PERMIAN

motivation

Internal climate variability represents the naturally occurring variations in climate resulting from interactions between different components of the Earth system. These variations typically dominate at daily to multi-decadal timescales [Hyun et al., 2022], which are also the timescales at which ecosystems respond to environmental change. Previous modelling studies of the Permian-Triassic transition overlook these most relevant timescales of environmental change.

research questions

Therefore, the first part of my thesis (Appendix A) works towards bridging geological and ecological timescales by exploring internal climate variability and its implications to the evolution of the End-Permian Mass Extinction. I pose the following research questions to guide my investigation into the first overarching research question of this thesis:

1A: What was the dominant mode of internal climate variability?

1B: What was the pattern of marine heatwaves?

Additionally, I aim to verify my hypothesis that the End-Permian Mass Extinction proceeded more rapidly and earlier in response to PTB climate perturbations than previously described.

methods

I use the coarse-resolution of the Max-Planck Institute Earth System model version which contributed to the 6th-phase of the Coupled Model Intercomparison Project [Mauritsen et al., 2019]. I develop a novel configuration to represent the latest Permian using the latest topographic data [Kocsis & Scotese, 2021] but deepen the ocean by 21% to achieve an ocean volume consistent with present-day ocean without ice sheets.

I apply solar radiation and orbital boundary conditions following previous modelling studies [Kiehl & Shields, 2005] but use the most recent constraints on atmospheric CO_2 mixing ratios at 500 ppm [H. Li et al., 2019; Joachimski et al., 2022]. I also define a reduced range of Plant Functional Types in the land surface model JSBACH to better represent the latest Permian [Bercovici et al., 2015; Nowak et al., 2020] and initialised the ocean with a higher mean salinity following Hay et al. [2006].

I characterise the dominant mode of internal climate variability through statistical analyses. I use covariance Empirical Orthogonal Function analysis to identify the pattern of variability. Then I perform power spectrum analyses on the associated principal component time series of the identified mode to determine the periodicity of the signal.

I characterise marine heatwaves using fixed percentile thresholds to account for local SST variability [Frölicher et al., 2018; Hu et al., 2021; Le Grix et al., 2022]. I select the 95th-percentile due to the length of the time series examined and the necessity of using monthly mean data.

key results

For the first time, I successfully reproduce temperatures in an Earth System Model consistent with temperature proxies while using the current best estimate of atmospheric pCO_2. Previous modelling studies required

significantly higher atmospheric CO_2 mixing ratios in order to reproduce PTB temperature proxies [Kiehl & Shields, 2005; A. Winguth & Maier-Reimer, 2005; A. Winguth & Winguth, 2013]. I relate this to the Equilibrium Climate Sensitivity (ECS) of 4.7°K per doubling CO_2 of the latest Permian configuration of the MPI-ESM. This ECS is higher than the MPI-ESM configurations of the present and also higher than other modelling studies of the Permian-Triassic transition. I suggest this represents an ECS state-dependency as studies have previously shown for the Eocene [J. Zhu et al., 2019; Anagnostou et al., 2020].

I illustrate the tropical climate of the latest Permian with a prevailing warm pool feature in the SSTs and Walker-type Circulation in the atmosphere. The warm pool is associated with convergent surface winds and strong convection over the Cathaysian peninsula. The region is also characterised by large cloud cover fractions and precipitation rates. The tropical ocean is characterised by strong westward surface currents in the Panthalassic Ocean and shallow mixed-layer depths.

I reveal the dominant mode of internal climate variability to be a pattern of tropical sea surface temperature variability. This variability mode represents 16.2% of variability with a positive core in the western equatorial Panthalassic Ocean. I determine a periodicity of 2-4 years in the principal component time series of the dominant mode. Using linear regression of anomalies, I demonstrate that this mode is likely explained by an atmosphere-ocean feedback where warming in the western equatorial Panthalassic drives divergent wind anomalies over the Cathaysian peninsula resulting in thermocline shoaling in the western Panthalassic and deepening in the eastern Panthalassic.

I characterise the pattern of tropical marine heatwaves with high intensities in the East Panthalassic Ocean. The central Panthalassic is revealed to experience the longest median marine heatwave durations with a maximum of 3.0 months. The Eastern Panthalassic is exposed to the greatest median intensities with a maximum of 2.6°C and the highest mean frequencies are found in the western Panthalassic with a maximum of 0.48 year^{-1}. These statistics represent the medians and means and it should be noted that longer durations, greater intensities and larger frequencies occur.

conclusions

I reveal a dominant mode of interannual tropical variability in the latest Permian with a periodicity of 2-4 years. I link this leading mode of variability with an atmosphere-ocean feedback. I conclude that this variability mode will have similar impacts on latest Permian ecosystems as the El Niño Southern Oscillation has on ecosystems in the present [Kleypas et al., 2015; Holbrook et al., 2021].

I characterise the pattern of tropical marine heatwaves which have maximum median intensities much lower than expected warming across the Permian-Triassic transition. Ecosystem thermal tolerances are determined by environmental variability [Stuart-Smith et al., 2015; Sunday et al., 2019] and the extreme events we simulate are expected to have negative ecosystem impacts. Therefore, we conclude that ecosystems would be extinguished before the peak warming of 8-10∘C occurs. This supports my hypothesis that the End-Permian Mass Extinction was more rapid and occurred earlier than previously described.

3

PAPER II: THE DEADLY TRIO OF MARINE STRESSORS VARIED REGIONALLY IN THE LATEST PERMIAN

motivation

Ocean warming, acidification and deoxygenation, the deadly trio of marine stressors, are negatively impacting marine ecosystems in the present [Gruber, 2011; Bijma et al., 2013; Stuart-Smith et al., 2015; Doney et al., 2020; Sampaio et al., 2021]. Evidence of the deadly trio has been identified in geologic record of the End-Permian Mass Extinction [Harnik et al., 2012; Bijma et al., 2013; Dal Corso et al., 2022]. Previous modelling studies have neglected the combined influence of the deadly trio and the implications for the pattern and pacing of the End-Permian Mass Extinction.

research questions

Therefore, the second part of my thesis (Appendix B) investigates the pattern of extremes across the latest Permian shelves, which likely represent the most vulnerable ecosystems to environmental change. I formulate the following guiding research questions to target my response to the second overarching research question of my thesis:

2A: What was the spatial pattern of temperature, oxygen and pH extreme events?

2B: How does this pattern relate to the extratropical latitudinal extinction selectivity of the End-Permian Mass Extinction?

Again, I seek to test my hypothesis that the pace of extinction during the PTB was more rapid and occurred earlier with respect to environmental change than previously described.

methods

As with my first study, I use the coarse-resolution of the Max-Planck Institute Earth System model version which contributed to CMIP6 [Mauritsen et al., 2019] but now with HAMOCC6. I continue to use the novel configuration I developed to represent the latest Permian with the same boundary conditions described in Section 2.

I modify HAMOCC6 to better represent the latest Permian by removing shell-producing phytoplankton and implementing shell-producing zooplankton. I initialise the ocean using homogeneous nutrient concentrations assuming a present-day nutrient inventory. I prescribe homogeneous surface weathering fluxes due to a lack of weathering flux proxy data.

I characterise extreme events using fixed percentile thresholds to account for local variability of temperature, oxygen and pH at the depth of the continental shelves [Frölicher et al., 2018; Hu et al., 2021; Le Grix et al., 2022]. As with my investigation of marine heatwaves, I select the 95^{th}-percentile.

key results

For the first time, I describe temperature, oxygen and pH extreme events relevant to latest Permian shelf ecosystems. I find strong latitudinal gradients of temperature and oxygen, while the maximum pH levels are found in the mid-latitudes in the climatological mean-state. I find no clear pattern in the durations and frequencies of temperature and pH extreme events and reveal that hypoxic extreme events are limited to the tropical shelf regions.

I clearly show regional variations in extremes across 5 major shelf regions. The tropical Tethys shelf regions have the highest exposure to hypoxic extreme events and also high maximum intensity pH extremes but only

moderate temperature extremes. In contrast, the East Panthalassic shelf region experiences high maximum intensities of temperature, pH and also hypoxic extreme events, and therefore the full stress of the deadly trio. The southern high latitudes experience the greatest maximum intensities of marine heatwaves but only moderate pH extremes, while the northern high latitudes experiences moderate intensities of both temperature and pH extremes.

I show that the distribution of dissolved oxygen and pH are linked to global ocean circulation patterns and biological carbon cycling. Oxygen Minimum Zones (OMZs) are found in the East Tethys and East Panthalassic Oceans. These OMZs develop to depths where rate of oxygen consumption by aerobic remineralisation is balanced by replenishment by ocean ventilation. The restricted exchange and complex ventilation of the Tethys Ocean leads to the formation of an OMZ despite the much lower rates of biological carbon cycling compared to the East Panthalassic. Ventilation of deep water enriched with dissolved inorganic carbon and reductions in total alkalinity through aerobic remineralisation are used to explain the distribution of pH.

conclusions

I find a spatially varying pattern of temperature, oxygen and pH extreme events where only the East Panthalassic Ocean experiences the combined stress of the deadly trio. Ecosystem tolerances are determined by environmental variability and extinctions will be driven by changes in the pattern of extremes [Stuart-Smith et al., 2015; Sunday et al., 2019]. I suggest different regions have different tolerances to the deadly trio of marine stressors but the change in magnitudes and pattern of extremes will determine the extinction triggers. Contrary to previous studies, I find it unlikely that the high latitude shelf regions will experience wide-spread hypoxic conditions.

I support the hypothesis of previous studies that ocean acidification drove the extratropical extinction selectivity preserved in the fossil record [Knoll et al., 2007; Clapham & Payne, 2011; Clarkson et al., 2015; Reddin et al., 2019; Dal Corso et al., 2022]. Either the high latitudes experienced mass extinction at different stages driven by different killing mechanisms or they experienced a similar rate of stress. The southern high latitudes are exposed to considerably greater maximum intensities of marine heatwaves than the northern high latitudes, while they both experience similar intensities of pH extremes. Furthermore, high latitude amplification should result in higher rates of acidification at high latitudes.

4

CONCLUSIONS & OUTLOOK

4.1 SUMMARY AND CONCLUSIONS

summary

In this thesis, I explore the internal climate variability and the spatial pattern of marine stressors of the latest Permian at ecologically-relevant scales to better understand the evolution of the End-Permian Mass Extinction. My primary focus is in representing rapid environmental change at interannual timescales that have not been addressed by previous research. Investigations of rapid environmental change of the Permian-Triassic transition are not possible using the isotopic record, due to limitations of temporal resolution and uncertainty, and can only be conducted through the application of Earth System Models. My research supports the hypothesis that the End-Permian Mass Extinction occurs more rapidly and earlier in the Permian-Triassic transition than previously discussed.

addressing research questions

The main results of this thesis are divided into two parts, represented by the appended manuscripts, which I summarise in Sections 2 and 3. Here, I summarise my conclusions in the frame of my research questions:

RQ1: What was the dominant mode of internal climate variability at interannual timescales in the latest Permian?

For the first time, I successfully reproduce the range of tropical SSTs using an Earth System Model with the recently improved constraints on atmospheric CO_2 mixing ratios of the latest Permian period. The Max Planck Institute Earth System Model simulates a higher Equilibrium Climate Sensitivity in the latest Permian configuration of 4.7°K per doubling of CO_2 than other Earth System Models applied to investigations of the Permian-Triassic transition. This configuration reproduces Sea Surface Temperatures in the tropical Tethys Ocean that compare well with estimates derived from the sparse $\delta^{18}O$ isotopic record. Previous modelling studies required higher atmospheric CO_2 mixing ratios than predicted by the geochemical record to achieve similar agreement with temperature estimates.

I reveal a 2-4 year periodicity of the atmosphere-ocean feedback system as the dominant mode of interannual tropical variability of the latest Permian. Empirical Orthogonal Function analysis of tropical Sea Surface Temperature anomalies exposes a pattern of variability dominated by a positive mode in the equatorial West Panthalassic Ocean. Power Spectrum analysis of the Principal Component time series associated with the leading mode of variability identifies a 2-4 year frequency peak. I conclude that this mode of variability is linked to the atmosphere-ocean feedback with diverging zonal wind anomalies over the Cathaysian peninsula leading to strong shoaling of the thermocline and surface warming in the equatorial West Panthalassic and weak deepening of the thermocline in the equatorial East Panthalassic.

I characterise latest Permian tropical Marine Heatwaves, their duration, intensity and frequency, and how they contribute to perspectives on the pacing of the End-Permian Mass Extinction. The tropical Tethys Ocean is estimated to warm by 8-10°C through the Permian-Triassic transition.

The maximum intensity of simulated tropical Marine Heatwaves of 5.8°C indicates that it is unlikely that organisms and ecosystem could tolerate such environmental conditions. Therefore it is likely that tropical marine ecosystems were exposed to lethal environmental temperatures much earlier than peak climate change was achieved across the Permian-Triassic transition.

RQ2: What was the spatial pattern of the deadly trio of marine stressors in the latest Permian?

I identify a spatially-varying pattern of temperature, dissolved oxygen and pH extreme events across the major shelf regions in the latest Permian. Southern extratropical latitude shelf regions experience intense marine heatwaves of up to 10.2°C, while tropical shelf regions are exposed to widespread hypoxic and acidification extreme events. The model simulation also indicates that it is unlikely that extratropical high latitude shallow shelf environments will be exposed to persistent hypoxic conditions.

The spatial-pattern of marine stressors across the latest Permian shelf environments has profound implications for the evolution of the End-Permian Mass Extinction. It is well-established that extreme events will become more intense, more frequent and longer lasting in response to carbon emissions over time. However, this also indicates that it will take longer for mean state conditions to exceed environmental tolerance thresholds of organisms and ecosystems in different regions. Despite this, low oxygen conditions are considered non-selective and lethal to even well-adapted aerobic organisms over long enough durations. Therefore, I propose that the primary threat to tropical Tethys shelf ecosystems is deoxygenation. I suggest that decreasing pH will present more stress than temperature at southern high latitudes and temperature and pH may be equally stressful at northern high latitudes. Only the East Panthalassic shelf is exposed to all three of the deadly trio of marine stressors. Furthermore, the simulated extremes indicate that organisms and ecosystems are unlikely to tolerate the magnitude of environmental change over the Permian-Triassic boundary. Therefore, I conclude that large-scale extinctions will occur as environmental conditions exceed extreme tolerance thresholds and on much shorter timescales than those required for peak environmental.

4.2 OUTLOOK

My research opens further avenues for future research to explore the evolution of extreme events into the Permian-Triassic transition, the latest Permian climate with refined boundary conditions and to test model-developed hypotheses against targeted sampling of the geologic record. Transient Earth system simulations of the Permian-Triassic boundary using CO_2 forcing scenarios would allow investigations of the evolution of the identified extreme events and their implications for the End-Permian Mass Extinction. Therefore testing my hypothesis that the extinction was more rapid and occurred earlier than previously described.

Further model development and investigations of the geologic record could also improve the fidelity of future model simulations. Developing novel model features such as representations of calcareous corals and siliceous sponges or forcing the Earth system models with better constrained sources and rates of weathering fluxes to the ocean would improve representations of

the marine carbonate system and composition of deposited marine sediments. However, more information is required from the geologic record to determine the sources and rates of weathering fluxes to permit such advances. There is also potential for targeted investigations of the geologic record to compare with model-developed hypothesis regarding the spatial pattern and extent of warming and hypoxia across the Permian-Triassic transition.

Part II

APPENDICES

A

CHARACTERISING INTERANNUAL TROPICAL VARIABILITY AND MARINE HEATWAVES IN THE LATEST PERMIAN

The attached manuscript is in preparation for submission to the journal *Climate of the Past*.

Burt, D.J., Putrasahan, D., Günther, M. & Ilyina, T. (in preparation). Characterising interannual tropical variability and marine heatwaves in the latest Permian [*to be submitted to Climate of the Past*].

AUTHOR CONTRIBUTIONS: D.J.B. designed the research question, performed analysis, created the figures and drafted the manuscript. D.P. and M.G. supported analysis and provided scientific guidance. D.P., M.G. and T.I. provided feedback. All authors contributed to editing and revising the manuscript.

Characterising interannual tropical variability and marine heatwaves in the latest Permian

Daniel Jonathan Burt[1,2], Dian Putrasahan[1], Moritz Günther[1,2] and Tatiana Ilyina[3,4,1]

[1] Max Planck Institute for Meteorology, Max Planck Society, Hamburg, Germany
[2] International Max Planck Research School for Earth System Modelling, Max Planck Society, Hamburg, Germany
[3] Universität Hamburg, Hamburg, Germany
[4] Helmholtz-Zentrum Hereon, Geesthacht, Germany

ABSTRACT

It is well established that over 90% of marine species became extinct during the End Permian Mass Extinction in response to massive climate change driven by volcanic carbon emissions. Previous modelling studies of the Permian-Triassic Boundary focus on the long term external climate forcing of these carbon emissions but have been unable to explain the pattern and magnitude of extinctions. To date, no studies have investigated rapid environmental changes in the latest Permian at which ecosystems typically respond, which may be explained by interannual climate variability. For the first time, we use the Max-Planck Institute Earth System Model to simulate the latest Permian and successfully reproduce sea surface temperatures that agree well with the available proxy record using a pCO_2 of 500 ppmV in the range of the latest pCO_2 proxy estimates. We identify the leading mode of tropical SST variability, which explains 16.2% of variability, and determine a periodicity of 2-4 years using power density spectrum analysis. The identified dominant mode of tropical SST variability is an ocean-atmosphere feedback system related to Walker-type Circulation variability and convergence strength over the Cathaysian peninsula. We find a spatially varying pattern of SST extreme events with highest median intensities of 2.6°C in the northeastern tropical Panthalassic and highest mean frequencies of 0.48 $year^{-1}$ in the western Panthalassic Ocean. We expect the dominant mode of interannual tropical variability to have a similar impact on ecosystems in the latest Permian, as the El Niño Southern Oscillation has in the present. The changes in thermocline depth linked to the atmosphere-ocean feedback system we identify, agrees with descriptions of episodic anoxia at the Cathaysian peninsula from previous studies of the Meishan section. We suggest that the strong SST variability of the latest Permian, may have interacted synergistically with long-term climate forcing to provide the abrupt climate change required to explain the severity of the End Permian Mass Extinction.

A.1 INTRODUCTION

The latest Permian is the background climate to the Permian-Triassic Boundary (PTB) mass extinction event (~252 Ma), which coincided with climate perturbations somewhat analogous to anthropogenic climate change in the

twenty-first century [Payne & Clapham, 2012]. Over 90% of marine and 70% of terrestrial species became extinct across the PTB [Song et al., 2013] in a geologically abrupt event linked with Siberian Trap volcanic activity [Burgess et al., 2017; Cui, Li, et al., 2021]. However, a disparity remains between the millennial to sub-millennial "abrupt timescales" of the geologic record [Kemp & Sexton, 2014] and the annual to decadal timescales at which ecosystems respond to climate change [Bestelmeyer et al., 2011; Di Lorenzo & Ohman, 2012]. Previous modelling studies have highlighted the need to investigate climate variability at these annual to decadal timescales in the context of the PTB [A. Winguth & Winguth, 2013; Black et al., 2018]. Here, we investigate the dominant mode of interannual climate variability in the latest Permian and its relationship with climate-relevant stressors which impact marine life.

Increased environmental stress and the subsequent End-Permian Mass Extinction (EPME) resulted from the PTB climate perturbations, which were driven by greenhouse gas emissions [Burgess et al., 2017; Black et al., 2018; Cui, Li, et al., 2021; Y. Wu et al., 2021]. The geologic record illustrates a 450-500 kyr period of carbon cycle disturbance, which is attributed to carbon dioxide and methane emissions related to Siberian Trap volcanism [Song et al., 2013; Burgess et al., 2014]. Uncertainty remains regarding the composition [Black et al., 2018; Jurikova et al., 2020; Cui, Li, et al., 2021], rate [Jurikova et al., 2020; Cui, Li, et al., 2021] and magnitude [Cui, Li, et al., 2021; Y. Wu et al., 2021; Joachimski et al., 2022] of these greenhouse gas emissions. However, it is clear from isotopic evidence that tropical sea surface temperatures (SSTs) rose by 8-10°C [Joachimski et al., 2012; Joachimski et al., 2020] concurrent with increased marine hypoxia [Kaiho et al., 2012; Feng & Algeo, 2014; Cui, Zhang, et al., 2021] and ocean acidification [Payne et al., 2010; Clarkson et al., 2015; Jurikova et al., 2020; Cui, Zhang, et al., 2021]. This enhanced environmental stress provided the killing mechanism during the 64±48 kyr extinction interval [Burgess et al., 2014] and delayed biotic recovery into the early Triassic [Song et al., 2012; Lau et al., 2016].

Despite the duration of this extinction interval, ecosystems respond to environmental stress much more quickly [Bestelmeyer et al., 2011; Di Lorenzo & Ohman, 2012]. Extinctions occur when the rate of environmental change exceeds the rate of organisms' ability to adapt [Bürger & Lynch, 1995; Hoffmann & Sgrò, 2011]. There is even evidence that organisms can adapt to the much faster rates of anthropogenic climate change [Gonzalez et al., 2013; Klausmeier et al., 2020]. Given the evidence of external climate forcing by carbon emissions on scales of tens of thousands of years [Jurikova et al., 2020; Cui, Li, et al., 2021], then it is more likely that ecosystems passed critical thresholds and transitioned from one state to another [Bestelmeyer et al., 2011] as a result of periodic extreme events [Y. Shen et al., 2011; Kaiho et al., 2012].

Modelling studies of the PTB also find long-term external climate forcing insufficient to account for the rapid environmental change required for widespread extinction [A. Winguth & Winguth, 2013; Black et al., 2018]. Fully-coupled Earth system modelling is required to investigate Permian-Triassic climate perturbations within the constraints of the geological, palaeontological and geochemical data [Kiehl & Shields, 2005; Montenegro et al., 2011; Cui et al., 2013]. Earth System Models (ESMs) present the opportunity to resolve the spatiotemporal scales at which episodic environmental change would occur [Y. Shen et al., 2011; Kaiho et al., 2012]. To date, no modelling studies

have been conducted to quantify the background internal climate variability of the latest Permian or the implications of such variability on the EPME.

We apply the Max-Planck Institute Earth System Model (MPI-ESM) to simulate the latest Permian climate within the constraints of available geological and geochemical proxy data. First, we present the mean tropical climate simulated by the MPI-ESM and then we identify the dominant mode of interannual climate variability. Finally, we illustrate the relationship between this dominant mode of interannual climate variability and the simulated thermal stress which could act on ecosystems present.

A.2 METHODS

A.2.1 *Model Description*

The latest Permian climate is simulated with a modified version of the Max-Planck Institute Earth System Model (MPI-ESM) version 1.2 used in the 6th-phase of the Coupled Model Intercomparison Project [Mauritsen et al., 2019]. The MPI-ESM couples the atmospheric general circulation model ECHAM6.3 and the land surface scheme JSBACH3.2 to the ocean general circulation model MPIOM1.6 through the OASIS3 Model Coupling Toolkit version 2.0 [Mauritsen et al., 2019]. We perform simulations with a coarse-resolution MPI-ESM configuration, which runs with a T31 spectral truncation (nominal resolution 3.75°) and with 31 vertical hybrid (sigma-pressure coordinate) levels up to 10 hPa in ECHAM6.3 [Mauritsen et al., 2019], but implement a novel curvilinear grid based on the standard coarse-resolution MPIOM grid with nominal resolution of 3.0° but with shifted poles. Our new grid configuration shifts the poles to 57°N 55°E and 75°S 100°E. In addition to the novel grid, other model features are configured to represent the latest Permian (Section A.2.2).

A.2.2 *Latest Permian Configuration*

The position of continents changes through geologic time and we use the continental configuration of Kocsis and Scotese [2021] in our simulation (Fig. 1). The MPI-ESM has previously been configured for palaeo-settings including the last glacial maximum [Riddick et al., 2018; Kleinen et al., 2020; Kapsch et al., 2021; Extier et al., 2022; Kapsch et al., 2022] and the Paleocene-Eocene thermal maximum [M. Heinze & Ilyina, 2015a, 2015b; Ilyina & Heinze, 2019]. However, each palaeo-setting requires a different continental configuration and we use the continental configuration for 250 Ma described by Kocsis and Scotese [2021] which assumes a flat-bottom ocean but we increase the depth of all ocean grid cells by 21% to achieve an ocean volume comparable with the present-day oceans without ice-sheets.

The Earth also experienced a distinct radiative forcing conditions as a result of different atmospheric composition, orbital parameters and solar irradiance during the latest Permian (Table 1). We use the atmospheric CO_2 mixing ratio of 500 ppmV following H. Li et al. [2019] and Joachimski et al. [2022] but use the pre-industrial atmospheric mixing ratios of methane (CH_4) and nitrous oxide (N_2O) as the other key greenhouse gases considered in the MPI-ESM. We implement a reduced solar insolation following Kiehl and Shields [2005] to reflect the reduced solar irradiance. While H. Wu et al. [2012] constrain the orbital parameters through the late Permian, and

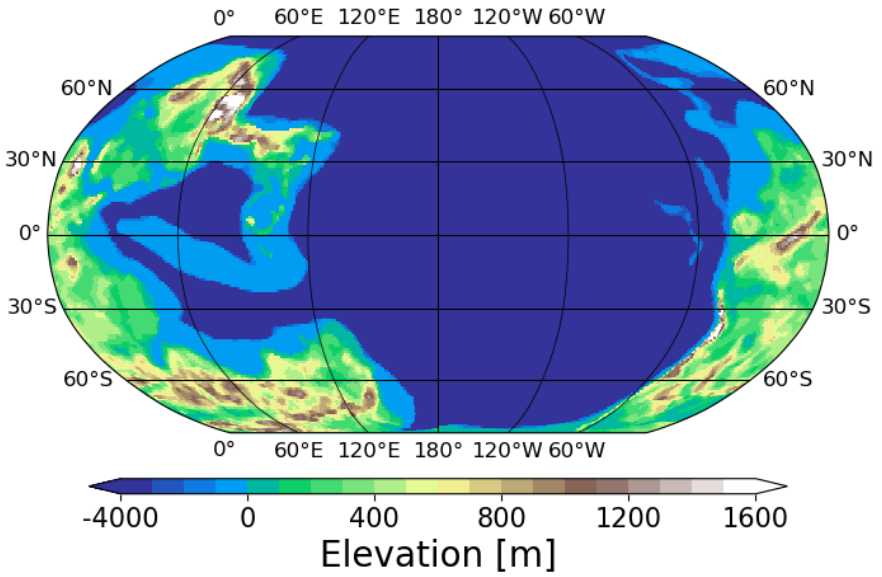

Figure 1: Contour map of elevation for the latest Permian (252 Ma). Data provided by Kocsis and Scotese [2021]. Note the change in scale below 0 m.

these parameters may significantly influence climate on long timescales [A. Winguth & Winguth, 2013], our goal is to simulate a quasi-equilibrium at significantly shorter timescales than Milankovitch Cycles. Therefore, we fix eccentricity and obliquity at the MPI-ESM pre-industrial settings which compare well with those used by Kiehl and Shields [2005].

Table 1: Boundary conditions for the latest Permian simulation.

	CO_2 [ppmV]	CH_4 [ppbV]	N_2O [ppbV]	S_0 [W m^{-2}]	Eccentricity	Obliquity [°]
Value	500.0	808.2	273.0	1338	0.01676	23.46

This configuration of the MPI-ESM is further modified from the version described by Mauritsen et al. [2019] to represent conditions in the latest Permian. Terrestrial flora was significantly different from the present-day and dominated by *Gigantopteris* flora, Cordaitales and pteridosperms [Bercovici et al., 2015; Nowak et al., 2020]. We alter the Plant Functional Type (PFT) library of JSBACH to reflect a reduced 7 PFTs, which include: 4 PFTs to represent extra-/tropical evergreen and deciduous single hard-stemmed plants; 2 PFTs to represent raingreen and deciduous hard multi-stemmed plants; and 1 PFT to represent single soft-stemmed plants. Following Hay et al. [2006], we increase the global mean ocean salinity from 35 to 40 in the MPIOM initial condition. This model version has undergone additional tuning of the ECHAM6 cloud parameters since the version described by Mauritsen et al. [2019]: the relative humidity threshold for cloud formation in the lowest model level is increased from 0.95 to 0.98, which decreases cloud cover, especially low clouds; and the threshold determining the separation between cloud liquid water and cloud ice is increased from 7×10^{-7} to 9×10^{-6}, which increases cloud liquid water.

A.2.3 *Analysis Methods*

To identify the dominant mode of interannual climate variability we perform covariance Empirical Orthogonal Function (EOF) and power density spectrum analyses on the deseasonalised, detrended tropical SST anomalies (Fig. 7). We divide the Principal Component (PC) time series associated with the leading mode of variability into 80 segments of 50 years and perform power density spectrum analysis on the segments.

The ocean-atmosphere feedbacks illustrated in Fig. 8 are computed by linear regression and correlation. We deseasonalise and detrend all of the time series used for computing the atmosphere-ocean feedbacks. We linearly regress the mean of the SST anomalies within the region from 150°E to 170°W and 5°S to 5°N against the zonal wind stress anomalies. Similarly, we linearly regress the mean of the zonal wind stress anomalies within the region from 125°E to 170°E and 6°S to 8°N against the 20°C isotherm depth anomalies. Finally, we correlate of the SST anomalies with 20°C isotherm depth anomalies.

We identify extreme SST events using a fixed percentile threshold to account for local SST variability in the selection [Frölicher et al., 2018; Hu et al., 2021; Le Grix et al., 2022] (Fig. 9). The 90^{th} percentile is a frequently used identification threshold for SST extreme events [Hu et al., 2021; Le Grix et al., 2022] but due to the long time series examined, we examine monthly mean SST data and use the 95^{th} percentile threshold. We report the median event intensities and event durations to represent their right-skewed distributions and the mean of event frequencies to illustrate the event characteristics [Oliver et al., 2020].

A.3 RESULTS AND DISCUSSION

A.3.1 *Tropical Climate of the latest Permian*

The latest Permian configuration of the MPI-ESM simulates climatological mean SSTs between -9.5°C to 30.0°C (Fig. 2A). There is a strong latitudinal temperature gradient with the coldest temperatures present in the southern high latitudes and warmest temperatures in the equatorial West Panthalassic. The tropical Tethys and West Panthalassic Oceans are dominated by a warm pool of SSTs more than 28°C from 30°E to 135°W. In the East Panthalassic there are tongues of cooler water along the west coast of Pangaea, diverging from the coastline around 20°N and 20°S respectively. The SSTs of the equatorial Tethys compare well with available temperature proxies from the $\delta^{18}O$ isotopic record [Grossman & Joachimski, 2022]. The temperature proxies indicate a range of mean SSTs across the equatorial Tethys Ocean of 26.0°C to 32.8°C. The simulated SSTs in the western Tethys Ocean are -1.8°C and -4.2°C colder than the proxy means at the same locations and the model mean SSTs also deviate from the proxy mean SSTs for the eastern Tethys around 10°N by 1.3°C, -3.2°C and 2.9°C from east-to-west respectively.

Comparing the model monthly mean SSTs against available proxy SST estimates for the latest Permian [Grossman & Joachimski, 2022] shows better agreement than when considering only the climatological means (Fig. 2B). In the western Tethys Ocean, there is insufficient proxy data for statistical comparison, however it should be noted that approximately 71% of available proxy SSTs lie within the range of simulated SSTs at the same location, with an potential positive outlier in the proxy record of 37.0°C at 1.85°S 40.13°E.

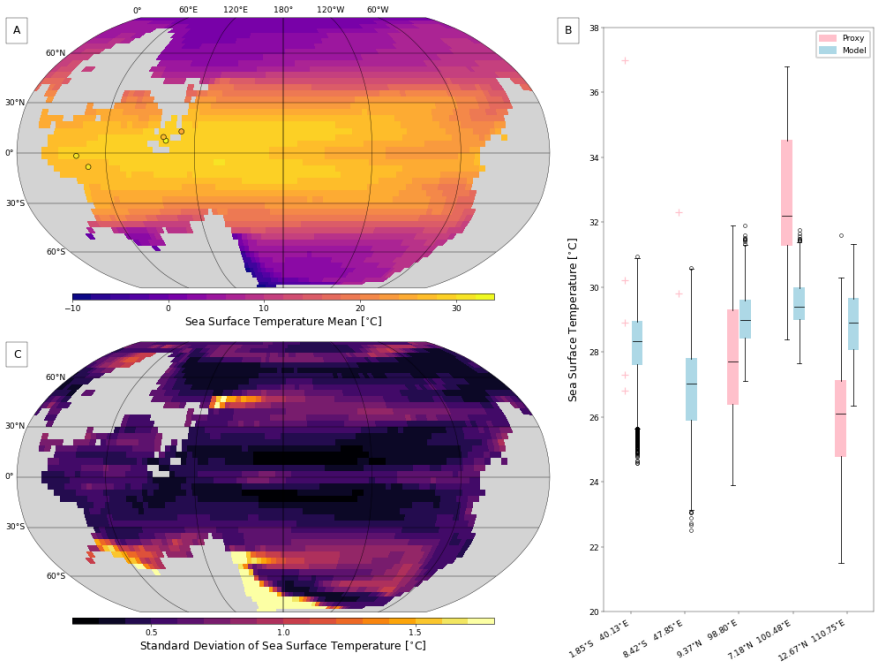

Figure 2: Contour maps of (A) the simulated climatological mean sea surface temperature [°C] with circles representing the proxy means and (C) the standard deviation of deseasonalised, detrended sea surface temperature anomalies [°C] of the model. (B) Box-whisker plot of sea surface temperatures [°C] from (pink) available proxy data and (blue) model monthly means at comparable palaeolatitudes and palaeolongitudes; individual data points are marked with coloured crosses at locations where 5 or fewer proxy temperatures were available ($n \leq 5$).

Excluding this estimate, allows a mean proxy SST of 28.3°C which is more comparable to the model climatological mean (28.2°C) at the same location. In the Tethys-Panthalassic boundary region, the model SST range is more consistent than the proxy SST estimate across the three sites. We find no statistically significant difference between the model and proxy SST distributions at 9.37°N 98.80°E. However, we do find statistically significant differences between the model and proxy distributions at the other two sites, such that the model mean is significantly lower at 7.18°N 100.48°E and significantly higher at 12.67°N 110.75°E than the available proxy SST estimates.

Given the reasonable agreement between the model monthly mean SST and proxy estimate [Grossman & Joachimski, 2022] distributions at specific locations (Fig. 2)B), we examine the pattern of SST variability simulated by the model and find spatially heterogeneous variability (Fig. 2C). Regions of low variability extend from approximately 150°E to 120°W at around 10°N and 10°S with a minimum at 13° 139°W. The greatest standard deviation of the tropics, 0.91°C, is located at 20°N on the eastern boundary of the Panthalassic Ocean, with relatively large standard deviations (0.7-0.9) in the equatorial East and West Panthalassic and north tropical Tethys Oceans. The greatest standard deviations globally are located in the southern high latitudes from around 46°S to the South Pole, following the South Panthalassic continental

shelf region. Large standard deviations also occur in the South Tethys Ocean and around 45°SN in the West Panthalassic.

We evaluate our simulation against available sparse proxy temperatures and it is important to consider this evaluation in the context of both the model and proxy estimate limitations. The primary challenge for model evaluation is the absence of proxy SST estimates for the Panthalassic Ocean, which is unavoidable due to the 64.2 Myr present-day mean age of ocean crust material [Seton et al., 2020]. The uncertainties in the age-models of the SST proxies, ranging from millions to tens of millions of years [Burgess et al., 2014; Baresel et al., 2017], and the existence of multiple tectonic models for palaeo-location transformations [Cao et al., 2017; Kocsis & Scotese, 2021] further confounds the issue. It is crucial to consider the spatiotemporal uncertainties when considering the background climate-state of the latest Permian, given that evidence suggests the decrease in the $\delta^{13}C$ record and climate warming began as early as 300 kyr before the End Permian Mass Extinction [Joachimski et al., 2020; Y. Wu et al., 2021; Gliwa et al., 2022]. These uncertainties may go towards explaining the large temperature differences in the proxy estimates in the East Tethys, which represent the South China sections (Fig. 2B). Though Chen et al. [2016] propose the warmer temperatures estimated for the Liangfengya and Daijiagou sections may be the result of differences in depositional environment or potentially thermal alteration but no other physical process or mechanism are discussed in literature to explain the SST differences.

It should also be noted that the model is limited by resolution and boundary condition assumptions. This configuration of the MPI-ESM requires a coarse-resolution to produce long period simulations for analysis. We use fixed pre-industrial orbital parameters in this configuration, which has a significant impact on the climate system as illustrated in CCSM3 by A. Winguth and Winguth [2013]. We implement the latest topographical data [Kocsis & Scotese, 2021] in this configuration which as yet lacks details of deep ocean bathymetry. Therefore, we assume a flat-bottom ocean, though this was found by Osen et al. [2013] to have a negligible impact on circulation and the distribution of water masses globally at coarse-resolutions. Furthermore, we increase the initial ocean salinity to 40 following Hay et al. [2006] while other studies such as Kiehl and Shields [2005] implement an initial ocean salinity of 35.

Previous earth and climate system models have been applied to simulate the latest Permian, however, unlike previous studies, we achieve a good agreement with both current best estimates for atmospheric CO_2 mixing ratios [H. Li et al., 2019; Joachimski et al., 2022] and Tethys Ocean SST proxies [Grossman & Joachimski, 2022]. Early studies of the latest Permian performed with climate system models required atmospheric CO_2 mixing ratios in the range of 2760-3550 ppmV to achieve agreement with temperature proxies at the time [Hotinski et al., 2001; Kiehl & Shields, 2005; A. Winguth & Maier-Reimer, 2005; A. Winguth & Winguth, 2013]. As estimates of pCO_2 became better constrained [H. Li et al., 2019; Joachimski et al., 2022] it became apparent that the mixing ratios implemented in previous studies were not appropriate. More recent studies with earth system models approximate these newer pCO_2 estimates but underestimate the Tethys Ocean SSTs [Black et al., 2018; Cui, Li, et al., 2021; Hülse et al., 2021]. It is unclear why the MPI-ESM is able to achieve this agreement where other studies were not and is possibly due to model configuration or boundary condition differences.

Black et al. [2018] describe an equilibrium climate sensitivity (ECS) of CESM1 of 3.2°K per doubling of CO_2 while we note an ECS of 4.7°K per doubling of CO_2 in our simulation. This ECS deviates significantly from the 3.0°K per doubling of CO_2 of the MPI-ESM configurations which contributed to CMIP6 [Meehl et al., 2020] but may be possible as a result of ECS state-dependency of greenhouse climates as studies have shown for the Eocene [J. Zhu et al., 2019; Anagnostou et al., 2020].

We demonstrate that our global simulations with MPI-ESM reproduce temperatures in agreement with the range of available proxy SSTs (Fig. 2B) but now we focus on the tropical climate of the latest Permian. We have greatest confidence in the tropical SSTs in the model due to the availability of tropical SST proxies [Grossman & Joachimski, 2022]. In the present, tropical variability plays a dominant role in global climate variability on interannual timescales [De Viron et al., 2013]. Furthermore, the largest biodiversity of the present is located in the tropics and has the greatest potential for biodiversity loss [García Molinos et al., 2016; Ramírez et al., 2017]. We now proceed by describing the tropical climate system with a focus on components which are related to SSTs. Deser et al. [2010] state that SSTs are governed primarily by surface winds, air temperatures, cloudiness, heat transport by ocean currents, vertical transport and mixing in the ocean and the ocean mixed-layer depth. Given that we analyse monthly mean data, we propose that the differences between surface air temperatures and SSTs are negligible and therefore exclude these from further analysis.

The tropical surface winds simulated by the model are dominated by a prevailing westward and equatorward direction (Fig. 3A). The 10 m wind

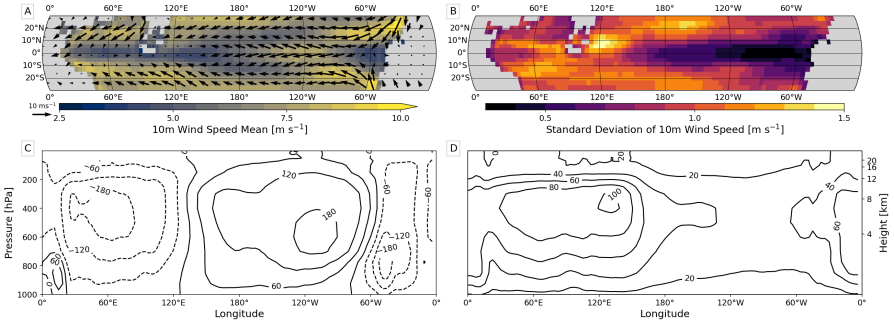

Figure 3: Contour maps of (A) 10 m wind speed climatological mean [m s^{-1}] overlain with quiver plot of 1000 hPa velocity vector climatological means and (B) standard deviation of deseasonalised, detrended monthly mean 10 m wind speed anomalies [m s^{-1}] and contour plots of the 5°S-5°N meridional mean of the zonal divergent wind [$\times 10^9$ kg s^{-1}] (C) climatological mean and (D) standard deviation of deseasonalised, detrended monthly mean anomalies.

speed mean exhibits a maxima at around 20°N over the eastern boundary of the Panthalassic Ocean, associated with north-easterly winds at 1000 hPa and are matched by a similarly strong south-easterly winds at around 25°S. The 10 m wind speed mean minimum is located at approximately 90°E at the equator with a region of low magnitudes extending from the western boundary of the Tethys Ocean along the equator to around 180° and an additional minimum located at approximately 60°W over the equatorial Panthalassic. The direction of 1000 hPa velocity vectors associated with

each of these minima regions which indicate regions of convergence and divergence respectively.

These convergent and divergent winds are also reflected in the meridional mean mass streamfunction of the zonal component of the divergent wind and force the surface components of a Walker-type Circulation (Fig. 3C). This Walker Circulation is composed of a clockwise rotation, represented by the positive cell in the streamfunction, which extends from the convergence region at 125°E to the divergence region at 80°W with a maximum of 200×10^9 kg s^{-1} at 600 hPa at 110°W. A prevailing anti-clockwise rotation, represented by the negative cell in the streamfunction, over the Tethys Ocean from 20°E to 125°E with a minimum at 500 hPa at approximately 65°E forms a second dominant cell in the circulation system.

The region of convergence indicated in Fig. 3A, C is also associated with high variability in the simulated 10 m wind speed with low variability in the eastern Panthalassic Ocean (Fig. 3B). Standard deviations of 10 m wind speed are lowest in the equatorial Panthalassic Ocean, decreasing across the central Panthalassic from approximately 180° to the eastern boundary with minima (0.35 ms^{-1}) at 100°W and 45°W. Higher standard deviations are found in the central Panthalassic Ocean north of 20°N and south of 20°S with the greatest variabilities present in the equatorial Tethys-Panthalassic boundary region with a maxima of 1.5 ms^{-1} at 10°N 120°E.

The standard deviation of the meridional mass streamfunction (Fig. 3D) also exhibits higher variability above the convergence region with low standard deviations associated with the prevailing positive cell of the mean-state (Fig. 3C). The lowest variability is located above the central and eastern equatorial Panthalassic Ocean from 170°E to 35°W. There are larger standard deviations over the equatorial Tethys and western equatorial Panthalassic oceans with the greatest standard deviation of 103×10^9 kg s^{-1} at 400 hPa at approximately 130°E.

The convergence region noted in Fig. 3A, C is also associated with a region of large mean total cloud cover fraction (Fig. 4A). The distribution of mean

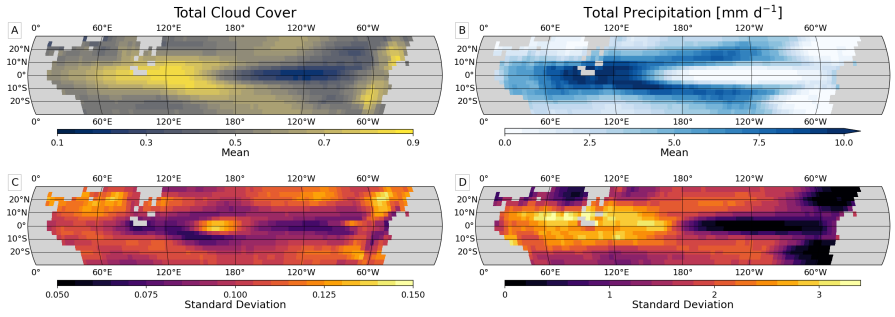

Figure 4: Contour maps of total cloud cover fraction (A) climatological mean and (C) standard deviation of deseasonalised, detrended monthly mean anomalies and total precipitation [mm day^{-1}] (B) climatological mean and (C) standard deviation of deseasonalised, detrended monthly mean anomalies.

total cloud cover is dominated by equatorial cloud cover over the western and eastern boundary regions of the Panthalassic Ocean with the least cloud cover over the central and eastern equatorial Panthalassic Ocean. The maximum of mean total cloud cover fraction (0.86) is located at the equator around 125°E with total cloud cover fractions exceeding 0.75 found from 70°E to 170°E

and also at 10°N 40°W and 10-20°N around 60°W. The lowest mean total cloud cover fractions are found over the equatorial Panthalassic Ocean from around 175°W to 80°W reaching 0.20 at the minimum.

Both the regions associated with highest and lowest mean total cloud cover are also associated with regions of low cloud cover variability (Fig. 4C). The western and central equatorial Panthalassic Ocean exhibits the lowest variability with a minimum of 0.07 at 10°S 150°E and another region of low variability at the eastern boundary. However, there is region of relatively high standard deviation of total cloud cover above 0.12 between 150-180°E over the equatorial Panthalassic Ocean. The largest standard deviation of total cloud cover (0.14) is located near the eastern boundary of the Panthalassic Ocean around 20°N 50°W as part of a meridional band roughly following the shape of the eastern boundary. Variability is also higher above 20°N in the central and eastern Panthalassic Ocean and above 10°N in the Tethys Ocean.

Total cloud cover does not indicate the types of cloud present, however, evidence for the approximate co-location of prevailing intense precipitation (>8.0 mm day^{-1}) (Fig. 4B) with high total cloud cover from 75°E to 170°E further supports the indications of deep convection (Fig. 3A, C). The most intense total precipitation rates are present in the western equatorial Panthalassic Ocean from 75°E to 170°E with regions of low precipitation rates dominating the central and eastern equatorial Panthalassic and eastern boundary. The intense total precipitation in the western equatorial Panthalassic Ocean typically leads to the formation of a freshwater 'lens', like those identified in present-day warm pools. The maximum mean precipitation rate of 11.1 mm day^{-1} is located at 105°E in the equatorial Panthalassic Ocean with regions of moderate precipitation rates extending across the equatorial Tethys and the central Panthalassic Ocean at 10-20°N and 10-20°S. The northern Tethys Ocean and eastern Panthalassic Ocean are dominated by regions of precipitation rates below 2.5 mm day^{-1} with a minimum of 0.06 mm day^{-1} at 125°W in the equatorial Panthalassic. The low precipitation rates over the eastern Panthalassic suggest that the high total cloud cover in the eastern Panthalassic (Fig. 4A) results from subsidence associated with the downward limb of the clockwise Walker Cell (Fig. 3C).

The standard deviation of total precipitation also exhibits a strong longitudinal pattern with high variability in the west and low variability in the east (Fig. 4D). The smallest standard deviations are located in the central and eastern equatorial Panthalassic with a minimum of 0.06 mm day^{-1} at 125°W and north of 10°N and south of 10°S at the eastern boundary. The northeastern Tethys ocean also features relatively low variability to a minimum of 0.34 mm day^{-1}. The greatest variability is in the western Panthalassic Ocean and across the Tethys Ocean from 10°S to 10°N with a maximum of 3.48 mm day^{-1} at approximately 5°N 65°E.

SSTs are present at the interface between the atmosphere and ocean and subject to the dynamics of both. Therefore, we must also consider the dynamics in the surface ocean, horizontal and vertical currents and the thickness of the mixed-layer depth [Deser et al., 2010].

The mean barotropic mass streamfunction and surface current velocities of the ocean model illustrate well-defined gyre structures and a prevailing strong equatorial current across the Panthalassic Ocean (Fig. 5A). The maximum and minimum transport rates of the mean barotropic mass streamfunction are associated with the equator-ward limbs of the wind-driven

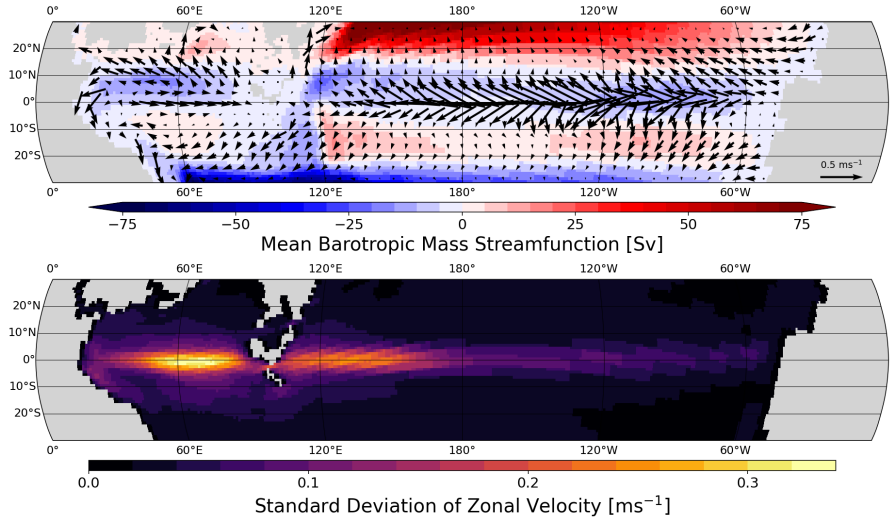

Figure 5: Contour maps of (A) climatological mean barotropic mass streamfunction [Sv] with quiver plot overlay of climatological mean surface (0-15 m) horizontal velocity vectors [ms^{-1}] and (B) the standard deviation of deseasonalised, detrended monthly mean zonal velocity anomalies [ms^{-1}].

subtropical gyres, such that the positive maximum (113.9 Sv) is located at approximately 30°N 140°E and the negative minimum (-71.7 Sv) is located at approximately 30°S 60°E. These surface gyres are also clearly illustrated by the horizontal surface current vectors, with the strongest currents present in the prevailing westward currents across the equatorial Panthalassic Ocean and western intensification also producing relatively strong surface currents at the western boundaries. The mean barotropic mass streamfunction indicates a clockwise rotation around 10-20°S from 120°E to 60°W and an anti-clockwise rotation from approximately 10°S to 15°N also from 120°E to 60°W. This suggests a dominant eastward current at the equator in contrast to the westward surface currents illustrated by the vectors and in fact reflects the strong equatorial undercurrent across the Panthalassic Ocean. Both the surface currents and the mean barotropic mass streamfunction indicate an anti-clockwise rotation in the north equatorial and clockwise rotation in the northern Tethys Ocean. A southward current follows the western boundary of the Tethys Ocean from around 15°N and joining the north equatorial sub-gyre and the western boundary of the southern subtropical gyre.

The greatest variability of the zonal surface current velocities is located around the equator (Fig. 5B). The standard deviation of zonal current velocity generally increases east-to-west in the equatorial Panthalassic Ocean with a maximum of around 0.25 ms^{-1} at around 130°E. Conversely, variability in the Tethys Ocean generally increases west-to-east with a maximum of 0.34 ms^{-1} at 65°E.

The fingerprint of horizontal circulation is apparent in near-surface (15 m) vertical velocities with downwelling associated with the subtropical gyres and coastal upwelling at the eastern boundary of the Panthalassic Ocean associated with offshore currents (Fig. 6A). The maximum vertical velocity of 13.9 μms^{-1} occurs in the western equatorial Tethys Ocean, with velocities exceeding 10 μms^{-1} also occurring from 170-100°W in the equatorial Pan-

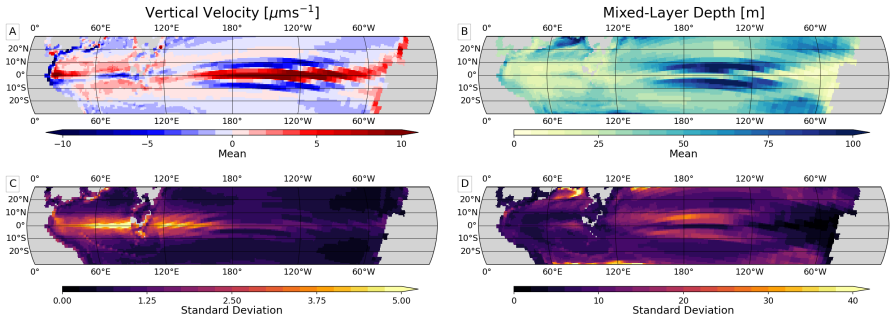

Figure 6: Contour maps of near-surface (15 m) vertical velocity [ms^{-1}] (A) climatological mean and (C) standard deviation of deseasonalised, detrended monthly mean anomalies and mixed-layer depth [m] (B) climatological mean and (D) standard deviation of deseasonalised, detrended monthly mean anomalies.

thalassic Ocean, likely related to the co-located equatorial currents (Fig. 5A). There are also relatively large vertical velocities along the eastern boundary of the Panthalassic associated with the regions of prevailing westward, offshore surface currents (Fig. 5A). Weak positive vertical velocities largely dominate from 15°S-15°N in the Tethys Ocean, which can be explained by Ekman pumping of the anti-clockwise gyre (Fig. 5A). Similarly, the weak negative vertical velocities in the northern Tethys can be related to the prevailing clockwise sub-gyre system (Fig. 5A). The largest negative vertical velocities are located along the western boundary of the Tethys Ocean from around 20°N to 10°S, associated with the relatively strong southward western boundary current (Fig. 5A). There are also relatively large negative vertical velocities above and below the equator in the central Panthalassic Ocean from 180° to 110°W, which can be related to the poleward-components of water transport immediately north and south of the westward equatorial current (Fig. 5A) responsible for the equatorial upwelling.

Variability in the near-surface vertical velocities is dominated by large standard deviations in the eastern equatorial Tethys Ocean and western equatorial Panthalassic Ocean (Fig. 6C). The largest standard deviation of near-surface vertical velocity (6.9 μms^{-1}) is in the eastern equatorial Tethys Ocean at approximately 90°E. Variability in vertical velocity exceeds 4.0 μms^{-1} across the equatorial Tethys from 50-90°E and approximately 115-150°E in the Panthalassic Ocean. The smallest vertical velocity standard deviations are present in the eastern Panthalassic Ocean north of 10°N and south of 10°S. The pattern of variability in near-surface vertical velocities is similar to the pattern of zonal current variability illustrated in Fig. 5B.

The latest Permian simulation exhibits a strongly-stratified surface tropical ocean with a mean mixed-layer depth of 40.8 m (Fig. 6B). The maximum mixed-layer depth of 147.4 m occurs in the northern Tethys Ocean at approximately 29°N 80°E within the sub-gyre identified in the northern Tethys Ocean (Fig. 5A). Deeper mixed-layer depths also occur north and south of the equator in the central Panthalassic Ocean associated with the poleward-component of the strong westward surface equatorial current (Fig. 5A). The regions of deeper mixed layers in the Tethys and Panthalassic Oceans are also related to downwelling in the vertical velocity fields (Fig. 6A). The mixed-layer depths are shallowest in the Panthalassic Ocean with mixed-layer depths less than 25 m across an approximate triangular region extending

from 120°W at the equator to the eastern boundary from 30°S to 15°N with a minimum of 7.8 m at 12°S 50°W. Shallow mixed-layer depths are also found across the equatorial Tethys Ocean. The shallow mixed-layer depths across the Tethys and Panthalassic Oceans are generally associated with positive vertical velocities (Fig. 6A) representing upwelling regions.

The simulated tropical mixed-layer depths display limited variability with a mean of 9.7 m (Fig. 6D) and more variability linked to regions of deeper mixing. The eastern equatorial Panthalassic Ocean shows the least variability, with a minimum of 0.1 m and much of the region with mean mixed-layer depths less than 25 m also have standard deviations of less than 4 m. Similarly, the mixed-layer depth standard deviation is less than 10 m across the majority of the Tethys Ocean and also from 15-25°N and 10-30°S in the Panthalassic Ocean. There are regions with mixed-layer depth standard deviations of 15-25 m in the western and central Panthalassic north and south of the equator from 10°S to 10°N but the greatest mixed-layer depth variability occurs in the northern Tethys Ocean and from 130-160°E north of 25°N and 60-150°E below 27°S.

A.3.2 *Latest Permian SST Variability*

The dominant EOF mode of tropical SST in the latest Permian illustrates a pattern of variability centred around the western equatorial Panthalassic Ocean (Fig. 7A). The 1st EOF mode represents 16.2% of the variability in

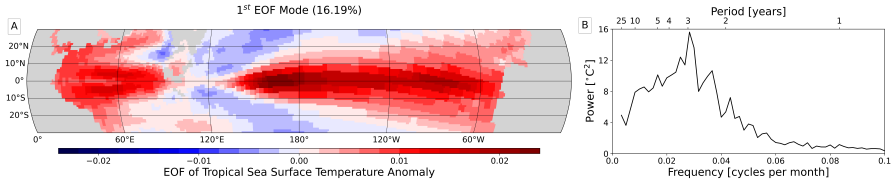

Figure 7: (A) Contour map of the 1st mode of the Empirical Orthogonal Function of deseasonalised, detrended monthly mean Sea Surface Temperature anomalies for the tropics and (B) power spectrum of the associated Principal Component time series.

the signal, with the 2nd mode representing 5.5% of signal variability and following modes representing diminishing fractions of the variability. There are two apparent positive regions, located across the Tethys Ocean and in a triangular-shape across the Panthalassic Ocean with a negative region forming diagonals from around 120°E near the equator to approximately 160°E at 30°S and 30°N. The maximum of 0.024 is located in the equatorial Panthalassic at 165°E and continuing to around 70°W with a second, lower maxima of 0.020 at around 100°W. The lowest value of -0.007 is located in the north-east Tethys Ocean at 16°N 90°E. The positive cores of the 1st EOF are co-located with the regions of high SST variability between 10°S and 10°N (Fig. 2C).

The PC time series associated with the leading EOF mode of tropical SST (Fig. 7A) in the latest Permian exhibits a periodicity of approximately 2-4 years (Fig. 7B). The associated power spectrum is characterised as a red-noise signal, which is typical of long-term climate variability [Vasseur & Yodzis, 2004; Fraedrich et al., 2009]. A peak power density of 15.6°C^2 is detected at approximately 3 years with power densities exceeding a corresponding "red noise" (1/f) signal across the periods from 2-4 years.

It is well established in the present-day climate system that tropical SST variability is strongly related to the coupling between the ocean and the atmosphere [Deser et al., 2010]. Therefore, we explore the ocean-atmosphere feedback system related to the leading EOF mode of tropical SST in these simulations of the latest Permian. Regressing the mean SST anomaly of the region of highest variability indicated in Fig. 7 against zonal wind stress anomalies, reveals the impact of SST on zonal wind in the tropics. Fig. 8A illustrates a strong positive relationship in the western equatorial Panthalassic Ocean at around 145°E, which forms the westerly component in a pattern of divergent zonal wind anomalies. This indicates that a warming

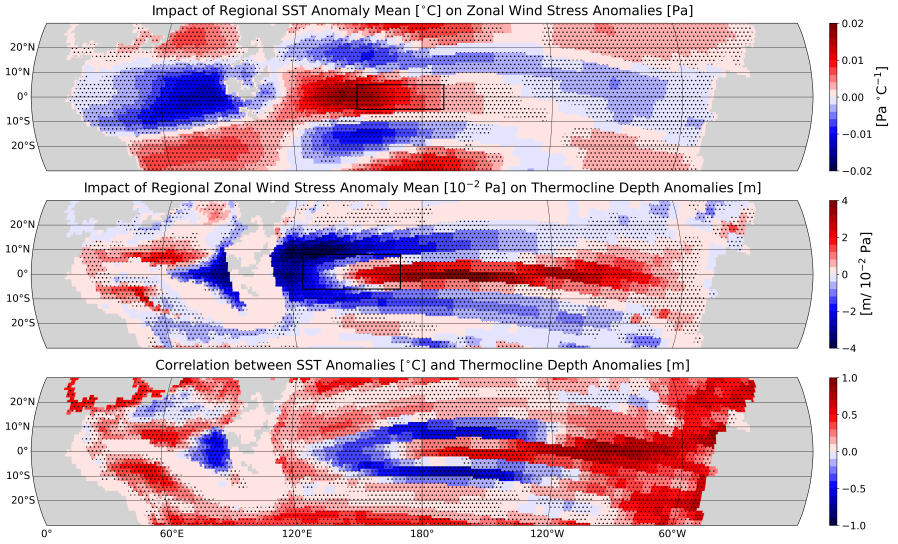

Figure 8: Contour maps of (A) linear regression of the regional mean deseasonalised, detrended monthly mean SST anomaly [°C] for 5°S-5°N 150°E-170°W (outlined) against deseasonalised, detrended monthly mean zonal wind stress anomalies [Pa], (B) linear regression of the regional mean deseasonalised, detrended monthly zonal wind stress anomaly [$\times 10^{-2}$ Pa] for 6°S-8°N 125°E-170°E (outlined) against deseasonalised, detrended monthly mean 20°C isotherm depth anomalies [m] and (C) point-wise correlation between deseasonalised, detrended monthly mean SST anomalies [°C] and deseasonalised, detrended monthly mean 20°C isotherm depth anomalies [m]. Stippling indicates significance using two-tailed student's t-test at 99.75% confidence threshold.

of the west equatorial Panthalassic Ocean SSTs is linked with a weakening of the prevailing easterly winds over the western Panthalassic Ocean and the prevailing westerly winds over the Tethys Ocean concurrent with a strengthening of the prevailing easterly winds over the eastern Panthalassic Ocean. This pattern is also associated with convergent zonal wind anomalies north of 10°N and south of 10°S around 120°E.

These zonal wind anomalies subsequently impact the ocean stratification, Fig. 8B illustrates the shoaling of the thermocline depth in the west Panthalassic in response to positive zonal wind anomalies over the western equatorial Panthalassic Ocean. While initially counter-intuitive, the positive zonal wind anomaly indicates a weakening of the prevailing easterly wind that entrains water across the surface of the equatorial Panthalassic, which results in

the shoaling of the thermocline depth. Concurrently, water in the central and eastern equatorial Panthalassic Ocean is transported more slowly, and coupled with the prevailing low cloud cover fraction (Fig. 4A), experiences greater warming, which results in a deepening of the thermocline depth. The shoaling of the thermocline in the eastern Tethys may be related to decreased downwelling in response to the weakened westerlies in the region.

To close this feedback system, we show the strong positive correlation between thermocline depth and SST anomalies across the majority of the tropical Panthalassic and Tethys oceans (Fig. 8C). The SST and thermocline depth anomalies are most strongly correlated in the eastern Panthalassic with a maxima of 0.86 at around 1.5°N 115°W. There are notable extensive negative correlations in the eastern equatorial Tethys Ocean and in a horseshoe-like pattern across the western and central equatorial Panthalassic Ocean but it is unclear at this time what mechanism is responsible for this inverted response.

The ocean-atmosphere feedback system illustrated in Fig. 8 provides greater understanding of the climate variability described previously. The divergent zonal wind anomalies at the Tethys-Panthalassic boundary (Fig. 8A) are co-located with the longitudes of greatest variability in the Walker Circulation (Fig. 3D) and in total precipitation (Fig. 4D). This suggests that warming in the western equatorial Panthalassic is associated with a weakening of convergence around 120°E leading to a dispersal or shifting of the region of maximum precipitation over the equatorial Tethys and western equatorial Panthalassic oceans. The change in zonal wind intensity and distribution of freshwater flux affects stratification and mixing across the region with a subsequent shoaling of the thermocline. The weaker easterlies reduce the western extent of the surface equatorial current (Fig. 5A) leading to a reduced transport of warm water to the western equatorial Panthalassic and a cooling of the SSTs, acting as a negative feedback on warming in the western equatorial Panthalassic.

We identify a pattern of SST variability in our latest Permian simulations (Fig. 7A) which shares some similarities to the El Niño Southern Oscillation (ENSO), the present-day dominant mode of SST variability [Deser et al., 2010]. The present-day ENSO is associated with a pattern of SST variability with a positive centre in the central to eastern Pacific Ocean and negative centre in the western Pacific and has an interannual frequency of 3-8 years. This association is well studied and the signal pattern can be extracted by a variety of statistical methods [Deser et al., 2010; X. Zhang et al., 2017; X. Zhu, 2021; Xu et al., 2023]. In our simulation, we do not see a comparably strong longitudinal dipole across the Panthalassic as is described for the canonical Pacific ENSO pattern but neither do we note a tripole pattern linked with the ENSO Modoki pattern [Ashok et al., 2007; Ashok & Yamagata, 2009; Kug et al., 2009]. The pattern of SST variability we identify in the Panthalassic Ocean is also similar to the Tropical Mode identified using the correlation matrix-based EOF method by X. Zhu [2021] in that there is a extensive positive core across the Panthalassic Ocean and an equivalent positive core across the Tethys Ocean with maxima above and below the equator, although the identified Tropical Mode does not express the similar horseshoe pattern of negatives that we find. It may be that the differences between the SST variability pattern identified for the latest Permian and the present-day ENSO could be attributed to the absence of the Atlantic Ocean, altering the teleconnections influencing the variability in this mode

[Cai et al., 2019], or the absence of the cold-tongue which is associated with the SST variability of the canonical ENSO mode [Kug et al., 2009; Takahashi et al., 2011; Timmermann et al., 2018]. Regardless, the latest Permian SST variability indicates a distinct mode of SST variability and has an apparent higher frequency (2-4 years) than the present-day ENSO mode (3-8 years) although both are related to tropical ocean-atmosphere interactions and variability in the Walker Circulation.

We expect that the dominant mode of SST variability impacted tropical ecosystems in the latest Permian in a comparable manner to the present-day ENSO. The relatively low variability in thermocline depth associated with the dominant mode of SST variability (Fig. 8), mixed-layer depth and vertical velocities (Fig. 6) associated with the eastern Panthalassic Ocean suggests a less pronounced impact on ecosystems as a result of shifts in upwelling position and intensity that affect the eastern Pacific Ocean in the present [Holbrook et al., 2021; Lehodey et al., 2021]. However, we expect significant impacts during positive phases associated with warming. Present-day studies have highlighted ENSO impacts on shallow shelf ecosystems where warm anomalies are linked with coral bleaching and mortality events within the Coral Triangle [Kleypas et al., 2015; McManus et al., 2019] and reduced productivity across open-ocean equatorial ecosystems [Lehodey et al., 2021]. There is evidence in the fossil record of abundant sponge reef ecosystems across the shallow shelves of the Tethys Ocean in the latest Permian [Rigby & Senowbari-Daryan, 1995; G. Liu et al., 2008; Tian & Wang, 2021] which are expected to be similarly vulnerable to ocean warming as coral ecosystems in the present-day [Bell et al., 2018].

Y. Shen et al. [2011] relate sulphur isotopic fractionation in the Meishan section with episodic shoaling of anoxic water along the continental slope associated with the Cathaysian peninsula, a region in which the model simulates a strong response of the thermocline depth in the tropical ocean-atmosphere feedback system we identify (Fig. 8). The Meishan section is associated with a depositional environment on the upper continental slope at 50-200 m depth [S.-Z. Shen et al., 2013] and the model simulates a thermocline depth along the Tethys-Panthalassic boundary shelf of 67-260 m depth, which gives further support to the shoaling hypothesis of Y. Shen et al. [2011]. The limited thermocline response to the feedback in the eastern Panthalassic may be a potential reason why similar episodic events have not been noted in the Quinn River section. Though it should also be noted that this section is associated with an bathyal/ abyssal depth deposition environment [Sperling & Ingle, 2006] and therefore may be too deep for such shoaling events to be impactful.

A.3.3 *SST Extreme Events of the latest Permian*

We illustrate the mean pattern and the leading mode of variability of SSTs simulated by the MPI-ESM for the latest Permian and now frame these in the context of potential susceptibility to the EPME. Studies of present-day ecosystems find that many organisms live in environments where the mean temperature is below their optimum, indicating that the upper limits of normal environmental variability may in fact determine species' thermal tolerances [Stuart-Smith et al., 2015; Sunday et al., 2019]. Therefore, when the typical range of variability is exceeded, we consider these as extreme events, which represent conditions that ecosystems that may cause tolerable or intolerable stress to populations or ecosystems. Therefore, we examine

from a climatological perspective how long populations or ecosystems must endure extremely high SSTs, how hot the extreme SSTs being endured are, and how often the extremely high SSTs must be endured, to better understand which regions may be more or less resilient to high SSTs in the latest Permian climate in advance of the climate change related to the EPME.

The longest median duration of tropical SST extreme events illustrated in Fig. 9A of 3.0 months is located in the eastern equatorial Panthalassic Ocean (8°N 105°W), with median durations exceeding 2.2 months present across the central and into the western equatorial Panthalassic Ocean. The eastern

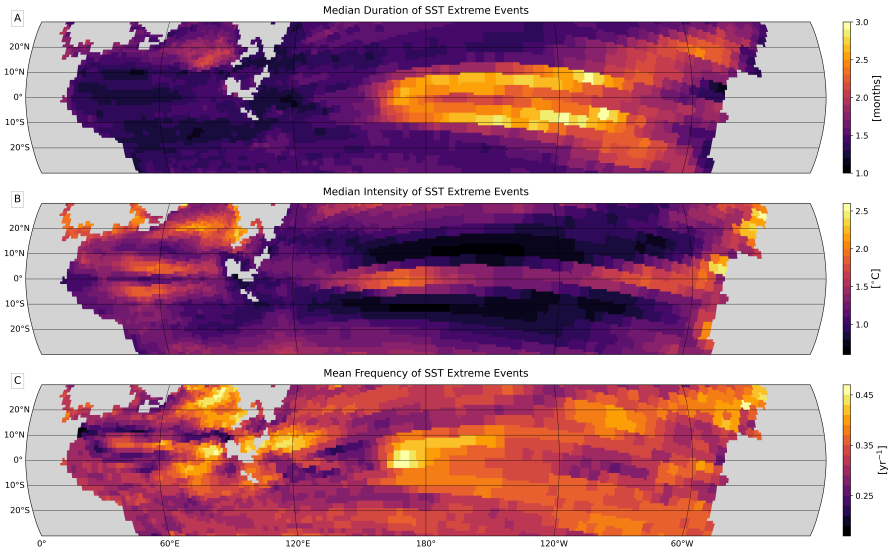

Figure 9: Contour maps of the (A) median duration [months], (B) median intensity [°C] and (C) mean frequency [year^{-1}] of SST extreme events.

Panthalassic Ocean generally experiences longer duration extreme events than the western Panthalassic. The northeastern Tethys Ocean indicates median durations of 1.7-2.2 months. However, the Tethys Ocean experiences shorter durations than the majority of the Panthalassic Ocean, despite the shortest median duration of 1.2 months occurring in the western equatorial Panthalassic Ocean around 2°S 120°E.

The greatest median extreme event intensities are located along the eastern boundary of the Panthalassic Ocean, with a maximum of 2.6°C at 25°N 25°W (Fig. 9B). Median intensities exceeding 2.0°C can also be found along the northeastern boundary of the Tethys Ocean and greater than 1.5°C in the western and eastern equatorial Panthalassic Ocean and equatorial Tethys Ocean. The extreme events in the Tethys Ocean tend to be more intense than those across the tropical Panthalassic Ocean. The weakest median intensities are located around 10°N and °S in the Panthalassic Ocean with a minimum of 0.7°C at 12°S 170°E.

Extreme SST events are found to occur with the greatest mean frequency (0.48 year^{-1}) in the western equatorial Panthalassic Ocean around 170°E (Fig. 9C). Mean frequencies greater than 0.33 year^{-1} are present across the eastern Panthalassic north of 10°N and south of 10°S, in the northeastern and eastern equatorial regions of the Tethys Ocean and in the Tethys-Panthalassic boundary region. The northwestern Tethys Ocean exhibits the least frequent

SST extreme events at 0.18 year^{-1} at 12°N 25°E with low mean frequencies also present in the western equatorial Panthalassic Ocean.

When considered together, these durations, intensities and frequencies present insight into the thermal stress of latest Permian tropical marine ecosystems (Fig. 9). The northeastern tropical shelf region of the Panthalassic Ocean experiences high median intensity (2.6°C) and high mean frequency (0.44 year^{-1}) extreme SSTs but with relatively short median durations (1.5 months), which could be crucially important in a continental shelf region adjacent to a region of strong upwelling. In contrast, region around 170°E experiences a high mean frequency of extremes and relative long median durations (2.6 months) but only moderate median intensities (1.9°C). The equatorial shelf region at the Tethys-Panthalassic boundary also experiences relatively high mean frequencies (0.43 year^{-1}) but only moderately low median intensities (1.0°C) and short median durations (1.5 months).

Extreme temperature events of 0.5-2.0° in the present-day are associated with negative impacts to tropical ecosystems [McManus et al., 2019; Holbrook et al., 2021] and our simulation of the latest Permian indicates that median SST extreme event intensities (Fig. 9B) are found within this range. While the frequencies of the simulated extreme events may indicate ecosystems in these regions which are tolerant to these temperatures [Stuart-Smith et al., 2015; Sunday et al., 2019], these extremes will exert stress on the associated populations. The study of Gonzalez and Bell [2013] indicates that stress may positively or negatively impact the vulnerability of populations to environmental change. While it is unclear if the populations of these regions would be more or less vulnerable to the climate change associated with the EPME, it is clear that ecosystem states track with climate forcing [Bestelmeyer et al., 2011; Di Lorenzo & Ohman, 2012]. Furthermore, it is expected that ecosystems within regions of red-shift climate variability will be at greater risk of extinction [Lawton, 1988] and that ecosystems will respond to changes in the pattern of extreme events, rather than changes in mean temperatures [Stuart-Smith et al., 2015; Sunday et al., 2019].

A.4 SUMMARY & CONCLUSIONS

We successfully simulate tropical Sea Surface Temperatures in agreement with latest Permian proxies using the most recent constraints of atmospheric pCO_2. The MPI-ESM latest Permian configuration simulates an Equilibrium Climate Sensitivity of 4.7°K per doubling of CO_2, which is both higher than the present-day model configuration and other Earth System Models used to simulation the Permian-Triassic Boundary. Previous modelling studies required atmospheric CO_2 mixing ratios significantly higher than current best estimates in order to reproduce tropical Tethys Sea Surface Temperatures.

For the first time, we reveal the dominant mode of latest Permian interannual tropical variability to be an atmosphere-ocean feedback system with a 2-4 year periodicity. The identified mode is characterised by a pattern of Sea Surface Temperature variability with a positive core in the western equatorial Panthalassic Ocean. We link the tropical atmosphere-ocean feedback system to shifts in the thermocline depth in the western equatorial Panthalassic Ocean of 67-260 m depth. These shifts are co-located with the depositional setting of the Meishan section and may explain the episodic upwelling of anoxia described in the sulphur isotopic record. Furthermore, we expect this interannual tropical variability to have a comparable impact in the lat-

est Permian as the El Niño Southern Oscillation has on ecosystems in the present.

We characterise tropical marine heatwaves and determine intensities much lower than expected warming across the Permian-Triassic Boundary. We find a median intensity of marine heatwaves of 2.6°, indicating that ecosystems would be extinguished much earlier than the peak ocean warming. Therefore, the End-Permian Mass Extinction may have occurred earlier and more rapidly in response to climate perturbations than previously described.

B

THE DEADLY TRIO OF MARINE STRESSORS VARIED REGIONALLY IN THE LATEST PERMIAN

The attached manuscript is in preparation for submission to the journal *Climate of the Past*.

Burt, D.J. & Ilyina, T. (in preparation). The Deadly Trio of marine stressors varied regionally in the latest Permian [*to be submitted to Climate of the Past*].

AUTHOR CONTRIBUTIONS: D.J.B. designed the research question, performed analysis, created the figures and drafted the manuscript. T.I. provided scientific guidance and feedback. All authors contributed to editing and revising the manuscript.

The significance of the Deadly Trio of marine stressors varied regionally in the latest Permian

Daniel Jonathan Burt[1,2] and Tatiana Ilyina[3,4,1]

[1] Max Planck Institute for Meteorology, Max Planck Society, Hamburg, Germany
[2] International Max Planck Research School for Earth System Modelling, Max Planck Society, Hamburg, Germany
[3] Universität Hamburg, Hamburg, Germany
[4] Helmholtz-Zentrum Hereon, Geesthacht, Germany

ABSTRACT

The deadly trio of ocean warming, acidification and deoxygenation are negatively impacting marine ecosystems in the present. The severity of the End-Permian Mass Extinction, where more than 90% of all life was extinguished, is also attributed to the deadly trio of marine stressors. As the Earth faces the potential of a modern mass extinction, it is crucial that we better understand the pattern and evolution of extinction in past analogues such as the End-Permian Mass Extinction. Previous research of the End-Permian Mass Extinction overlooks the most relevant spatiotemporal timescales at which ecosystems respond. Here, we use the Max-Planck Institute Earth System Model to characterise extreme events of temperature, oxygen and pH and their implications for the pattern and pacing of the End-Permian Mass Extinction. We reveal, for the first time, a spatially varying pattern of extreme events, where hypoxic extreme events dominate across the tropical Tethys shelf regions, marine heatwaves of up to 10.2°C dominate across the southern high latitude shelf regions and pH extremes of up to -0.61 dominate the tropical shelf regions. We conclude that contrary to previous studies, it is unlikely that deoxygenation plays a role in extratropical extinction across the shallow shelf regions. Furthermore, due to the magnitudes of the extreme events, we suggest that the End-Permian Mass Extinction was more rapid and occurred earlier in response to the Permian-Triassic transition climate perturbations.

B.1 INTRODUCTION

Ocean warming, acidification and deoxygenation, referred to as the deadly trio, [Gruber, 2011; Bijma et al., 2013] negatively impact marine ecosystems globally in the present [Stuart-Smith et al., 2015; Doney et al., 2020; Sampaio et al., 2021]. The deadly trio are expected to worsen and their extremes will become longer lasting, more intense and more frequent in response to anthropogenic carbon emissions [Eyring et al., 2021]. The End-Permian Mass Extinction (EPME), the Earth's most severe biotic crisis, is linked to analogous climate perturbations in response to volcanic carbon emissions [Payne & Clapham, 2012; Burgess et al., 2017; Dal Corso et al., 2022]. Here, we explore the spatial distribution of deadly trio extreme events in an Earth

System Model (ESM) and their implications for the pattern and pacing of the EPME.

The ocean has taken up 91% of excess heat from the enhanced atmospheric greenhouse effect [Forster et al., 2021] and 26% of anthropogenic carbon emissions [Friedlingstein et al., 2023] since the pre-industrial era. The uptake of excess heat leads directly to ocean warming but also indirectly to sea-level rise and increased stratification, which reduces ventilation of the ocean interior [Fox-Kemper et al., 2021]. The uptake of carbon by the ocean alters the existing chemical balance of dissolved inorganic carbon species and leads to acidification [Doney et al., 2020]. The deadly trio of ocean warming, deoxygenation and acidification negatively impact the survival, metabolism, reproduction and many other biological processes of marine biota [Stuart-Smith et al., 2015; Doney et al., 2020; Sampaio et al., 2021]. With continuing anthropogenic carbon emissions, these marine stressors are expected to worsen [Eyring et al., 2021] and may threaten a modern mass extinction [Penn & Deutsch, 2022].

The severity of the EPME (252 Ma), where 90% of all species were extinguished, is attributed to the impacts of the deadly trio [Harnik et al., 2012; Bijma et al., 2013; Dal Corso et al., 2022]. The mass extinction is linked to the climate perturbations during the Permian-Triassic transition, which are associated with large-scale carbon emissions from Siberian Traps volcanism [Burgess et al., 2017; Cui, Li, et al., 2021; Dal Corso et al., 2022]. Evidence in the isotopic record of the latest Permian clearly indicate global patterns of ocean warming, acidification and deoxygenation [Harnik et al., 2012; Bijma et al., 2013] concurrent with massive biodiversity loss [Cui et al., 2013; Foster & Twitchett, 2014; Dal Corso et al., 2022].

Previous investigations of the EPME focus on impacts of the deadly trio on single species [Götze et al., 2020] or changes in climate conditions on geologic timescales [Penn et al., 2018] and therefore overlook the spatiotemporal scales at which ecosystems respond. It is clear from present-day studies that species have a variety of responses and impacts from ocean warming, acidification and deoxygenation [Vaquer-Sunyer & Duarte, 2008; Keeling et al., 2010; Yao & Somero, 2014; Stuart-Smith et al., 2015; Cattano et al., 2018; Wang et al., 2018; Doney et al., 2020; Cornwall et al., 2021; Sampaio et al., 2021] and single-species studies cannot provide a holistic perspective of environmental stress in the latest Permian. Penn et al. [2018] seek to explain the EPME through the different mean states of the latest Permian and earliest Triassic but this approach does not account for the pacing of the EPME, nor do they consider the combined influence of the deadly trio.

We apply the Max-Planck Institute Earth System Model (MPI-ESM) to characterise the spatial pattern and intensity of temperature, oxygen and pH extreme events across the latest Permian continental shelves. First, we illustrate the temperature, oxygen and pH climatological mean-states and the duration, intensity and frequency of their extreme events. Then we explore the physical dynamics and biogeochemical cycling of the Tethys and Panthalassic Oceans to explain the spatial patterns we identify.

B.2 METHODS

B.2.1 *Model Description*

We simulate the latest Permian climate using the MPI-ESM version 1.2 used in the 6th-phase of the Coupled Model Intercomparison Project [Mauritsen et al., 2019]. The MPI-ESM couples the atmospheric general circulation model ECHAM6.3 and the land surface scheme JSBACH3.2 to the ocean general circulation model MPIOM1.6 and ocean biogeochemistry model HAMOCC6 through the OASIS3 Model Coupling Toolkit version 2.0 [Mauritsen et al., 2019]. We perform simulations with a coarse-resolution MPI-ESM configuration with a T31 spectral truncation (nominal resolution 3.75°) and 31 vertical hybrid (sigma-pressure coordinate) levels up to 10 hPa in ECHAM6.3 [Mauritsen et al., 2019] and a coarse-resolution MPIOM grid with a 3.0° nominal resolution [Burt et al., *in preparation*]. Further configuration of model features to represent the latest Permian are described in Section B.2.2.

The HAMOCC6 ocean biogeochemistry model simulates the transport and evolution of tracers at the air-sea interface and within the water-column and surface sediment layers [Ilyina et al., 2013; Paulsen et al., 2017; Mauritsen et al., 2019; B. Liu et al., 2021]. Air-sea fluxes are calculated for gaseous tracers such as CO_2, O_2, N_2O and N_2. HAMOCC6 computes the transport of 25 tracers within the water column including dissolved inorganic carbon, total alkalinity, phosphate, nitrate and oxygen using the 3D hydrodynamic field from MPIOM in the same manner as salinity. The organic compartments are resolved through an extended Nutrient, Phytoplankton, Zooplankton and Detritus scheme [Six & Maier-Reimer, 1996] with prognostic parameterisations of bulk phytoplankton, cyanobacteria and zooplankton. Below the model-defined export depth of 100 m, the sinking speed of particulate organic matter increases linearly with depth to achieve a power-law-like attenuation of fluxes in accordance with observations [Martin et al., 1987; Kriest & Oschlies, 2008]. Constant sinking speeds are prescribed for opal and dust, which are considerably faster than horizontal velocities in the hydrodynamic field and therefore opal and dust are not advected.

The sediment module simulates porous sediment layers over a single solid burial layer in order to accommodate remineralisation and dissolution processes C. Heinze et al. [1999]. Pelagic sedimentation fluxes of opal and organic matter are added to the solid component of the sediment. The single solid burial layer represents the removal of material from the active layer and is balanced by homogeneous addition of opal and organic matter to the ocean surface.

B.2.2 *Latest Permian Configuration*

We configure the MPI-ESM for the distinct boundary conditions of the latest Permian. We use the continental configuration for 250 Ma from Kocsis and Scotese [2021] for our simulations of the latest Permian climate (Fig. 1). The continental configuration of Kocsis and Scotese [2021] provides relatively detailed topographic data for the land but limited bathymetric data for the ocean. The continental shelves are represented but due to the 64.2 Myr present-day mean age of ocean crust material [Seton et al., 2020], there is almost no ocean crust from the Permian in the present with which to determine palaeobathymetry.

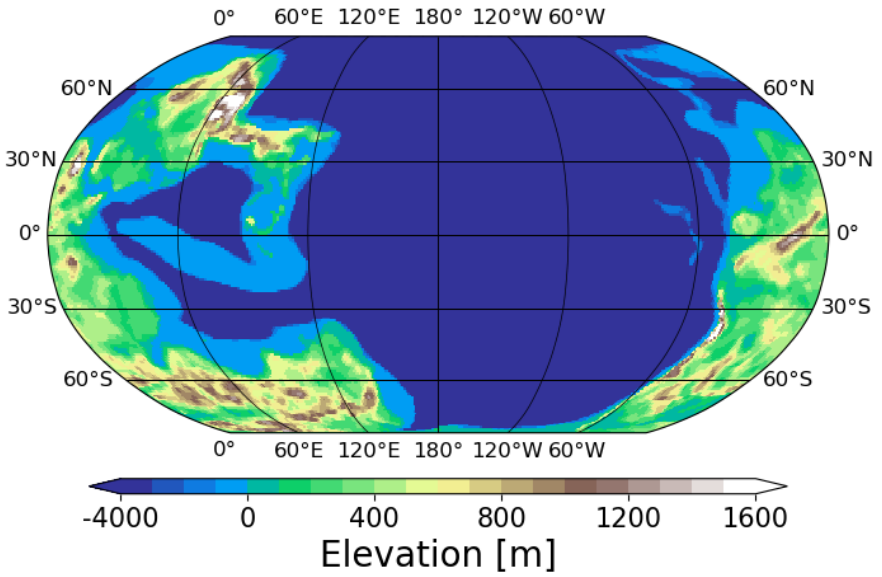

Figure 1: Contour map of elevation for the latest Permian (252 Ma). Data provided by Kocsis and Scotese [2021]. Note the change in scale below 0 m.

We summarise the atmospheric mixing ratios, orbital parameters and solar irradiance boundary conditions of our latest Permian configuration in Table 2. We use the current best estimate of atmospheric pCO_2 of 500 ppmV [H. Li et al., 2019; Joachimski et al., 2022] and the pre-industrial atmospheric mixing ratios for methane (CH_4) and nitrous oxide (N_2O). We implement a reduced solar insolation to reflect the younger latest Permian sun and fix the MPI-ESM orbital parameters to pre-industrial settings, which compare well with those used by Kiehl and Shields [2005].

Table 2: Boundary conditions for the latest Permian simulation.

	CO_2 [ppmV]	CH_4 [ppbV]	N_2O [ppbV]	S_0 [W m^{-2}]	Eccentricity	Obliquity [°]
Value	500.0	808.2	273.0	1338	0.01676	23.46

We modify HAMOCC6 in order to better represent biogeochemical cycling in the latest Permian. We remove the representation of calcareous and siliceous shell-producing phytoplankton and instead implement siliceous shell-producing zooplankton to represent the dominance of radiolarians in the latest Permian. We initialise the ocean with a homogeneous distribution of nutrients assuming present-day inventories but spin-up the model to permit the inventories to achieve a new quasi-equilibrium in the latest Permian configuration. We also homogenise the pre-industrial dust forcing of [Albani et al., 2016] due to a lack of boundary condition information for the period.

B.3 RESULTS

B.3.1 *Characterising temperature, oxygen and pH extreme events*

In order to investigate the marine stressors that organisms and ecosystems associated with the benthic environment could have been exposed to in the latest Permian, we focus our analyses on the model level at the base of the water column above the continental shelves. This model level represents the depths 65-78 m in the adjusted bathymetry following Kocsis and Scotese [2021]. This depth level also represents the base of the euphotic zone and is within or near the mixed-layer depth in the majority of regions. Throughout our analyses, we focus on descriptions around 5 generalised shelf regions: the tropical Tethys shelves (including the western coastal shelf and Cathaysian peninsula shelf), the South Tethys shelf (including the marginal sea), the North Panthalassic shelf, the East Panthalassic shelf and the South Panthalassic shelf.

climatological mean state

The climatological mean-states of temperature, dissolved oxygen (DO) and seawater pH in Fig. 2 illustrate the long-term environmental conditions in which latest Permian ecosystems may have existed. Globally seawater temperatures ranged from -1.7°C to 29.8°C with the warmest region in the west tropical Panthalassic and the coolest region located at the South Panthalassa shelf. There is a strong latitudinal gradient through the Panthalassic and a longitudinal gradient across the equatorial Panthalassic. The tropical Tethys shelves are simulated with an average temperature of 25.0°C, considerably warmer than the 14.3°C average of the East Panthalassic shelf or other cooler shelves. The DO concentration also exhibits strong latitudinal and longitudinal gradients with the lowest concentrations of 0.3 mmol m^{-3} in the East equatorial Panthalassic and up to 348.8 mmol m^{-3} at the high latitudes. Low DO concentrations are also found in the western Panthalassic and equatorial Tethys Oceans. HAMOCC simulates seawater pH ranging from maxima around 8.1 at the subtropics and decreases towards the poles and the equator, with a minimum of 6.2 in the East equatorial Panthalassic. The pH ranges from 7.66 to 7.93 across the continental shelves with the lowest values occurring across the East Panthalassic and tropical Tethys shelves.

The climatological mean states of temperature, DO and pH reveal the impact of the prevailing tropical Walker Circulation described in Burt et al. [*in preparation*]. The warm pool across the equatorial Tethys and West Panthalassic Ocean is evident in the western Panthalassic warm pool shown in Fig. 2 and a related cool region associated with upwelling of deep water. The relationship between temperature and DO is also apparent, where oxygen solubility is dependent on temperature at approximately 4 mmol m^{-3} $°C^{-1}$.

The magnitude and pattern of DO concentrations and pH also indicate the limits of the model. The fidelity of lower DO concentrations across the Cathaysian peninsula shelf and higher DO concentrations across the coastal shelves may be related to the application of homogeneous weathering rather than coastal or riverine weathering fluxes. HAMOCC has the functionality to support both coastal or riverine weathering fluxes but there is insufficient proxy data regarding the locations and magnitudes of riverine weathering fluxes to support these boundary conditions. Furthermore, the persistent oxygen minimum zone around 3°N 100°E is likely a result of restricted circulation. The locality map for South China described by S.-Z. Shen et al. [2013] shows bathymetric channels across the shelf and between islands that are not represented at our coarse resolution. Additionally, many studies

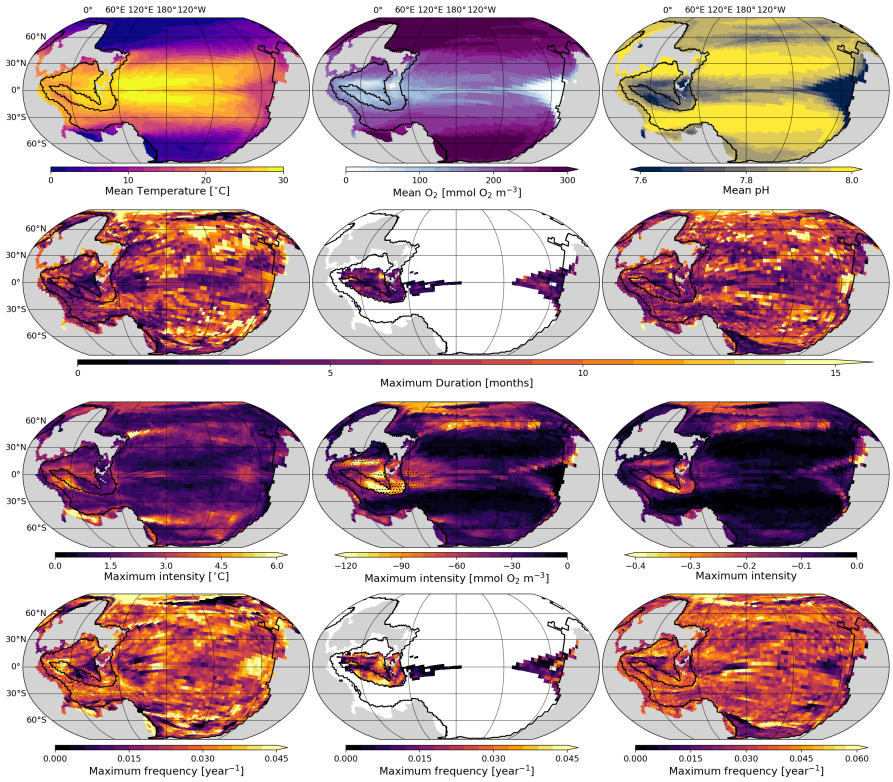

Figure 2: Contour maps relating to (left) temperature, (centre) dissolved oxygen and (right) seawater pH reported on total scale at standard temperature and pressure at 71.5 m depth. Row one illustrates the climatological mean state and the following rows illustrate extreme event descriptions for (row two) maximum duration, (row three) maximum intensity and (row four) the mean frequency. The (centre, row two) maximum duration and (centre, row four) mean frequency of dissolved oxygen are illustrated only for hypoxic extreme events. Stippling in (centre, row three) of maximum intensity of dissolved oxygen extreme events indicates locations where the extreme event induced hypoxia from climatological mean oxic conditions.

indicate that the pH levels simulated would negatively impact biota [Kroeker et al., 2013; Gobler & Baumann, 2016; Wang et al., 2018; Götze et al., 2020; Steckbauer et al., 2020; Santos et al., 2021; Sampaio et al., 2021], and it is unclear if this is the result of the simple representation of the marine biological carbon cycle in HAMOCC, no biological feedback from pH, or the high atmospheric CO_2 mixing ratio of the forcing condition.

temperature extremes

We illustrate the pattern and impact of marine heatwaves in our simulations of the latest Permian by describing the maximum duration, maximum intensity and mean annual frequency of extreme temperature events (Fig. 2). The pattern of extremes at depth is less clear than described by Burt et al. [*in preparation*], however the durations tend to be longer at higher latitudes, with a maximum of 46 months, and shorter in the tropics and Tethys Ocean. The longest marine heatwave simulated on the continental shelves is 31 months on the East Panthalassic shelf with an average of 9.7 months across the whole shelf, while the North Panthalassic shelf has the shortest duration extreme events at 5.0 months. The greatest maximum intensity extreme of 10.2°C

occurs on the South Tethys shelf, though the shelf average is 3.8°C and the East Panthalassic shelf has the lowest shelf average maximum intensity of 1.7°C. There is also no clear pattern of mean annual frequencies but the highest frequency of 0.08 yr^{-1} occurs in the northern high latitudes and the South Panthalassic shelf has the highest mean frequency of 0.06 yr^{-1} at 76°S 160°E.

We highlight the similarity between the pattern of global maximum marine heatwave intensities at 71.5 m shown in Fig. 2 and the pattern of surface tropical median marine heatwave intensities described by Burt et al. [*in preparation*]. We note a similar pattern of higher intensities north and south of the equatorial Tethys, in the west and east equatorial Panthalassa and onto the East Panthalassic shelf but not that the maximum intensities experienced at higher latitudes. However, the interannual mode of tropical SST variability described by Burt et al. [*in preparation*] does not explain the magnitude or pattern of maximum intensities in the extratropics, which may be related to long-term variability in gyre circulation patterns.

The average maximum marine heatwave intensities across the tropical Tethys (2.0°C) and East Panthalassic (1.7°C) shelves are of magnitudes considered to have significant negative impacts on the organisms and ecosystems present [Harris et al., 2018; Smale et al., 2019; Jacox et al., 2020; K. Smith et al., 2023]. Furthermore, under the Climate Extremes Hypothesis of thermal tolerances [Stuart-Smith et al., 2015; Sunday et al., 2019], changes in environmental temperature extremes rather than changes in means are expected to drive extinction. It is therefore unlikely that tropical marine organisms and ecosystems of the latest Permian could tolerate the 8-10°C warming described in the geologic record [Joachimski et al., 2020] and extinctions would occur much earlier and faster than the pace and magnitude of climate warming across the Permian-Triassic transition.

DO extremes

As with marine heatwaves, DO extreme events occur across the ocean but extremes which induce hypoxic conditions are largely constrained to the tropics (Fig. 2). We use the definition of "Critical Hypoxia" of 83.2 mmol m^{-3} following Monteiro and van der Plas [2006] as the threshold at which "organisms require physiological adaptations to survive". The maximum duration of a marine hypoxic extreme event simulated is 14 months in the tropical Tethys on the western edge of the Cathaysian peninsula shelf. Hypoxic extreme conditions occur on both the tropical Tethys and East Panthalassic shelves at mean maximum durations of 3.8 and 3.6 months respectively. Greater magnitudes of maximum intensities occur at northern high latitudes and the least in the subtropical gyre regions. Despite the relatively low magnitude of maximum intensities in the tropics, it is only the tropics that experience shifts from oxic to hypoxic conditions. An additional 5.0×10^6 km^2 is exposed to hypoxia across the southern Cathaysian peninsula shelf (10-20°S) compared to 0.6×10^6 km^2 additional shelf area exposure in the East Panthalassic. The Cathaysian peninsula shelf also experiences higher mean frequencies of hypoxic extreme events with a maximum of 0.05 yr^{-1} compared to the East Panthalassic shelf.

The tropical Tethys Ocean experiences warm temperatures and low oxygen solubility and is therefore has the greatest sensitivity to extremes of dissolved oxygen. Low oxygen is recognised as having consistently negative impacts on complex life which is dependent upon aerobic respiration [Vaquer-Sunyer & Duarte, 2008; Keeling et al., 2010; Sampaio et al., 2021]. The frequency and intensity of hypoxia across the Cathaysian peninsula shelf may have

significant implications for the types of organisms and ecosystems that may survive and thrive there, whether they are adapted to survive these conditions or whether the region was periodically recolonised. However, changes in oxygen conditions are not typically considered as the primary trigger for the EPME because the severity of the impacts on biota are non-selective [Knoll et al., 2007]. However, Penn et al. [2018] do propose aerobic habitat loss due to warming as the driver for extinction selectivity across the Permian-Triassic transition.

The occurrence of episodic hypoxia across the Cathaysian peninsula continental shelf is also consistent with geochemical evidence. Y. Shen et al. [2011] identify potential indicators of a bioturbation shutdown associated with hypoxic conditions in the S-isotopic geochemical record from the Meishan section. The Meishan section is associated with the Panthalassic edge of the Cathaysian peninsula shelf north of the equator.

pH extremes

Fig. 2 shows the duration, intensity and frequency of extreme pH events with respect to variability thresholds only and not specific biological constraints due to the variety of responses by marine biota to acidity [Orr et al., 2005; Doney et al., 2009; Doney et al., 2020]. As with the maximum duration and mean frequency of marine heatwaves, there is no apparent pattern for pH extremes. The shortest durations occur at southern high latitudes with short durations across the tropics and longer maximum durations at northern high latitudes and the East equatorial Panthalassa. The longest maximum duration of 51 months occurs in the marginal sea of the South Tethys shelf region. The South Tethys and South Panthalassic shelves have the longest average maximum durations of 7.4 and 6.7 months respectively. The greatest maximum intensity pH event of -0.61 occurs on the East Panthalassic shelf at 17°N 31°W and the tropical Tethys and East Panthalassic shelves have similar averaged maximum intensities of -0.16 and -0.17 respectively. The North and South Panthalassic shelves have the lowest average maximum intensity pH events at -0.07 and -0.09 respectively. There is only minimal differences in mean frequency of pH extremes across the continental shelves. The North Panthalassic shelf experiences the lowest averaged mean frequency at 0.029 yr^{-1}, while the South Tethys and South Panthalassic experience the highest averaged mean frequencies at 0.034 yr^{-1}.

The short maximum durations and low mean frequencies of pH extreme events across the continental shelves indicate that these were relatively stable pH environments in the latest Permian. With the exception of the tropical Tethys and East Panthalassic shelves, the greatest maximum pH extreme intensities occur in the open ocean at high latitudes. The low intensities of pH extremes across the continental shelves indicate a potentially low tolerance of organisms and ecosystems to changes in pH conditions. Ocean acidification is widely proposed in literature as the mechanism for extinction selectivity in the EPME [Knoll et al., 2007; Clapham & Payne, 2011; Clarkson et al., 2015; Dal Corso et al., 2022]. The faster shift in seawater pH in response to increasing atmospheric CO_2 mixing ratios at high latitudes than low latitudes [Canadell et al., 2021] could also explain the higher latitudinal extinction selectivity of the EPME detected in the fossil record [Reddin et al., 2019]. However, there remains the absence of shell damage in the fossil record and the presence of ooidal limestones in the geological record in the Early Triassic, indicating that if ocean acidification did occur, it was limited to the latest Permian and extinction interval [Dal Corso et al., 2022; Foster et al., 2022].

regional stressor significance

We expect the simulated pattern of extremes indicates regionally varying significance of the deadly trio of marine stressors to latest Permian continental shelf ecosystems. Regional variations could suggest that a single trigger or stressor does not explain the extinction selectivity in the fossil record and may compliment previous efforts to identify the driver of extinction selectivity in the latest Permian [Penn et al., 2018; Reddin et al., 2019].

The tropical Tethys shelves are exposed to the most widespread and intense extreme oxygen events while also being exposed to potentially harmful marine heatwaves and pH extremes (Fig. 2). The pattern of durations and frequencies suggest that in the benthic environment that marine heatwaves and low oxygen extremes and pH extremes are unlikely to be concurrent events. We suggest ocean deoxygenation may be the primary stressor across the tropical Tethys continental shelves, in the absence of dramatic adaptations by biota across the region.

In contrast to the tropical Tethys, the East Panthalassic shelf experiences relatively minor extension of the existing low oxygen regions during extreme oxygen events. Instead the East Panthalassic shelf experiences the longest duration marine heatwaves and most intense pH extremes. These long lasting and low intensity marine heatwaves coupled with loss of aerobic habitat as described by Penn et al. [2018] and pH extremes may indicate that warming and acidification are more significant to extinction selectivity in the region.

We find it unlikely that the North Panthalassic shelf region will be exposed to stressful oxygen concentrations but may be sensitive to warming and acidification. Due to high latitude amplification, which may be weaker than in the present due to low sea-ice in the latest Permian, [Forster et al., 2021; Previdi et al., 2021] the high latitudes may experience higher rates of warming and acidification than low latitudes. The mild extreme intensities across the North Panthalassic shelf indicate that only limited warming and acidification would exceed the tolerances of organisms and ecosystems in the region.

The South Tethys and South Panthalassa shelves experience relatively intense and frequent marine heatwaves and relatively mild pH extremes, with the exception of the South Tethys marginal sea. This could indicate that despite high latitude amplification, the South Tethys and South Panthalassa shelf ecosystem are relatively tolerant to warming and more vulnerable to acidification.

We find that the North Panthalassa, South Panthalassa and South Tethys shelf regions each exhibit indications of vulnerability to acidification. This could agree with hypotheses that acidification was the primary driver of extinction selectivity in the latest Permian and agree with the latitudinal extinction selectivity described by [Reddin et al., 2019]. We do not make any conclusions regarding nektonic taxa in the overlying water column of these regions, nor the open ocean or the deep ocean ecosystems of the latest Permian.

B.3.2 *Drivers/ Mechanisms*

oxygen minimum zones

Further examination of the climatological mean state of DO at the tropics (Fig. 3) indicates the presence of a persistent low oxygen region in the East equatorial Panthalassic, referred to as an Oxygen Minimum Zone (OMZ). The East equatorial Panthalassic OMZ has a minimum surface depth of 21.5 m with a shallow surface gradient until around 110°W where it deepens dramatically. We also identify an OMZ in the East Tethys Ocean which is surrounded by the Cathaysian peninsula shelf and open to the north, the

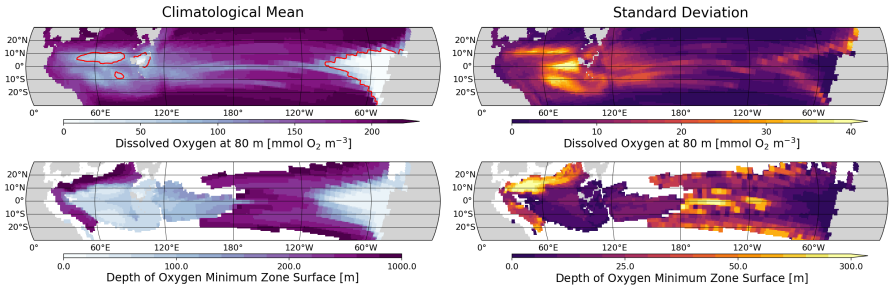

Figure 3: Contour maps of (left) climatological mean states of (top) dissolved oxygen concentration at 71.5 m with red contour indicating hypoxic threshold and (bottom) depth of oxygen minimum zone upper surface and (right) standard deviations of (top) dissolved oxygen concentration and (bottom) depth of oxygen minimum zone upper surface.

shallowest surface of the OMZ at 51.8 m is visible as a persistent hypoxic region in the central tropical Tethys from 52-84°E and an even deeper OMZ in the western Panthalassic with a minimum surface depth of 84.1 m. The greatest standard deviations of DO concentration occur in the East Tethys Ocean and East Panthalassic shelf with large standard deviations in the western and equatorial Panthalassic Ocean and the boundaries of the East equatorial Panthalassic OMZ. The deeper surface depths of ocean hypoxia are associated with larger standard deviations with only relatively small standard deviations at the shallowest OMZ surfaces and across the continental shelves.

Our distribution of DO concentrations agrees better with evidence from the geochemical record than it does with another recent ESM study. It is unclear if Penn et al. [2018] find similar latest Permian OMZs in their simulations with CESM1 although their simulation illustrates widespread hypoxic conditions in the Early Triassic. We use a different definition of anoxia from Penn et al. [2018], selecting the higher threshold of 20.8 mmol m^{-3} described by Monteiro and van der Plas [2006]. Penn et al. [2018] describe seafloor DO concentrations of 50-100 mmol m^{-3} in the deep Tethys Ocean in the Early Triassic, which are potentially hypoxic under the definition we use here, but the Cathaysian shelf peninsula region does not display hypoxic conditions. Furthermore, in the continental configuration used by Penn et al. [2018], there are two passages between the Tethys and Panthalassic Oceans at 3000 m, which could significantly increase exchange between these bodies [Kiehl & Shields, 2005]. In contrast, Müller et al. [2023] identify evidence of low oxygen conditions in the latest Permian geochemical record at the northern margin and western equatorial sections on the Cathaysian shelf, which agree with our distribution of DO concentrations at continental shelf depths in the Tethys Ocean. Their results indicate that oxygen concentrations may have been persistently low in the western equatorial Tethys through the Changhsingian and decreased through the Changhsingian at the northern margin in the latest Permian.

The high variability of DO conditions in the Tethys and the persistent OMZs in the East Tethys and West Panthalassic suggest the occurrence of hypoxia on the Cathaysian peninsula continental shelf is related to decreasing DO concentrations from below. Likely mechanisms that raise deeper hypoxic water or more rapidly deplete seawater DO are ventilation through physical

circulation (Fig. 4) or aerobic remineralisation (Fig. 5) or a combination of both.

ocean ventilation

Water mass ventilation age, the age since the water mass was last in contact with the atmosphere, gives an indication of the circulation regime across the latest Permian ocean (Fig. 4). At the 71.5 m model level, a water mass

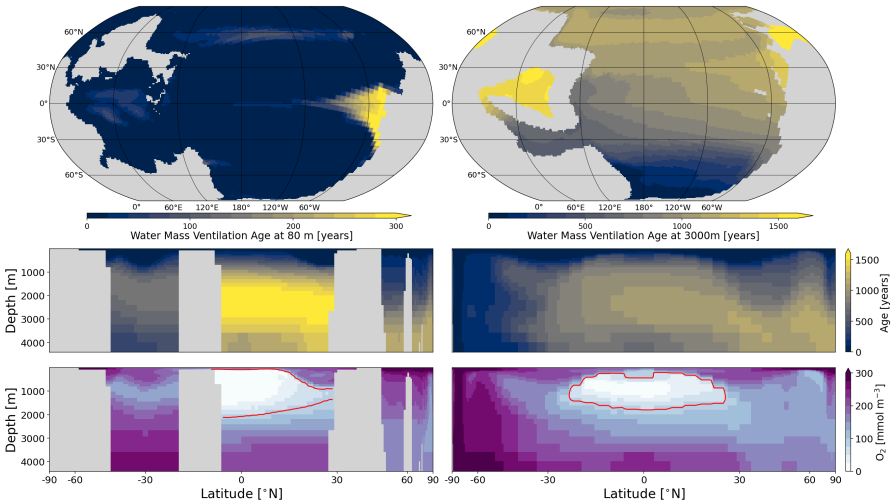

Figure 4: Contour maps of climatological mean water mass age since surface contact at (top-left) 71.5 m and (top-right) 3000 m. Contour plots of meridional sections of (centre) water mass age since surface contact and of (bottom) dissolved oxygen concentration at (left) 80°E and (right) 120°W. Red contour in dissolved oxygen meridional sections denotes hypoxic conditions at 83.2 mmol m^{-3} following Monteiro and van der Plas [2006].

of ventilation age between 30 and 70 years is present across the equatorial Tethys, an older water mass of 20-100 years is present around 60°N and the eastern Equatorial Panthalassic indicates a ventilation age of 200-350 years. The water masses present across the South Tethys and North and South Panthalassic shelves have average ages of less than 3 years. However, the tropical Tethys shelf is influenced by the older water mass and has an average ventilation age of 12.8 years with the oldest 76.9 years, while the East Panthalassic shelf is similarly affected with a maximum age of 272.0 years and an average age of 17.1 years. Comparing these with the ventilation ages at around 3000 m reveals that the oldest water mass ages of over 1700 years are found in an isolated basin in the North Panthalassic and in the Tethys Ocean of over 1500 years. The southern high latitudes ventilate the deep ocean and interact with the Tethys Ocean through a restricted channel of deep water exchange. The northern high latitudes act as a less efficient source of deep and intermediate water ventilation.

The pattern of ventilation (Fig. 4) suggests that the cooler, hypoxic and low pH water present in the East equatorial Panthalassic (Fig. 2) are associated with older ventilation ages. The water mass has lost heat during its time in the ocean interior and been depleted of oxygen through aerobic respiration, which has also reduced the total alkalinity and increased the dissolved inorganic carbon leading to reduced pH. The water mass is eventually transported to the East equatorial Panthalassic associated with intense upwelling where it is returned to the surface. The age of the water mass suggests that

did not originate in a high latitude region of deep water formation and is likely associated with a different source closer to the surface and the tropics.

The pattern of ventilation is further illustrated by the meridional sections, where northern hemisphere deep water rises to intermediate depths of 2-3 km at the tropics and entrains and mixes with younger water masses. The hypoxic conditions at the 120°W extension of the East equatorial Panthalassa OMZ are also not associated with the oldest water associated with deep water formation with the lowest DO concentrations at around 850 m depth with an age of 816 years and the deepest extent of hypoxia associated with 1000 year old water at 1700 m depth and extends from 23°S to 25°N. This suggests that DO is depleted from above and reaches an equilibrium with the rate of replenishment from the rising older water which is less depleted in DO than the OMZ.

A similar situation is apparent in the Tethys Ocean OMZ, which extends to greater depth than its East equatorial Panthalassic counterpart (Fig. 4). The Tethys Ocean OMZ extends to a maximum depth of 2080 m with a ventilation age of over 1600 years but the minimum DO concentration occurs at around 600 m depth with a ventilation age of 600 years. Given the maximum ventilation age in the 80°E meridional section of 1612.8 years occurs at a depth of 2293 m with younger ventilation ages below and in the Panthalassic water south of the Cathaysian peninsula, we infer that the Tethys Ocean is ventilated by a complex circulation system due to restricted exchange with the Panthalassic Ocean.

biological carbon pump

The differences in equilibration depths of the OMZs with ventilation age can be explained by examining the biological carbon pump (Fig. 5). The

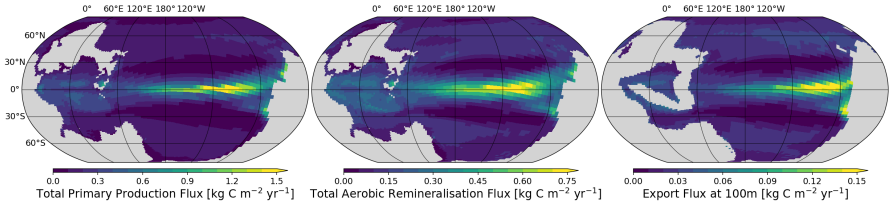

Figure 5: Contour maps of climatological means of the (left) total integrated primary production flux, (centre) total integrated aerobic remineralisation flux and (right) export flux of particulate organic carbon at 100 m depth.

central and eastern equatorial Panthalassic exhibit the greatest integrated primary production with a maximum of 1.6 kg C m^{-2} yr^{-1} at 116°W. The tropical Tethys Ocean exhibits more moderate productivity with a maximum of 1.0 kg C m^{-2} yr^{-1} at 5°N 100°E and an average of 0.3 kg C m^{-2} yr^{-1}. The tropical Tethys and East Panthalassic shelf regions are 3-4 times more productive on average than the other shelf regions. The pattern of primary production is largely reflected in the pattern of aerobic remineralisation at lower magnitudes. However, the maximum of aerobic remineralisation has a less eastward extent in the equatorial Panthalassic, which we attribute to the presence of the OMZ. This also explains the larger magnitudes of the particulate organic carbon (POC) export flux in the East equatorial Panthalassic. As the POC approaches the OMZ, the rate of aerobic remineralisation decreases and eventually ceases as anaerobic remineralisation processes dominate within the OMZ. The broad, shallow continental shelves also exhibit relatively high productivity as organic matter is remineralised and nutrients

released back into the euphotic zone rather than being remineralised below the nutricline.

The higher rates of primary production and aerobic remineralisation in the East equatorial Panthalassic (Fig. 5) explain the younger ventilation age compared to the Tethys Ocean (Fig. 4). The higher rates of aerobic remineralisation deplete the seawater of oxygen faster and require faster replenishment from deep water of younger ventilation age but still produce a more intense, shallower and widespread OMZ than the Tethys Ocean. In the Tethys Ocean, the productivity is supported by remineralisation across the broad Cathaysian peninsula shelf and moderate equatorial upwelling rather than an intense eastern boundary upwelling system. The lower productivity and aerobic remineralisation lead to a slower depletion of oxygen which is slowly replenished by the complex circulation system in the Tethys Ocean with waters of significantly older ventilation age.

Both primary production and aerobic remineralisation are temperature dependent processes and therefore sensitive to seawater temperature variability. This also explains why the highest carbon fixation and remineralisation rates occur in the tropics. Hülse et al. [2021] also note the importance of temperature dependent remineralisation when reproducing the pattern of hypoxia and euxinia in model simulations of the Permian-Triassic boundary.

pH balance

The pattern of ventilation and biological carbon cycling also explains the simulated mean pattern and variability of seawater pH (Fig. 6). The

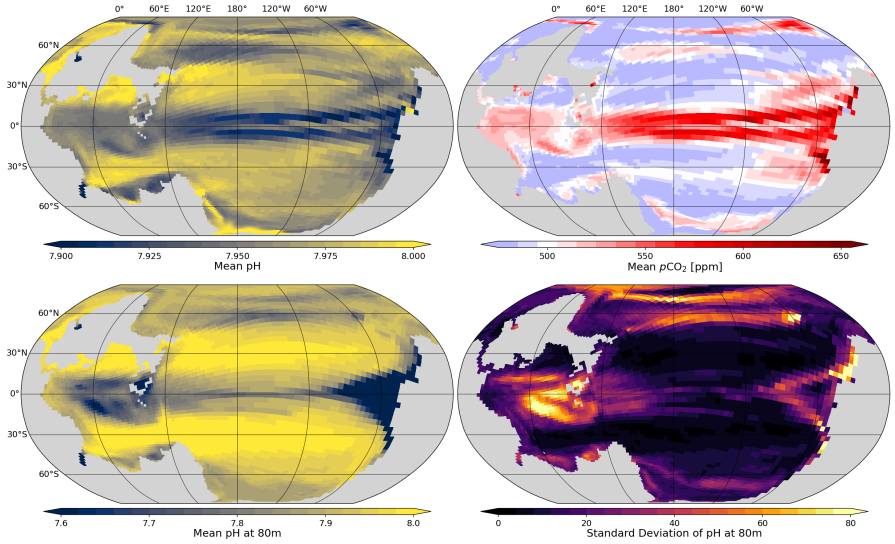

Figure 6: Contour maps of climatological means of (top-left) surface pH, (bottom-left) pH at 71.5 m depth and (top-right) pCO_2, where the white contour around 500 ppm represents the atmospheric pCO_2 mixing ratio and quasi-equilibrium, and (bottom-right) standard deviation of pH at 71.5 m depth.

simulated surface seawater pH ranges from 7.73 to 8.15 with a global mean of 7.96 which is lower than the present day but at quasi-equilibrium with a significantly higher atmospheric CO_2 mixing ratio. The lowest seawater pH occurs in the marginal sea linked with the South Tethys continental shelf region, with low pHs also present across the equatorial Panthalassic and at locations along the western coastline of Pangaea. These low pH regions are also associated with high pCO_2 levels and ocean outgassing

associated with regions of upwelling, across the equatorial and East tropical Panthalassic and high latitude regions, and therefore ventilation or patterns of remineralisation, such as the tropical Tethys and South Tethys marginal sea. There is an apparent low pCO_2 region across the central and eastern equatorial Panthalassic concurrent with high primary productivity (Fig. 5). This region also exhibits higher pH levels, indicating that the rate of carbon fixation in the region keeps pace with the upwelling of dissolved inorganic carbon enriched deep water.

These patterns also hold at the continental shelf depth, with high productivity and remineralisation regions on the tropical Tethys and East Panthalassic shelves (Fig. 5) associated with low pH levels and high standard deviations (Fig. 6). This may suggest that variations in aerobic remineralisation drive the variability in OMZ surface depths and pH levels in the tropics and that elevated rates of remineralisation that deplete oxygen also lead to reduced pH levels generating stressful marine conditions for biota in these regions.

B.4 CONCLUSIONS

spatial pattern of stress

Our study represents a pioneering investigation of marine extreme events at ecologically-relevant timescales in the latest Permian and their implications for the End-Permian Mass Extinction. We identify regional variations in the significance of marine heatwaves and hypoxic and pH extreme events across major shelf regions of the latest Permian. Hypoxic extreme events present the greatest stress to tropical Tethys Ocean shelf ecosystems and pH extremes present the greatest stress to the southern extratropical shelf regions. Marine heatwaves and pH extreme events may be equally impactful at northern high latitudes while the East Panthalassic continental shelf region is exposed to the full deadly trio of marine stressors.

pace of extinction

The regional variations of marine stressor significance we identify may have profound implications for the evolution of the End-Permian Mass Extinction. It is well established that extreme events will become more intense, longer lasting and more frequent in response to environmental change such as that associated with the Permian-Triassic transition. During the Permian-Triassic transition, carbon emissions will lead to climate warming, subsequently increasing stratification, decreasing gas solubility and increasing aerobic remineralisation. However, unlike previous studies, we find it unlikely that low oxygen conditions will become widespread across shallow extratropical shelf regions even with the projected intense warming of the Permian-Triassic transition. Therefore, we consider the maximum extreme events across the marine environment in the context of expected environmental change and which tolerance thresholds are likely to be exceeded earliest in each region. We conclude that low oxygen conditions are likely to pose the greatest risk to tropical Tethys shelf ecosystems and acidification and pH extremes will pose the greatest threat to southern extratropical shelf ecosystems. We expect northern extratropical shelf ecosystems will be exposed equally to ecologically relevant increases in the intensity and frequency of both thermal and acidity extremes. Finally, the East Panthalassic shelf regions are likely to be exposed to the full deadly trio of marine stressors due to proximity to the intense East equatorial Panthalassic OMZ and the cascade of deoxygenation and acidification in response to elevated remineralisation from frequent, long lasting marine heatwaves. This pattern of marine stressor

significance could also explain the extratropical latitudinal extinction selectivity previously identified in the fossil record and suggest that the extinctions may have occurred more rapidly in response to environmental change and earlier in the extinction interval than previously thought.

BIBLIOGRAPHY

Agostini, S., Harvey, B., Milazzo, M., Wada, S., Kon, K., Floc'h, N., Komatsu, K., Kuroyama, M., & Hall-Spencer, J. (2021). Simplification, not "tropicalization", of temperate marine ecosystems under ocean warming and acidification. *Global Change Biology*, *27*, 4771–4784. https://doi.org/10.1111/gcb.15749

Albani, S., Mahowald, N., Murphy, L., Raiswell, R., Moore, J., Anderson, R., McGee, D., Bradtmiller, L., Delmonte, B., Hesse, P., & Mayewski, P. (2016). Paleodust variability since the last glacial maximum and implications for iron inputs to the ocean. *Geophysical Research Letters*, *43*, 3944–3954.

Altieri, K., Spence, K., & Smith, S. (2021). Air-sea ammonia fluxes calculated from high-resolution summertime observations across the atlantic southern ocean. *Geophysical Research Letters*, *48*(e2020GL091963), 9. https://doi.org/10.1029/2020GL091963

Anagnostou, E., John, E., Babila, T., Sexton, P., Ridgwell, A., Lunt, D., Pearson, P., Chalk, T., Pancost, R., & Foster, G. (2020). Proxy evidence for state-dependence of climate sensitivity in the eocene greenhouse. *Nature Communications*, *11*(4436). https://doi.org/10.1038/s41467-020-17887-x

Arias, P., Bellouin, N., Coppola, E., Jones, R., Krinner, G., Marotzke, J., Naik, V., Palmer, M., Plattner, G.-K., Rogelj, J., Rojas, M., Sillmann, J., Storelvmo, T., Thorne, P., Trewin, B., Achuta Rao, K., Adhikary, B., Allan, R., Armour, K., ... Zickfeld, K. (2021). Technical summary. In V. Masson-Delmotte, P. Zhai, A. Pirani, S. Connors, C. Péan, S. Berger, N. Caud, Y. Chen, L. Goldfarb, M. Gomis, M. Huang, K. Leitzell, E. Lonnoy, J. Matthews, T. Maycock, T. Waterfield, O. Yelekçi, R. Yu, & B. Zhou (Eds.), *Climate change 2021: The physical science basis. contribution of working group i to the sixth assessment report of the intergovernmental panel on climate change* (pp. 33–144). Cambridge University Press. https://doi.org/10.1017/9781009157896.002

Ashok, K., Behera, S., Rao, S., Weng, H., & Yamagata, T. (2007). El niño modoki and its possible teleconnection. *Journal of Geophysical Research*, *112*(C11007), 481–484. https://doi.org/10.1029/2006JC003798

Ashok, K., & Yamagata, T. (2009). The el niño with a difference. *Nature*, *461*(7263), 481–484. https://doi.org/10.1038/461481a

Baag, S., & Mandal, S. (2022). Combined effects of ocean warming and acidification on marine fish and shellfish: A molecule to ecosystem perspective. *Science of the Total Environment*, *802*(149807). https://doi.org/10.1016/j.scitotenv.2021.149807

Baresel, B., Bucher, H., Brosse, M., Cordey, F., Guodun, K., & Schaltegger, U. (2017). Precise age for the permian-triassic boundary in south china from high-precision u-pb geochronology and bayesian age–depth modeling. *Solid Earth*, *8*, 361–378. https://doi.org/10.5194/se-8-361-2017

Bell, J., Bennett, H., Rovellini, A., & Webster, N. (2018). Sponges to be winners under near-future climate scenarios. *BioScience*, *68*(12), 955–968. https://doi.org/10.1093/biosci/biy142

Bercovici, A., Cui, Y., Forel, M.-B., Yu, J., & Vajda, V. (2015). Terrestrial paleoenvironment characterization across the permian-triassic boundary in south china. *Journal of Asian Earth Sciences*, *98*, 225–246. https://doi.org/10.1016/j.jseaes.2014.11.016

Berner, R. (2002). Examination of hypotheses for the permo–triassic boundary extinction by carbon cycle modeling. *Proceedings of the National Academy of Sciences*, *99*, 4172–4177. https://doi.org/10.1073/pnas.032095199

Bestelmeyer, B., Ellison, A., Fraser, W., Gorman, K., Holbrook, S., Laney, C., Ohman, M., Peters, D., Pillsbury, F., Rassweiler, A., Schmitt, R., & Sharma, S. (2011). Analysis of abrupt transitions in ecological systems. *Ecosphere*, *2*(129). https://doi.org/P10.1890/ES11-00216.1

Bijma, J., Pörtner, H.-O., Yesson, C., & Rogers, A. (2013). Climate change and the oceans - what does the future hold? *Marine Pollution Bulletin*, *74*, 495–505. https://doi.org/10.1016/j.marpolbul.2013.07.022

Black, B., Neely, R., Lamarque, J.-F., Elkins-Tanton, L., Kiehl, J., Shields, C., Mills, M., & Bardeen, C. (2018). Systemic swings in end-permian climate from siberian traps carbon and sulfur outgassing. *Nature Geoscience*, *11*, 949–954. https://doi.org/10.1038/s41561-018-0261-y

Brand, U., Posenato, R., Came, R., Affek, H., Angiolini, L., Azmy, K., & Farabegoli, E. (2012). The end-permian mass extinction: A rapid volcanic co2 and ch4-climatic catastrophe. *Chemical Geology*, *322-323*, 121–144. https://doi.org/10.1016/j.chemgeo.2012.06.015

Bürger, R., & Lynch, M. (1995). Evolution and extinction in a changing environment: A quantitative-genetic analysis. *Evolution*, *49*, 151–163. https://doi.org/10.1111/j.1558-5646.1995.tb05967.x

Burgess, S., Bowring, S., & Shen, S.-Z. (2014). High-precision timeline for earth's most severe extinction. *Proceedings of the National Academy of Sciences of the United States of America*, *111*(9), 3316–3321. https://doi.org/10.1073/pnas.1317692111

Burgess, S., Muirhead, J., & Bowring, S. (2017). Initial pulse of siberian traps sills as the trigger of the end-permian mass extinction. *Nature Communications*, *8*(164). https://doi.org/10.1038/s41467-017-00083-9

Burls, N., & Sagoo, N. (2022). Increasingly sophisticated climate models need the out-of-sample tests paleoclimates provide. *Journal of Advances in Modeling Earth Systems*, *14*(e2022MS003389). https://doi.org/10.1029/2022MS003389

Burt, D., Putrasahan, D., Günther, M., & Ilyina, T. (*in preparation*). Identifying episodic regional sea surface temperature extremes in the dominant-mode of latest permian internal climate variability in the max-planck institute earth system model.

Cai, W., Wu, L., Lengaigne, M., Li, T., McGregor, S., Kug, J.-S., Yu, J.-Y., Steucker, M., Santoso, A., Li, X., Ham, Y.-G., Chikamoto, Y., Ng, B., McPhaden, M., Du, Y., Dommenget, D., Jia, F., Kajtar, J., Keenlyside, N., … Chang, P. (2019). Pantropical climate interactions. *Science*, *363*, 11. https://doi.org/10.1126/science.aav4236

Canadell, J., Monteiro, P., Costa, M., Cotrim da Cunha, L., Cox, P., Eliseev, A., Henson, S., Ishii, M., Jaccard, S., Koven, C., Lohila, A., Patra, P., Piao, S., Rogelj, J., Syampungani, S., Zaehle, S., & Zickfeld, K. (2021). Global carbon and other biogeochemical cycles and feedbacks. In V. Masson-Delmotte, P. Zhai, A. Pirani, S. Connors, C. Péan, S. Berger, N. Caud, Y. Chen, L. Goldfarb, M. Gomis, M. Huang, K. Leitzell, E. Lonnoy, J. Matthews, T. Maycock, T. Waterfield, O. Yelekçi, R. Yu, & B. Zhou (Eds.), *Climate change 2021: The physical science basis. contribution of working group i to the sixth assessment report of the intergovernmental panel on climate change* (pp. 673–816). Cambridge University Press. https://doi.org/10.1017/9781009157896.007

Cao, W., Zahirovic, S., Flament, N., Williams, S., Golonka, J., & Müller, R. (2017). Improving global paleogeography since the late paleozoic using paleobiology. *Biogeosciences*, *14*, 5425–5439. https://doi.org/10.5194/bg-14-5425-2017

Cattano, C., Claudet, J., Domenici, P., & Milazzo, M. (2018). Living in a high co2 world: A global meta-analysis shows multiple trait-mediated fish responses to ocean acidification. *Ecological Monographs*, *88*(3), 320–335. https://doi.org/10.1002/ecm.1297

Chen, J., Shen, S.-Z., Li, X.-H., Xu, Y.-G., Joachimski, M., Bowring, S., Erwin, D., Yuan, D.-X., Chen, B., Zhang, H., Wang, Y., Cao, C.-Q., Zheng, Q.-F., & Mu, L. (2016). High-resolution sims oxygen isotope analysis on conodont apatite from south china and implications for the end-permian mass extinction. *Palaeogeography, Palaeoclimatology, Palaeoecology*, *448*, 26–38. https://doi.org/10.1016/j.palaeo.2015.11.025

Clapham, M., & Payne, J. (2011). Acidification, anoxia, and extinction: A multiple logistic regression analysis of extinction selectivity during the middle and late permian. *Geology*, *39*, 1059–1062. https://doi.org/10.1130/G32230.1

Clarkson, M., Kasemann, S., Wood, R., Lenton, T., Daines, S., Richoz, S., Ohnemueller, F., Meixner, A., Poulton, S., & Tipper, E. (2015). Ocean acidification and the permo-triassic mass extinction. *Science*, *348*, 229–232. https://doi.org/10.1126/science.aaa0193

Cornwall, C., Comeau, S., Kornder, N., Perry, C., van Hooidonk, R., DeCarlo, T., Pratchett, M., Anderson, K., Browne, N., Carpenter, R., Diaz-Pulido, G., D'Olivo, J., Doo, S., Figueiredo, J., Fortunato, S., Kennedy, E., Lantz, C., McCulloch, M., González-Rivero, M., ... Lowe, R. (2021). Global declines in coral reef calcium carbonate production under ocean acidification and warming. *Proceedings of the National Academy of Sciences*, *118*(e2015265118). https://doi.org/10.1073/pnas.2015265118

Cui, Y., & Kump, L. (2015). Global warming and the end-permian extinction event: Proxy and modeling perspectives. *Earth-Science Reviews*, *149*, 5–22. https://doi.org/10.1016/j.earscirev.2014.04.007

Cui, Y., Kump, L., & Ridgwell, A. (2013). Initial assessment of the carbon emission rate and climatic consequences during the end-permian mass extinction. *Palaeogeography, Palaeoclimatology, Palaeoecology*, *389*, 128–136. https://doi.org/10.1016/j.palaeo.2013.09.001

Cui, Y., Li, M., van Soelen, E., Peterse, F., & Kürschner, W. (2021). Massive and rapid predominantly volcanic co_2 emission during the end-permian mass extinction. *Proceedings of the National Academy of Sciences of the United States of America*, *118*(37), 11. https://doi.org/10.1073/pnas.2014701118

Cui, Y., Zhang, F., Wang, J., Jiang, S., & Shen, S. (2021). Marine anoxia and ocean acidification during the end-permian extinction: An integrated view from δ^{238}u and $\delta^{44/40}$ca proxies and earth system modelling. In R. Ernst, A. Dickson, & A. Bekker (Eds.), *Large igneous provinces* (pp. 325–340). American Geophysical Union (AGU). https://doi.org/10.1002/9781119507444.ch14

Dal Corso, J., H., S., Callegaro, S., Chu, D., Sun, Y., Hilton, J., Grasby, S., Joachimski, M., & Wignall, P. (2022). Environmental crises at the permian-triassic mass extinction. *Nature Reviews Earth and Environment*, 18. https://doi.org/10.1038/s43017-021-00259-4

De Viron, O., Dickey, J., & Ghil, M. (2013). Global modes of climate variability. *Geophysical Research Letters*, *40*, 1832–1837. https://doi.org/10.1002/grl.50386

Deser, C., Alexander, M., Xie, S.-P., & Phillips, A. (2010). Sea surface temperature variability: Patterns and mechanisms. *Annual Review of Marine Science*, *2*, 115–143. https://doi.org/10.1146/annurev-marine-120408-151453

Di Lorenzo, E., & Ohman, M. (2012). A double-integration hypothesis to explain ocean ecosystem response to climate forcing. *Proceedings of the National Academy of Sciences of the United States*

of America, *110*, 2496–2499. https://doi.org/10.1073/pnas.1218022110

Doney, S., Busch, D., Cooley, S., & Kroeker, K. (2020). The impacts of ocean acidification on marine ecosystems and reliant human communities. *Annual Review of Environment and Resources*, *45*, 83–112. https://doi.org/10.1146/annurev-environ-012320-083019

Doney, S., Fabry, V., Feely, R., & Kleypas, J. (2009). Ocean acidification: The other co2 problem. *Annual review of marine science*, *1*, 169–192. https://doi.org/10.1146/annurev.marine.010908.163834

Erwin, D. (1994). The permo-triassic extinction. *Nature*, *367*, 231–236. https://doi.org/10.1038/367231a0

Extier, T., Six, K., Liu, B., Paulsen, H., & Ilyina, T. (2022). Local oceanic co_2 outgassing triggered by terrestrial carbon fluxes during deglacial flooding. *Climate of the Past*, *18*(2), 273–292. https://doi.org/10.5194/cp-18-273-2022

Eyring, V., Gillett, N., Achuta Rao, K., Barimalala, R., Barreiro Parrillo, M., Bellouin, N., Cassou, C., Durack, P., Kosaka, Y., McGregor, S., Min, S., Morgenstern, O., & Su, Y. (2021). Human influence on the climate system. In V. Masson-Delmotte, P. Zhai, A. Pirani, S. Connors, C. Péan, S. Berger, N. Caud, Y. Chen, L. Goldfarb, M. Gomis, M. Huang, K. Leitzell, E. Lonnoy, J. Matthews, T. Maycock, T. Waterfield, O. Yelekçi, R. Yu, & B. Zhou (Eds.), *Climate change 2021: The physical science basis. contribution of working group i to the sixth assessment report of the intergovernmental panel on climate change* (pp. 423–552). Cambridge University Press. https://doi.org/10.1017/9781009157896.005

Feng, Q., & Algeo, T. (2014). Evolution of oceanic redox conditions during the permo-triassic transition: Evidence from deepwater radiolarian facies. *Earth-Science Reviews*, *137*, 34–51. https://doi.org/10.1016/j.earscirev.2013.12.003

Forster, P., Storelvmo, T., Armour, K., Collins, W., Dufresne, J.-L., Frame, D., Lunt, D., Mauritsen, T., Palmer, M., Watanabe, M., Wild, M., & Zhang, H. (2021). The earth's energy budget climate feedbacks and climate sensitivity. In V. Masson-Delmotte, P. Zhai, A. Pirani, S. Connors, C. Péan, S. Berger, N. Caud, Y. Chen, L. Goldfarb, M. Gomis, M. Huang, K. Leitzell, E. Lonnoy, J. Matthews, T. Maycock, T. Waterfield, O. Yelekçi, R. Yu, & B. Zhou (Eds.), *Climate change 2021: The physical science basis. contribution of working group i to the sixth assessment report of the intergovernmental panel on climate change* (pp. 923–1054). Cambridge University Press. https://doi.org/10.1017/9781009157896.009

Foster, W., Hirtz, J., Farrell, C., Reistroffer, M., Twitchett, R., & Martindale, R. (2022). Bioindicators of severe ocean acidification are absent from the end-permian mass extinction. *Scientific Reports*, *12*(1202). https://doi.org/10.1038/s41598-022-04991-9

Foster, W., & Twitchett, R. (2014). Functional diversity of marine ecosystems after the late permian mass extinction event. *Nature Geoscience*, *7*, 233–238. https://doi.org/10.1038/ngeo2079

Fourier, J. (1824). Remarques générales sur les températures du globe terrestre et des espaces planétaires. *Annales de Chimie et de Physique*, *27*, 136–167.

Fox-Kemper, B., Hewitt, H., Xiao, C., Aõalgeirsdóttir, G., Drijfhout, S., Edwards, T., Golledge, N., Hemer, M., Kopp, R., Krinner, G., Mix, A., Notz, D., Nowicki, S., Nurhati, I., Ruiz, L., Sallée, J.-B., Slangen, A., & Yu, Y. (2021). Ocean, cryosphere and sea level change. In V. Masson-Delmotte, P. Zhai, A. Pirani, S. Connors, C. Péan, S. Berger, N. Caud, Y. Chen, L. Goldfarb, M. Gomis, M. Huang, K. Leitzell, E. Lonnoy, J. Matthews, T. Maycock, T. Waterfield, O. Yelekçi, R. Yu, & B. Zhou (Eds.), *Climate change 2021: The physical science basis. contribution of working group i to the sixth assessment report of the intergovernmental panel on climate change* (pp. 1211–1362). Cambridge University Press. https://doi.org/10.1017/9781009157896.011

Fraedrich, K., Blender, R., & Zhu, X. (2009). Continuum climate variability: Long-term memory, scaling, and 1/f-noise. *International Journal of Modern Physics B*, *23*(28), 5403–5416. https://doi.org/10.1142/S0217979209063729

Friedlingstein, P., O'Sullivan, M., Jones, M., Andrew, R., Bakker, D., Hauck, J., Landschützer, P., Le Quére, C., Luijkx, I., Peters, G., Peters, W., Pongratz, J., Schwingshackl, C., Sitch, S., Canadell, J., Ciais, P., Jackson, R., Alin, S., Anthoni, P., … Zheng, B. (2023). Global carbon budget 2023. *Earth System Science Data*, *15*, 5301–5369. https://doi.org/10.5194/essd-15-5301-2023

Frölicher, T., Fischer, E., & Gruber, N. (2018). Marine heatwaves under global warming. *Nature*, *560*, 360–364. https://doi.org/10.1038/s41586-018-0383-9

Ganino, C., & Arndt, N. (2009). Climate changes caused by degassing of sediments during the emplacement of large igneous provinces. *Geology*, *37*, 323–326. https://doi.org/10.1130/G25325A.1

García Molinos, J., Halpern, B., Schoeman, D., Brown, C., Kiessling, W., Moore, P., Pandolfi, J., Poloczanska, E., Richardson, A., & Burrows, M. (2016). Climate velocity and the future global redistribution of marine biodiversity. *Nature Climate Change*, *6*, 83–88. https://doi.org/10.1038/NCLIMATE2769

Gliwa, J., Wiedenbeck, M., Schobben, M., Ullmann, C., Kiessling, W., Ghaderi, A., Struck, U., & Korn, D. (2022). Gradual warming prior to the end-permian mass extinction. *Palaeontology*, *65*(e12621). https://doi.org/10.1111/pala.12621

Gobler, C., & Baumann, H. (2016). Hypoxia and acidification in ocean ecosystems: Coupled dynamics and effects on marine life. *Bi-*

ology letters, *12*(20150976). https://doi.org/10.1098/rsbl.2015.0976

Godbold, J., & Calosi, P. (2013). Ocean acidification and climate change: Advances in ecology and evolution. *Philosophical Transactions of the Royal Society B: Biological Sciences*, *368*(20120448). https://doi.org/10.1098/rstb.2012.0448

Gonzalez, A., & Bell, G. (2013). Evolutionary rescue and adaptation to abrupt environmental change depends upon the history of stress. *Philosophical Transactions of the Royal Society B*, *368*(20120079). https://doi.org/10.1098/rstb.2012.0079

Gonzalez, A., Ronce, O., Ferriere, R., & Hochberg, M. (2013). Evolutionary rescue: An emerging focus at the intersection between ecology and evolution. *Philosophical Transactions of the Royal Society B*, *368*(20120404). https://doi.org/10.1098/rstb.2012.0404

Götze, S., Bock, C., Eymann, C., Lannig, G., Steffen, J., & Pörtner, H.-O. (2020). Single and combined effects of the "deadly trio" hypoxia, hypercapnia and warming on the cellular metabolism of the great scallop pecten maximus. *Comparative Biochemistry and Physiology Part B: Biochemistry and Molecular Biology*, *243*, 110438. https://doi.org/10.1016/j.cbpb.2020.110438

Grard, A., Francois, L., Dessert, C., Dupré, B., & Godderis, Y. (2005). Basaltic volcanism and mass extinction at the permo-triassic boundary: Environmental impact and modeling of the global carbon cycle. *Earth and Planetary Science Letters*, *234*, 207–221. https://doi.org/10.1016/j.epsl.2005.02.027

Grossman, E., & Joachimski, M. (2022). Ocean temperatures through the phanerozoic reassessed. *Scientific Reports*, *12*(8938), 13. https://doi.org/10.1038/s41598-022-11493-1

Gruber, N. (2011). Warming up, turning sour, losing breath: Ocean biogeochemistry under change. *Philosophical Transactions of the Royal Society A*, *369*, 1980–1996. https://doi.org/10.1098/rsta.2011.0003

Gulev, S., Thorne, P., Ahn, J., Dentener, F., Domingues, C., Gerland, S., Gong, D., Kaufman, D., Nnamchi, H., Quaas, J., Rivera, J., Sathyendranath, S., Smith, S., Trewin, B., von Schuckmann, K., & Vose, R. (2021). Changing state of the climate system. In V. Masson-Delmotte, P. Zhai, A. Pirani, S. Connors, C. Péan, S. Berger, N. Caud, Y. Chen, L. Goldfarb, M. Gomis, M. Huang, K. Leitzell, E. Lonnoy, J. Matthews, T. Maycock, T. Waterfield, O. Yelekçi, R. Yu, & B. Zhou (Eds.), *Climate change 2021: The physical science basis. contribution of working group i to the sixth assessment report of the intergovernmental panel on climate change* (pp. 287–422). Cambridge University Press. https://doi.org/10.1017/9781009157896.004

Harnik, P., Lotze, H., Anderson, S., Finkel, Z., Finnegan, S., Lindberg, D., Liow, L., Lockwood, R., McClain, C., McGuire, J., O'Dea,

A., Pandolfi, J., Simpson, C., & Tittensor, D. (2012). Extinctions in ancient and modern seas. *Trends in Ecology & Evolution*, *27*, 608–617. https://doi.org/10.1016/j.tree.2012.07.010

Harris, R., Beaumont, L., Vance, T., Tozer, C., Remenyi, T., Perkins-Kirkpatrick, S., Mitchell, P., Nicotra, A., McGregor, S., Andrew, N., Letnic, M., Kearney, M., Wernberg, T., Hutley, L., Chambers, L., Fletcher, M.-S., Keatley, M., Woodward, C., Williamson, G., … Bowman, D. (2018). Biological responses to the press and pulse of climate trends and extreme events. *Nature Climate Change*, *8*, 579–587. https://doi.org/10.1038/s41558-018-0187-9

Hay, W., Migdisov, A., Balukhovsky, A., Wold, C., Flögel, S., & Söding, E. (2006). Evaporites and the salinity of the ocean during the phanerozoic: Implications for climate, ocean circulation and life. *Palaeogeography, Palaeoclimatology, Palaeoecology*, *240*, 3–46. https://doi.org/10.1016/j.palaeo.2006.03.044

Haywood, A., Valdes, P., Aze, T., Barlow, N., Burke, A., Dolan, A., Von Der Heydt, A., Hill, D., Jamieson, S., Otto-Bliesner, B., Salzmann, U., Saupe, E., & Voss, J. (2019). What can palaeoclimate modelling do for you? *Earth Systems and Environment*, *3*, 1–18. https://doi.org/10.1007/s41748-019-00093-1

Heinze, C., Maier-Reimer, E., Winguth, A., & Archer, D. (1999). A global oceanic sediment model for long-term climate studies. *Global Biogeochemical Cycles*, *13*, 221–250. https://doi.org/10.1029/98GB02812

Heinze, M., & Ilyina, T. (2015a). Effects of changing ocean circulation on the marine carbon cycle during the paleocene-eocene thermal maximum. *Nova Acta Leopoldina NF*, *121*(408), 301–303.

Heinze, M., & Ilyina, T. (2015b). Ocean biogeochemistry in the warm climate of the late pleocene. *Climate of the Past*, *11*(1), 63–79. https://doi.org/10.5194/cp-11-63-2015

Herbert, F. (1976). *Children of Dune*. Gollancz.

Hoegh-Guldberg, O., Mumby, P., Hooten, A., Steneck, R., Greenfield, P., Gomez, E., Harvell, C., Sale, P., Edwards, A., Caldeira, K., Knowlton, N., Eakin, C., Iglesias-Prieto, R., Muthiga, N., Bradbury, R., Dubi, A., & Hatziolos, M. (2007). Coral reefs under rapid climate change and ocean acidification. *Science*, *318*(5857), 1737–1742. https://doi.org/10.1126/science.1152509

Hoffmann, A., & Sgrò. (2011). Climate change and evolutionary adaptation. *Nature*, *470*, 479–485. https://doi.org/10.1038/nature09670

Holbrook, N., Claar, D., Hobday, A., McInnes, K., Oliver, E., Sen Gupta, A., Widlansky, M., & Zhang, X. (2021). Enso-driven ocean extremes and their ecosystem impacts. In M. McPhaden, A. Santoso, & W. Cai (Eds.), *El niño southern oscillation in a*

changing climate (pp. 409–428). American Geophysical Union (AGU). https://doi.org/10.1002/9781119548164.ch18

Holser, W., Schönlaub, H., Boeckelmann, K., Magaritz, M., & Orth, C. (1991). The permian–triassic of the gartnerkofel-1 core (carnic alps, austria): Synthesis and conclusions. *Abhandlungen der Geologischen Bundesanstalt*, *45*, 213–232.

Hotinski, R., Bice, L., Karen, Kump, L., Najjar, R., & Arthur, M. (2001). Ocean stagnation and end-permian anoxia. *Geology*, *29*(1), 7–10. https://doi.org/10.1130/0091-7613(2001)029<0007:OSAEPA>2.0.CO;2

Hu, S., Li, S., Zhang, Y., Guan, C., Du, Y., Feng, M., Ando, K., Wang, F., Schiller, A., & Hu, D. (2021). Observed strong subsurface marine heatwaves in the tropical western pacific ocean. *Environmental Research Letters*, *16*(104024). https://doi.org/10.1088/1748-9326/ac26f2

Hülse, D., Lau, K., van de Velde, S., Arndt, S., Meyer, K., & Ridgwell, A. (2021). End-permian marine extinction due to temperature-driven nutrient cycling and euxinia. *Nature Geoscience*, *14*, 862–867. https://doi.org/10.1038/s41561-021-00829-7

Hyun, S.-H., Yeh, S.-W., Kirtman, B., & An, S.-I. (2022). Internal climate variability in the present climate and the change in enso amplitude in future climate simulations. *Frontiers in climate*, *4*(932978). https://doi.org/10.3389/fclim.2022.932978

Ilyina, T., & Heinze, M. (2019). Carbonate dissolution enhanced by ocean stagnation and respiration at the onset of the paleocene-eocene thermal maximum. *Geophysical Research Letters*, *46*(2), 842–852. https://doi.org/10.1029/2018GL080761

Ilyina, T., Six, K., Segschneider, J., Maier-Reimer, E., Li, H., & Núñez-Riboni, I. (2013). Global ocean biogeochemistry model hamocc: Model architecture and performance as component of the mpi-earth system model in different cmip5 experimental realizations. *Journal of Advances in Modeling Earth Systems*, *5*, 287–315. https://doi.org/10.1029/2012MS000178

Isozaki, Y. (1997). Permo-triassic boundary superanoxia and stratified superocean: Records from lost deep sea. *Science*, *276*, 235–238. https://doi.org/10.1126/science.276.5310.235

Jacox, M., Alexander, M., Bograd, S., & Scott, J. (2020). Thermal displacement by marine heatwaves. *Nature*, *584*, 82–86. https://doi.org/10.1038/s41586-020-2534-z

Joachimski, M., Alekseev, A., Grigoryan, A., & Gatovsky, Y. (2020). Siberian trap volcanism, global warming and the permian-triassic mass extinction: New insights from the armenian permian-triassic sections. *Geological Society of America Bulletin*, *132*(1-2), 427–443. https://doi.org/10.1130/B35108.1

Joachimski, M., Lai, X., Shen, S., Jiang, H., Luo, G., Chen, B., Chen, J., & Sun, Y. (2012). Climate warming in the latest permian and the

permian-triassic mass extinction. *Geological Society of America Bulletin*, *40*(3), 195–198. https://doi.org/10.1130/G32707.1

Joachimski, M., Müller, J., Gallagher, T., Mathes, G., Chu, D., Mouraviev, F., Silantiev, V., Sun, Y., & Tong, J. (2022). Five million years of high atmospheric co_2 in the aftermath of the permian-triassic mass extinction. *Geology*, *50*, 13. https://doi.org/10.1130/G49714.1

Jurikova, H., Gutjahr, M., Wallmann, K., Flögel, S., Liebetrau, V., Posenato, R., Angiolini, L., Garbelli, C., Brand, U., M., W., & Eisenhauer, A. (2020). Permian-triassic mass extinction pulses driven by major marine carbon cycle perturbations. *Nature Geoscience*, *13*, 745–750. https://doi.org/10.1038/s41561-020-00646-4

Kaiho, K., Oba, M., Fukuda, Y., Ito, K., Ariyoshi, S., Gorjan, P., Riu, Y., Takahashi, S., Chen, Z.-Q., Tong, J., & Yamakita, S. (2012). Changes in depth-transect redox conditions spanning the end-permian mass extinction and their impact on the marine extinction: Evidence from biomarkers and sulfur isotopes. *Global and Planetary Change*, *94-95*, 20–32. https://doi.org/10.1016/j.gloplacha.2012.05.024

Kapsch, M.-L., Mikolajewicz, U., Ziemen, F., Rodehacke, C., & Schannwell, C. (2021). Analysis of the surface mass balance for deglacial climate simulations. *The Cryosphere*, *15*(2), 1131–1156. https://doi.org/10.5194/tc-15-1131-2021

Kapsch, M.-L., Mikolajewicz, U., Ziemen, F., & Schannwell, C. (2022). Ocean response to transient simulations of the last deglaciation dominated by underlying ice-sheet reconstruction and method of meltwater distribution. *Geophysical Research letters*, *49*(3), 11. https://doi.org/10.1029/2021GL096767

Keeling, R., Körtzinger, A., & Gruber, N. (2010). Ocean deoxygenation in a warming world. *Annual review of marine science*, *2*, 199–229. https://doi.org/10.1146/annurev.marine.010908.163855

Kemp, D., & Sexton, P. (2014). Time-scale uncertainty of abrupt events in the geologic record arising from unsteady sedimentation. *Geology*, *42*, 891–894. https://doi.org/10.1130/G35783.1

Kiehl, J., & Shields, C. (2005). Climate simulation of the latest permian: Implications for mass extinction. *Geology*, *33*(9), 757–760. https://doi.org/10.1130/G21654.1

Klausmeier, C., Osmond, M., Kremer, C., & Litchman, E. (2020). Ecological limits to evolutionary rescue. *Philosophical Transactions of the Royal Society B*, *375*(20190453). https://doi.org/10.1098/rstb.2019.0453

Klein, S., Geraldi, N., Anton, A., Schmidt-Roach, S., Ziegler, M., Cziesielski, M., Martin, C., Rädecker, N., Frölicher, T., Mumby, P., Pandolfi, J., Suggett, D., Voolstra, C., Aranda, M., & Duarte, C. (2022). Projecting coral responses to intensifying marine

heatwaves under ocean acidification. *Global change biology*, *28*, 1753–1765. https://doi.org/10.1111/gcb.15818

Kleinen, T., Mikolajewicz, U., & Brovkin, V. (2020). Terrestrial methane emissions from the last glacial maximum to the preindustrial period. *Climate of the Past*, *16*(2), 575–595. https://doi.org/10.5194/cp-16-575-2020

Kleypas, J., Castruccio, F., Curchitser, E., & Mcleod, E. (2015). The impact of enso on coral heat stress in the western equatorial pacific. *Global Change Biology*, *21*(7), 2525–2539. https://doi.org/10.1111/gcb.12881

Knoll, A., Bambach, R., Payne, J., Pruss, S., & Fischer, W. (2007). Paleophysiology and end-permian mass extinction. *Earth and Planetary Science Letters*, *256*, 295–313. https://doi.org/10.1016/j.epsl.2007.02.018

Kocsis, Á. T., & Scotese, C. R. (2021). Mapping paleocoastlines and continental flooding during the phanerozoic. *Earth-Science Reviews*, *213*(103463), 15. https://doi.org/10.1016/j.earscirev.2020.103463

Kriest, I., & Oschlies, A. (2008). On the treatment of particulate organic matter sinking in large-scale models of marine biogeochemical cycles. *Biogeosciences*, *5*, 55–72. https://doi.org/10.5194/bg-5-55-2008

Kroeker, K., Kordas, R., Crim, R., Hendriks, I., Ramajo, L., Singh, G., Duarte, C., & Gattuso, J.-P. (2013). Impacts of ocean acidification on marine organisms: Quantifying sensitivities and interaction with warming. *Global change biology*, *19*, 1884–1896. https://doi.org/10.1111/gcb.12179

Kug, J.-S., Jin, F.-F., & An, S.-I. (2009). Two types of el niño events: Cold tongue el niño and warm pool el niño. *Journal of Climate*, *22*, 1499–1515. https://doi.org/10.1175/2008JCLI2624.1

Kwiatkowski, L., Torres, O., Bopp, L., Aumont, O., Chamberlain, M., Christian, J. R., Dunne, J. P., Gehlen, M., Ilyina, T., John, J. G., Lenton, A., Li, H., Lovenduski, N. S., Orr, J. C., Palmieri, J., Santana-Falcón, Y., Schwinger, J., Séférian, R., Stock, C. A., … Ziehn, T. (2020). Twenty-first century warming, acidification, deoxygenation and upper-ocean nutrient and primary production decline from cmip6 model projections. *Bigeosciences*, *17*, 3439–3470. https://doi.org/10.5194/bg-17-3439-2020

Lau, K., Maher, K., Altiner, D., Kelley, B., Kump, L., Lehrmann, D., Silva-Tamayo, J., Weaver, K., Yu, M., & Payne, J. (2016). Marine anoxia and delayed earth system recovery after the end-permian extinction. *Proceedings of the National Academy of Sciences of the United States of America*, *113*, 2360–2365. https://doi.org/10.1073/pnas.1515080113

Lawton, J. (1988). More time means more variation. *Nature*, *334*, 563. https://doi.org/10.1038/334563a0

Le Grix, N., Zscheischler, J., Rodgers, K., Yamaguchi, R., & Frölicher, T. (2022). Hotspots and drivers of compound marine heatwaves and low net primary production extremes. *Biogeosciences*, *19*, 5807–5835. https://doi.org/10.5194/bg-19-5807-2022

Lehodey, P., Bertrand, A., Hobday, A., Kiyofuji, H., McClatchie, S., Menkès, C., Pilling, G., Polovina, J., & Tommasi, D. (2021). Enso impact on marine fisheries and ecosystems. In M. McPhaden, A. Santoso, & W. Cai (Eds.), *El niño southern oscillation in a changing climate* (pp. 429–451). American Geophysical Union (AGU). https://doi.org/10.1002/9781119548164.ch19

Levin, L. (2018). Manifestation, drivers, and emergence of open ocean deoxygenation. *Annual review of marine science*, *10*, 229–260. https://doi.org/10.1146/annurev-marine-121916-063359

Lewandowska, A., Boyce, D., Hofmann, M., Matthiessen, B., Sommer, U., & Worm, B. (2014). Effects of sea surface warming on marine plankton. *Ecology letters*, *17*(5), 614–623. https://doi.org/10.1111/ele.12265

Li, C., Huang, J., Ding, L., Liu, X., Yu, H., & Huang, J. (2020). Increasing escape of oxygen from oceans under climate change. *Geophysical Research Letters*, *47*(e2019GL086345). https://doi.org/10.1029/2019GL086345

Li, H., Yu, J., McElwain, J., Yiotis, C., & Chen, Z.-Q. (2019). Reconstruction of atmospheric co_2 during the late changhsingian based on fossil conifers from the dalong formation in south china. *Palaeogeography, Palaeoclimatology, Palaeoecology*, *519*, 37–48. https://doi.org/10.1016/j.palaeo.2018.09.006

Li, Y., Gao, M., Zhang, Z., Duan, J., & Xue, Y. (2023). Phased human-nature interactions for the past 10000 years in the hexi corridor, china. *Environmental Research Letters*, *18*(044035). https://doi.org/10.1088/1748-9326/acc87b

Liu, B., Six, K., & Ilyina, T. (2021). Incorporating the stable carbon isotope ^{13}c in the ocean biogeochemical component of the max planck institute earth system model. *Biogeosciences*, *18*(14), 4389–4429. https://doi.org/10.5194/bg-18-4389-2021

Liu, G., Feng, Q., & Gu, S. (2008). Extinction pattern and process of siliceous sponge spicules in deep-water during the latest permian in south china. *Science in China Series D: Earth Sciences*, *51*(11), 1623–1632. https://doi.org/10.5194/bg-18-4389-2021

Maerz, J., Six, K., Stemmler, I., Ahmerkamp, S., & Ilyina, T. (2020). Microstructure and composition of marine aggregates as co-determinants for vertical particulate organic carbon transfer in the global ocean. *Biogeosciences*, *17*, 1765–1803. https://doi.org/10.5194/bg-17-1765-2020

Maier-Reimer, E. (1993). Geochemical cycles in an ocean general circulation model. preindustrial tracer distributions. *Global Bio-*

geochemical Cycles, *7*(3), 645–677. https://doi.org/10.1029/93GB01355

Martin, J., Knauer, G., Karl, D., & Broenkow, W. (1987). Vertex: Carbon cycling in the northeast pacific. *Deep-Sea Research Part A. Oceanographic Research Papers*, *34*(2), 267–285. https://doi.org/10.1016/0198-0149(87)90086-0

Mauritsen, T., Bader, J., Becker, T., Behrens, J., Bittner, M., Brokopf, R., Brovkin, V., Claussen, M., Crueger, T., Esch, M., Fast, I., Fiedler, S., Fläschner, D., Gayler, V., Giorgetta, M., Goll, D., Haak, H., Hagemann, S., Hedemann, C., … Roeckner, E. (2019). Developments in the mpi-m earth system model version 1.2 (mpi-esm1.2) and its response to increasing co_2. *Journal of Advances in Modeling Earth Systems*, *11*, 998–1038. https://doi.org/10.1029/2018MS001400

McManus, L., Vasconcelos, V., Levin, S., Thompson, D., Kleypas, J., Castruccio, F., Curchitser, E., & Watson, J. (2019). Extreme temperature events will drive coral decline in the coral triangle. *Global Change Biology*, *26*, 2120–2133. https://doi.org/10.1111/gcb.14972

Meehl, G., Senior, C., Eyring, V., Flato, J.-F., Lamarque, Stouffer, R., Taylor, K., & Schlund, M. (2020). Context for interpreting equilibrium climate sensitivity and transient climate response from the cmip6 earth system models. *Science Advances*, *6*(eaba1981), 10. https://doi.org/10.1126/sciadv.aba1981

Messerli, B., Grosjean, M., Hofer, T., Núñe, L., & Pfister, C. (2000). From nature-dominated to human-dominated environmental changes. *Quaternary Science Reviews*, *19*, 459–479. https://doi.org/10.1016/S0277-3791(99)00075-X

Meyer, K., Kump, L., & Ridgwell, A. (2008). Biogeochemical controls on photic-zone euxinia during the end-permian mass extinction. *Geology*, *36*(9), 747–750. https://doi.org/10.1130/G24618A.1

Monteiro, P., & van der Plas, A. (2006). Low oxygen water (low) variability in the benguela system: Key processes and forcing scales relevant to forecasting. *Large Marine Ecosystems*, *14*, 71–90. https://doi.org/10.1016/S1570-0461(06)80010-8

Montenegro, A., Spence, P., Meissner, K., Eby, M., Melchin, M., & Johnston, S. (2011). Climate simulations of the permian-triassic boundary: Ocean acidification and the extinction event. *Paleoceanography*, *26*(PA3207), 19. https://doi.org/10.1029/2010PA002058

Moore, J., Doney, S., Kleypas, J., Glover, D., & Fung, I. (2001). An intermediate complexity marine ecosystem model for the global domain. *Deep Sea Research Part II: Topical Studies in Oceanography*, *49*, 403–462. https://doi.org/10.1016/S0967-0645(01)00108-4

Morée, A., Clarke, T., Cheung, W., & Frölicher, T. (2023). Impact of deoxygenation and warming on global marine species in the

21st century. *Biogeosciences*, *20*, 2425–2454. https://doi.org/10.5194/bg-20-2425-2023

Müller, J., Sun, Y., Yang, F., Regelous, M., & Joachimski, M. (2023). Manganous water column in the tethys ocean during the permian-triassic transition. *Global and Planetary Change*, *222*(104067). https://doi.org/10.1016/j.gloplacha.2023.104067

Nguyen, H., Ralph, P., Marín-Guirao, L., Pernice, M., & Procaccini, G. (2021). Seagrasses in an era of ocean warming: A review. *Biological reviews*, *96*(5), 2009–2030. https://doi.org/10.1111/brv.12736

Nowak, H., Vérard, C., & Kustatscher, E. (2020). Palaeophytogeographical patterns across the permian-triassic boundary. *Frontiers in Earth Science*, *8*(613350), 16. https://doi.org/10.3389/feart.2020.613350

Ogden, D., & Sleep, N. (2012). Explosive eruption of coal and basalt and the end-permian mass extinction. *Proceedings of the National Academy of Sciences*, *109*, 59–62. https://doi.org/10.1073/pnas.1118675109

Oliver, E., Benthuysen, J., Darmaraki, S., Donat, M., Hobday, A., Holbrook, N., Schlegel, R., & Sen Gupta, A. (2020). Marine heatwaves. *Annual Review of Marine Science*, *13*, 313–342. https://doi.org/10.1146/annurev-marine-032720-095144

Orr, J., Fabry, V., Aumont, O., Bopp, L., Doney, S., Feely, R., Gnanadesikan, A., Gruber, N., Ishida, A., Joos, F., Key, R., Lindsay, K., Maier-Reimer, E., Matear, R., Monfray, P., Mouchet, A., Najjar, R., Plattner, G.-K., Rodgers, K., … Yool, A. (2005). Anthropogenic ocean acidification over the twenty-first century and its impact on calcifying organisms. *Nature*, *437*(7059), 681–686. https://doi.org/10.1038/nature04095

Osen, A., Winguth, A., Winguth, C., & Scotese, C. (2013). Sensitivity of late permian climate to bathymetric features and implications for the mass extinction. *Global and Planetary Change*, *105*, 171–179. https://doi.org/10.1016/j.gloplacha.2012.01.011

Paulsen, H., Ilyina, I., Six, K., & Stemmler, I. (2017). Incorporating a prognostic representation of marine nitrogen fixers into the global ocean biogeochemical model hamocc. *Journal of Advances in Modeling Earth Systems*, *9*, 438–464. https://doi.org/10.1002/2016MS000737

Payne, J., & Clapham, M. (2012). End-permian mass extinction in the oceans: An ancient analog for the twenty-first century? *Annual Reviews of Earth and Planetary Sciences*, *40*, 89–111. https://doi.org/10.1146/annurev-earth-042711-105329

Payne, J., Turchyn, A., Paytan, A., DePaolo, D., Lehrmann, D., Yu, M., & Wei, J. (2010). Calcium isotope constraints on the end-permian mass extinction. *Proceedings of the National Academy*

of Sciences of the United States of America, *107*, 8543–8548. https://doi.org/10.1073/pnas.0914065107

Penn, J., & Deutsch, C. (2022). Avoiding ocean mass extinction from climate warming. *Science*, *376*, 524–526. https://doi.org/10.1126/science.abe9039

Penn, J., Deutsch, C., Payne, J., & Sperling, E. (2018). Temperature-dependent hypoxia explains biogeography and severity of end-permian marine mass extinction. *Science*, *362*, eaat1327. https://doi.org/10.1126/science.aat1327

Previdi, M., Smith, K., & Polvani, L. (2021). Arctic amplification of climate change: A review of underlying mechanisms. *Environmental Research Letters*, *16*(093003). https://doi.org/10.1088/1748-9326/ac1c29

Ramírez, F., Afán, I., Davis, L., & Chiaradia, A. (2017). Climate impacts on global hot spots of marine biodiversity. *Science Advances*, *3*(e1601198). https://doi.org/10.1126/sciadv.1601198

Rampino, M., & Caldeira, K. (2005). Major perturbation of ocean chemistry and a 'strangelove ocean'after the end-permian mass extinction. *Terra Nova*, *17*, 554–559. https://doi.org/10.1111/j.1365-3121.2005.00648.x

Reddin, C., Kocsis, Á., & Kiessling, W. (2019). Climate change and the latitudinal selectivity of ancient marine extinctions. *Paleobiology*, *45*, 70–84. https://doi.org/10.1017/pab.2018.34

Riddick, T., Brovkin, V., Hagemann, S., & Mikolajewicz, U. (2018). Dynamic hydrological discharge modelling for coupled climate model simulations of the last glacial cycle: The mpi-dynamichd model version 3.0. *Geoscientific Model Development*, *11*(10), 4291–4316. https://doi.org/10.5194/gmd-11-4291-2018

Ridgwell, A., Hargreaves, J., Edwards, N., Annan, J., Lenton, T., Marsh, R., Yool, A., & Watson, A. (2007). Marine geochemical data assimilation in an efficient earth system model of global biogeochemical cycling. *Biogeosciences*, *4*, 87–104. https://doi.org/10.5194/bg-4-87-2007

Rigby, J., & Senowbari-Daryan, B. (1995). Permian sponge biogeography and biostratigraphy. In P. Scholle, T. Peryt, & D. Ulmer-Scholle (Eds.), *The permian of northern pangea* (pp. 153–166). Springer. https://doi.org/10.1007/978-3-642-78593-1_10

Sampaio, E., Santos, C., Rosa, I., Ferreira, V., Pörtner, H.-O., Duarte, C., Levin, L., & Rosa, R. (2021). Impacts of hypoxic events surpass those of future ocean warming and acidification. *Nature Ecology & Evolution*, *5*(3), 311–321. https://doi.org/10.1038/s41559-020-01370-3

Santos, C., Sampaio, E., Pereira, B., Pegado, M., Borges, F., Wheeler, C., Bouyoucos, I., Rummer, J., Frazao Santos, C., & Rosa, R. (2021). Elasmobranch responses to experimental warming, acidifica-

tion, and oxygen loss—a meta-analysis. *Frontiers in Marine Science*, *8*(735377). https://doi.org/10.3389/fmars.2021.735377

Schmidtko, S., Stramma, L., & Visbeck, M. (2017). Decline in global oceanic oxygen content during the past five decades. *Nature*, *542*(7641), 335–339. https://doi.org/10.1038/nature21399

Schobben, M., Foster, W., Sleveland, A., Zuchuat, V., Svensen, H., Planke, S., Bond, D., Marcelis, F., Newton, R., Wignall, P., & Poulton, S. (2020). A nutrient control on marine anoxia during the end-permian mass extinction. *Nature Geoscience*, *13*, 640–646. https://doi.org/10.1038/s41561-020-0622-1

Schobben, M., Stebbins, A., Ghaderi, A., Strauss, H., Korn, D., & Korte, C. (2015). Flourishing ocean drives the end-permian marine mass extinction. *Proceedings of the National Academy of Sciences of the United States of America*, *112*(33), 10298–10303. https://doi.org/10.1073/pnas.1503755112

Seton, M., Müller, R., Zahirovic, S., Williams, S., Wright, N., Cannon, J., Whittaker, J., Matthews, K., & McGirr, R. (2020). A global data set of present-day oceanic crustal age and seafloor spreading parameters. *Geochemistry, Geophysics, Geosystems*, *21*(e2020GC009214). https://doi.org/10.1029/2020GC009214

Shen, S.-Z., Cao, C.-Q., Zhang, H., Bowring, S., Henderson, C., Payne, J., Davydov, V., Chen, B., Yuan, D.-X., Zhang, Y.-C., Wang, W., & Zheng, Q. (2013). High-resolution $\delta^{13}c_{carb}$ chemostratigraphy from latest guadalupian through earliest triassic in south china and iran. *Earth and Planetary Science Letters*, *375*, 156–165. https://doi.org/10.1016/j.epsl.2013.05.020

Shen, S.-Z., Crowley, J., Wang, Y., Bowring, S., Erwin, D., Sadler, P., Cao, C.-Q., Rothman, D., Henderson, C., Ramezani, J., Zhang, H., Shen, Y., Wang, X.-D., Wang, W., Mu, L., Li, W.-Z., Tang, Y.-G., Liu, X.-L., Liu, L.-J., … Jin, Y.-G. (2011). Calibrating the end-permian mass extinction. *Science*, *334*, 1367–1372. https://doi.org/10.1126/science.1213454

Shen, Y., Farquhar, J., Zhang, H., Masterson, A., Zhang, T., & Wing, B. (2011). Multiple s-isotopic evidence for episodic shoaling of anoxic water during the late permian mass extinction. *Nature Communications*, *2*(210). https://doi.org/10.1038/ncomms1217

Shields, C., & Kiehl, J. (2018). Monsoonal precipitation in the paleo-tethys warm pool during the latest permian. *Palaeogeography, Palaeoclimatology, Palaeoecology*, *491*, 123–136. https://doi.org/10.1016/j.palaeo.2017.12.001

Six, K., & Maier-Reimer, E. (1996). Effects of plankton dynamics on seasonal carbon fluxes in an ocean general circulation model. *Global Biogeochemical Cycles*, *10*(4), 559–583. https://doi.org/10.1029/96GB02561

Smale, D., Wernberg, T., Oliver, E., Thomsen, M., Harvey, B., Straub, S., Burrows, M., Alexander, L., Benthuysen, J., Donat, M., Feng,

M., Hobday, A., Holbrook, N., Perkins-Kirkpatrick, S., Scannell, H., Sen Gupta, A., Payne, B., & Moore, P. (2019). Marine heatwaves threaten global biodiversity and the provision of ecosystem services. *Nature Climate Change*, *9*, 306–312. https://doi.org/10.1038/s41558-019-0412-1

Smith, K., Burrows, M., Hobday, A., King, N., Moore, P., Sen Gupta, A., Thomsen, M., Wernberg, T., & Smale, D. (2023). Biological impacts of marine heatwaves. *Annual Review of Marine Science*, *15*, 119–145. https://doi.org/10.1146/annurev-marine-032122-121437

Smith, R., Dubois, C., & Marotzke, J. (2004). Ocean circulation and climate in an idealised pangean oagcm. *Geophysical research letters*, *31*(L18207). https://doi.org/10.1029/2004GL020643

Song, H., Wignall, P., Tong, J., Bond, D., Song, H., Lai, X., Zhang, K., Wang, H., & Chen, Y. (2012). Geochemical evidence from bio-apatite for multiple oceanic anoxic events during permian-triassic transition and the link with end-permian extinction and recovery. *Earth and Planetary Science Letters*, *353-354*, 12–21. https://doi.org/10.1016/j.epsl.2012.07.005

Song, H., Wignall, P., Tong, J., & Yin, H. (2013). Two pulses of extinction during the permian-triassic crisis. *Nature geoscience*, *6*, 52–56. https://doi.org/10.1038/NGEO1649

Sperling, E., & Ingle, J. (2006). A permian-triassic boundary section at quinn river crossing, northwestern nevada, and implications for the cause of the early triassic chert gap on the western pangean margin. *Geological Society of America Bulletin*, *118*, 733–746. https://doi.org/10.1130/B25803.1

Steckbauer, A., Klein, S., & Duarte, C. (2020). Additive impacts of deoxygenation and acidification threaten marine biota. *Global change biology*, *26*, 5602–5612. https://doi.org/10.1111/gcb.15252

Stordal, F., Svensen, H., Aarnes, I., & Roscher, M. (2017). Global temperature response to century-scale degassing from the siberian traps large igneous province. *Palaeogeography, Palaeoclimatology, Palaeoecology*, *471*, 96–107. https://doi.org/10.1016/j.palaeo.2017.01.045

Stramma, L., Johnson, G., Sprintall, J., & Mohrholz, V. (2008). Expanding oxygen-minimum zones in the tropical oceans. *science*, *320*(5876), 655–658. https://doi.org/10.1126/science.1153847

Stramma, L., Schmidtko, S., Levin, L., & Johnson, G. (2010). Ocean oxygen minima expansions and their biological impacts. *Deep Sea Research Part I: Oceanographic Research Papers*, *57*(4), 587–595. https://doi.org/10.1016/j.dsr.2010.01.005

Stuart-Smith, R., Edgar, G., Barrett, N., Kininmonth, S., & Bates, A. (2015). Thermal biases and vulnerability to warming in the

world's marine fauna. *Nature*, *528*, 88–92. https://doi.org/10.1038/nature16144

Sun, Y., Zulla, M., Joachimski, M., Bond, D., Wignall, P., Zhang, Z., & Zhang, M. (2019). Ammonium ocean following the end-permian mass extinction. *Earth and Planetary Science Letters*, *518*, 211–222. https://doi.org/10.1016/j.epsl.2019.04.036

Sunday, J., Bennett, J., Calosi, P., Clusella-Trullas, S., Gravel, S., Hargreaves, A., Leiva, F., Verberk, W., Olalla-Tárraga, M., & Morales-Castilla, I. (2019). Thermal tolerance patterns across latitude and elevation. *Philosophical Transactions of the Royal Society B*, *374*(20190036). https://doi.org/10.1098/rstb.2019.0036

Svensen, H., Planke, S., Polozov, A., Schmidbauer, N., Corfu, F., Podladchikov, Y., & Jamtveit, B. (2009). Siberian gas venting and the end-permian environmental crisis. *Earth and Planetary Science Letters*, *277*, 490–500. https://doi.org/10.1016/j.epsl.2008.11.015

Takahashi, K., Montecinos, A., Goubanova, K., & Dewitte, B. (2011). Enso regimes: Reinterpreting the canonical and modoki el niño. *Geophysical Research Letters*, *38*(L10704). https://doi.org/10.1029/2011GL047364

Thomson, J., Burkholder, D., Heithaus, M., Fourqurean, J., Fraser, M., Statton, J., & Kendrick, G. (2015). Extreme temperatures, foundation species, and abrupt ecosystem change: An example from an iconic seagrass ecosystem. *Global change biology*, *21*(4), 1463–1474. https://doi.org/10.1111/gcb.12694

Tian, X., & Wang, Y. (2021). Compositional characteristics and paleoenvironmental significance of changhsingian (late permian) sponge reefs in south china. *Arabian Journal of Geosciences*, *14*(1067). https://doi.org/10.1007/s12517-021-07377-9

Timmermann, A., An, S.-I., Kug, J.-S., Jin, F.-F., Cai, W., Capotondi, A., Cobb, K., Lengaigne, M., McPhaden, M., Stuecker, M., Stein, K., Wittenberg, A., Yun, K.-S., Bayr, T., Chen, H.-C., Chikamoto, Y., Dewitte, B., Dommenget, D., Grothe, P., ... Zhang, X. (2018). El niño-southern oscillation complexity. *Nature*, *559*, 535–545. https://doi.org/10.1038/s41586-018-0252-6

Vaquer-Sunyer, R., & Duarte, C. (2008). Thresholds of hypoxia for marine biodiversity. *Proceedings of the National Academy of Sciences*, *105*(40), 15452–15457. https://doi.org/10.1073/pnas.0803833105

Vasseur, D., & Yodzis, P. (2004). The color of environmental noise. *Ecology*, *85*, 1145–1152. https://doi.org/10.1890/02-3122

Wang, M., Jeong, C.-B., Lee, Y., & Lee, J.-S. (2018). Effects of ocean acidification on copepods. *Aquatic Toxicology*, *196*, 17–24. https://doi.org/10.1016/j.aquatox.2018.01.004

Wignall, P., & Twitchett, R. (1996). Oceanic anoxia and the end permian mass extinction. *Science*, *272*(5265), 1155–1158. https://doi.org/10.1126/science.272.5265.1155

Wignall, P., & Twitchett, R. (2002). Extent, duration, and nature of the permian-triassic superanoxic event. In C. Koeberl & K. MacLeod (Eds.), *Catastrophic events and mass extinctions: Impacts and beyond* (pp. 395–413). The Geological Society of America, Inc.

Winguth, A., & Maier-Reimer, E. (2005). Causes of the marine productivity and oxygen changes associated with the permian-triassic boundary: A reevaluation with ocean general circulation models. *Marine Geology*, *217*, 283–304. https://doi.org/10.1016/j.margeo.2005.02.011

Winguth, A., & Winguth, C. (2013). Precession-driven monsoon variability at the permian-triassic boundary - implications for anoxia and the mass extinction. *Global and Planetary Change*, *105*, 160–170. https://doi.org/10.1016/j.gloplacha.2012.06.006

Winguth, A., Shields, C., & Winguth, C. (2015). Transition into a hothouse world at the permian-triassic boundary - a model study. *Palaeogeography, Palaeoclimatology, Palaeoecology*, *440*, 316–327. https://doi.org/10.1016/j.palaeo.2015.09.008

Winguth, C., & Winguth, A. (2012). Simulating permian-triassic oceanic anoxia distribution: Implications for species extinction and recovery. *Geology*, *40*(2), 127–130. https://doi.org/10.1130/G32453.1

Wu, H., Zhang, S., Hinnov, L., Jiang, G., Feng, Q., Li, H., & Yang, T. (2012). Time-calibrated milankovitch cycles for the late permian. *Nature Communications*, *4*(2452), 8. https://doi.org/10.1038/ncomms3452

Wu, Y., Chu, D., Tong, J., H., S., Dal Corso, J., Wignall, P., Song, H., Du, Y., & Cui, Y. (2021). Six-fold increase of atmospheric pco_2 during the permian-triassic mass extinction. *Nature Communications*, *12*, 8. https://doi.org/10.1038/s41467-021-22298-7

Xu, Z., Huang, G., Ji, F., & Liu, B. (2023). Multi-scale variability features of global sea surface temperature over the past century. *Frontiers in Marine Science*, *10*(1238320). https://doi.org/10.3389/fmars.2023.1238320

Yao, C.-L., & Somero, G. (2014). The impact of ocean warming on marine organisms. *Chinese Science Bulletin*, *59*, 468–479. https://doi.org/10.1007/s11434-014-0113-0

Zeebe, R., & Wolf-Gladrow, D. (2003). Equilibrium. In R. Zeebe, D. Wolf-Gladrow, & D. Halpern (Eds.), *Co_2 in seawater: Equilibrium, kinetics, isotopes* (2nd ed.). Elsevier Science B.V.

Zhang, R., Follows, M., Grotzinger, J., & Marshall, J. (2001). Could the late permian deep ocean have been anoxic? *Paleoceanography*, *16*, 317–329. https://doi.org/10.1029/2000PA000522

Zhang, X., Chen, C., Lian, T., & Chen, D. (2017). Spatiotemporal modes of global sea surface temperature variability. *Science China Earth Sciences*, *60*(3), 508–516. https://doi.org/10.1007/s11430-016-0160-9

Zhu, J., Otto-Bliesner, B., Brady, E., Gettelman, A., Bacmeister, J., Neale, R., Poulsen, C., Shaw, J., McGraw, Z., & Kay, J. (2022). Lgm paleoclimate constraints inform cloud parameterizations and equilibrium climate sensitivity in cesm2. *Journal of Advances in Modeling Earth Systems*, *14*(e2021MS002776). https://doi.org/10.1029/2021MS002776

Zhu, J., Poulsen, C., & Tierney, J. (2019). Simulation of eocene extreme warmth and high climate sensitivity through cloud feedbacks. *Science Advances*, *5*(eaax1874). https://doi.org/10.1126/sciadv.aax1874

Zhu, X. (2021). Characteristics of inherent coupling structure of model climates. *Journal of Climate*, *34*, 6891–6904. https://doi.org/10.1175/JCLI-D-20-0700.1

ACKNOWLEDGMENTS

I would like to take this opportunity to thank the many people that have supported me during my PhD journey, without whom this would not have been possible.

First, to my supervisors, Tatiana and Michael, for giving me the opportunity to explore a truly exciting research topic. I thank Tatiana for giving me the freedom and time to explore and develop this research in a way that expresses my interests and personality and for always meeting my enthusiasm for the science with greater enthusiasm. I would also like to thank Michael for inspiring my interest in a field of research that I had no idea would mean so much to me by the end of this PhD.

I would like to thank the whole of the Ocean Biogeochemistry group during my time in Hamburg for their support and patience as I developed as a modeller. There was always something new and exciting to learn. I offer special thanks to Bo, Fanny, Rike, Joeran, Tinka and Irene.

This PhD experience would have been entirely different without everyone at the IMPRS-ESM. Thank you to the whole administrative team but especially Antje for tirelessly going above and beyond every time and always making time to support me when I needed it. Thank you also to the many PhDs that I've met through the IMPRS-ESM and shared this experience with but especially to Jacqueline, Luca and Moritz.

Last but not least to my friends and family who kept me going through the most stressful and difficult times over these years. Thank you to Lucy, Marek, Teffy, Dian and Shubhankar and all my other friends, you always made sure to encourage me to take breaks and have fun. Finally, to my mum, Sharon, especially for always being prepared and eager to hear about my work and being even more excited to tell me when you understood it.

VERSICHERUNG AN EIDES STATT - DECLARATION OF OATH

Hiermit versichere ich an Eides statt, dass ich die vorliegende Dissertation mit dem Titel: „Unravelling climate conditions preceding the End-Permian Mass Extinction: Insights from latest Permian interannual tropical variability and extreme events “ selbstständig verfasst und keine anderen als die angegebenen Hilfsmittel – insbesondere keine im Quellenverzeichnis nicht benannten Internet-Quellen – benutzt habe. Alle Stellen, die wörtlich oder sinngemäß aus Veröffentlichungen entnommen wurden, sind als solche kenntlich gemacht. Ich versichere weiterhin, dass ich die Dissertation oder Teile davon vorher weder im In- noch im Ausland in einem anderen Prüfungsverfahren eingereicht habe und die eingereichte schriftliche Fassung der auf dem elektronischen Speichermedium entspricht.

Hamburg, April 2024

Daniel Burt

Hinweis / Reference

Die gesamten Veröffentlichungen in der Publikationsreihe des MPI-M
„Berichte zur Erdsystemforschung / Reports on Earth System Science“,
ISSN 1614-1199

sind über die Internetseiten des Max-Planck-Instituts für Meteorologie erhältlich:
https://mpimet.mpg.de/forschung/publikationen

All the publications in the series of the MPI -M
„Berichte zur Erdsystemforschung / Reports on Earth System Science“,
ISSN 1614-1199

are available on the website of the Max Planck Institute for Meteorology:
https://mpimet.mpg.de/en/research/publications